

HYDRAULICS OF
SUBMERGED ARCH BRIDGES

DECEMBER 1963

NO. 35

Joint
Highway
Research
Project

PURDUE UNIVERSITY
LAFAYETTE INDIANA

by
O. EIKERI
and
J.W. DELLEUR

Progress Report

HYDRAULICS OF SUBMERGED ARCH BRIDGES

TO: K. B. Woods, Director
Joint Highway Research Project

December 17, 1963

FROM: H. L. Michael, Associate Director
Joint Highway Research Project

Project: C-36-62B
File: 9-8-2

Progress Report No. 6 on the cooperative research entitled "Hydraulics of River Flow Under Arch Bridges" is attached. This report is titled "Hydraulics of Submerged Arch Bridges" and has been authored by Mr. Oddvar Eikeri, Graduate Assistant on our staff under the direction of Professor J. W. Delleur.

This is the last formal progress report on this project which has been in progress during the last six (6) years. A Final Report is now being prepared and will be submitted within a few weeks.

The attached report covers research performed on this project during the past year and supplements the earlier progress reports, extending the research to conditions not covered in earlier reports, specifically the case of submerged conditions.

The report is presented to the Board for the record and will be submitted to the cooperating agencies for review and comment.

Respectfully submitted,

Harold L. Michael
Harold L. Michael,
Secretary

HIM:bc

Attachment

Copy:

F. L. Ashbaucher
J. R. Cooper
W. L. Dolch
W. H. Goetz
F. F. Hovey
F. S. Hill
G. A. Leonards

J. F. McLaughlin
R. D. Miles
R. E. Mills
M. B. Scott
J. V. Smythe
E. J. Yoder

Hydraulics of River Flow Under Arch Bridges

Hydraulics of Submerged Arch Bridges

By

Oddvar Eikeri

Graduate Assistant

Joint Highway Research Project

Project: C-36-62B

File: 9-8-2

Prepared as Part of an Investigation

Conducted By

Joint Highway Research Project

Engineering Experiment Station

Purdue University

in cooperation with

Indiana State Highway Commission

and the

Bureau of Public Roads

U S Department of Commerce

Released for Publication

Subject to Change

Purdue University

Not Reviewed By

Indiana State Highway Commission

or the

Bureau of Public Roads

Lafayette, Indiana

December 17, 1963

ACKNOWLEDGMENTS

The author wishes to express his sincerest appreciation to Professor J. W. Delleur for his invaluable assistance and experienced guidance in all phases of the study and in the preparation and review of the manuscript.

Appreciation is also extended to Professor K. B. Woods, Head of the Civil Engineering School at Purdue University and Director of the Joint Highway Research Project, and to Professor H. L. Michael, Associate Director of the Joint Highway Research Project, for their help and cooperation.

The interest and help extended by the Joint Highway Research Project and Indiana State Highway Department is greatly appreciated.

Sincere thanks to Dr. G. H. Toebe, a member of his committee, for contributing of his time and advice.

Special acknowledgment is due to Mr. A. A. Sooky, doctoral candidate in hydraulics for his valuable advice and the permission to use the many apparatus he has developed.

Special thanks are extended to the staff of Civil Engineering at Purdue University and all other persons who have assisted the author with the completion of this project.

Finally, the author gratefully acknowledges the help, understanding and inspiration of his wife Toril during the time of preparation of this report.

TABLE OF CONTENTS

	<u>Page</u>
LIST OF TABLES	vii
LIST OF FIGURES	ix
ABSTRACT	xiii
CHAPTER I - INTRODUCTION	2
CHAPTER II - REVIEW OF LITERATURE	5
CHAPTER III - THEORETICAL ANALYSIS	10
Dimensional Considerations	13
Definition of Channel Opening Ratio and Channel Width Ratio	15
Orifice Flow	16
The Equation of Discharge for Orifice Flow	17
Backwater Ratio Equation for Submerged Inlet with Orifice Flow	20
Dimensionless Equation for Orifice Type Flow	21
Head Loss Due to Bridge Constriction	23
CHAPTER IV - EXPERIMENTAL APPARATUS	26
Flume	26
Water Supply and Measurement System	27
Test Station	33
Measuring Equipment	33
Instrument Carriage	33
Point Gage	35
Prandtl Tube	37
Variable-Reluctance Pressure Transducers	37
Calibration of Velocity Probe	45
Procedure for Measuring of the Velocity	49
CHAPTER V - DEFINITION OF TEST GEOMETRIES - SELECTION OF TESTS	51
Geometry I-a, Two-Dimensional Semicircle Arch Bridge Constrictions	51
Geometry I-b, Three Dimensional Semicircular Arch Bridges	51
Geometry II, Dual Parallel Three-Dimensional Arch Bridge Constrictions	52
Geometry III, Three Dimensional Arch Bridge Constriction with Wingwalls	53
Geometry IV, Two Dimensional Semicircular Arch Bridge Constrictions with Eccentricity	54

Digitized by the Internet Archive
in 2011 with funding from
LYRASIS members and Sloan Foundation; Indiana Department of Transportation

TABLE OF CONTENTS, continued

Page

Geometry V-a, Two-Dimensional Semicircular Arch Bridge	
Constrictions with Skew	54
Geometry V-b, Three Dimensional Semicircular Arch Bridge	
Constrictions with Skew	54
Geometry VI, Three Dimensional Two-Span Semicircular	
Arch Bridge Constrictions	55
Geometry VII, Two-Dimensional Segment Arch Bridge	
Constrictions	55
Submerged Test Geometries	57
Roughness	57
Construction of Models	58
Selection of Variables	60
 CHAPTER VI - TESTING PROCEDURE AND DATA PROCESSING	 70
Test Setup for Submerged Flow Conditions	70
Nomographic Charts	70
Data Processing	74
 CHAPTER VII - RESULTS AND THEIR ANALYSIS	 76
Geometry I-a - Smooth Boundaries	76
Coefficient of Contraction, of Discharge and of Velocity	
for Free Jet Outflow	77
Velocity Distribution at Vena Contracta for Free Jet Outflow	81
The Generalized Backwater Equation - Outflow Fully and	
Partly Submerged	85
Discharge Coefficient for Free, Submerged and Partly	
Submerged Outflow	87
Geometry I-b - Smooth Boundaries	89
Geometries I-a and I-b - Rough Boundaries	91
Comparison Between Smooth and Rough Boundary Tests	97
Skewed Bridges - Geometry V-b Rough Boundaries $n = 0.0238$	100
Geometry VI - Two Span Semicircular Arch Bridge Constriction	
Rough Boundaries $n = 0.0238$	103
Geometry VII - Segment Arch Bridge - Rough Boundaries	
$n = 0.0238$	103
Head Loss Considerations	106
General Backwater Equations for Geometries I-a, I-b, V-b,	
VI and VII - Smooth and Rough Boundaries	118
 CHAPTER VIII - FINDINGS, CONCLUSIONS AND RECOMMENDATIONS	 130
Findings	130
Conclusions	131
Recommendations	131

TABLE OF CONTENTS, continued

	<u>Page</u>
BIBLIOGRAPHY	132
APPENDIX A - NOTATIONS	134
APPENDIX B - DEVELOPMENT OF THEORETICAL DISCHARGE EQUATION FOR ORIFICE TYPE FLOW THROUGH SEMICIRCULAR OPENINGS	138
APPENDIX C - DIGITAL COMPUTERS AND PROGRAM NOTES	142
APPENDIX D - TABLES	166

LIST OF TABLES

Tables	Page
I Smooth Boundary Tests Geometry I-a	63
II " " " " I-b	64
III Rough Boundary Tests Geometry I-a	65
IV " " " " I-b	66
V " " " " V-b	67
VI " " " " VI	68
VII " " " " VII	69
VIII Raw data Run number 2 - 10	166
IX " " " " 11 - 18	167
X " " " " 19 - 26	168
XI " " " " 27 - 34	169
XII " " " " 35 - 42	170
XIII " " " " 43 - 51	171
XIV " " " " 52 - 59	172
XV " " " " 60 - 67	173
XVI " " " " 101 - 116	174
XVII " " " " 117 - 134	175
XVIII " " " " 135 - 152	176
XIX " " " " 153 - 170	177
XX " " " " 171 - 188	178

LIST OF TABLES, continued

Table		Page
XXI	Raw data Run number 189 - 206	179
XXII	" " " " 207 - 224	180
XXIII	" " " " 225 - 242	181
XXIV	" " " " 243 - 258	182
XXV	" " " " 259 - 276	183
XXVI	" " " " 277 - 296	184
XXVII	" " " " 297 - 307	185
XXVIII	" " " " 70 - 71	186
XXIX	" " " " 72 - 73	187
XXX	Calculated Values Run number 2 - 140	188
XXXI	" " " " 141 - 306	189

LIST OF FIGURES

<u>Figure</u>		<u>Page</u>
1.	Testing Flume, Models and Instrument Carriage	1
2.	Centerline Surface Profile Near Submerged Constriction .	11
3.	Plan View of Flow Through a Submerged Constriction . . .	12
4.	Definition Sketch for the Channel Opening Ratio	16a
5.	Definition Sketch for Orifice Flow Calculation	19
6.	Plan View of Jacks and Gears	28
7.	Jack Detail	29
8.	Tail Gate Construction	29
9.	General Layout of Testing Facility	30
10.	Calibration Curve for 6" Venturimeter	31
11.	Calibration Curve for 3" Venturimeter	32
12a.	Test Section	34
b.	Test Section Detail	34
13.	Top View of Instrument Carriage	36
14.	Point Gage and Prandtl Tube	36
15.	Accuracy of Velocity Readings as a Function of Angle of Attack	38
16.	Velocity Transducer System	40
17.	Diaphragm - Type Variable-Reluctance Pressure Transducer	41
18.	Carrier - Demodulator	43
19.	Diagram for Selection of Diaphragm in Transducer	44
20.	Calibration Apparatus for Prandtl tube	46
21.	Detail of Calibration Apparatus	47

LIST OF FIGURES, continued

<u>Figure</u>		<u>Page</u>
22.	Typical Calibration Curves for Probe	48
23.	Pressure Cells	
a	Right Cell Connected for High Velocity Measurement . . .	50
b	Left Pressure Cell Connected for Low Velocity Measurement	50
24.	Definition Sketches of Test Geometries	56
25.	Test Models	59
26.	Test Selection Curve-Large Flume-Smooth Boundaries . . .	72
27.	Test Selection Curve-Large Flume-Rough Boundaries . . .	73
28.	Upstream and Downstream Views of Typical Test Run . . .	75
29.	Coefficients of Velocity, Contraction and Discharge. Submerged Inlet and Unsubmerged Discharge Jet	79
30.	Isovelocity Curves at Vena Contracta	82
31.	Isovelocity Curves for Cross-Section at Vena Contracta .	83
32.	Velocity Distribution at Vena Contracta	84
33.	Generalized Backwater Ratio for Submerged Inlet Geometry I-a	86
34.	Discharge Coefficient Versus Channel Opening Ratio, Smooth Boundaries, Geometry I-a	88
35.	Discharge Coefficient for Free and Submerged Discharge and Partly Submerged Jet, Geometry I-a	90
36.	Dimensionless Curves for Geometries I-a and I-b Smooth Boundaries	92
37.	Dimensionless Curves for Geometries I-a and I-b Rough Boundaries	94
38 a.	Spiral Motion in Barrel Section Downstream of Vena Contracta	95
b.	Typical Flow Condition Through Constriction	95
39.	Slug Flow at Barrel Exit	96
40.	Free Discharge Jet	96

LIST OF FIGURES, continued

<u>Figure</u>		<u>Page</u>
41.	Comparison of Dimensionless Curves for Geometry I-a, for Smooth and Rough Boundaries	98
42 a.	Flow Through Left Skewed Bridge	101
b.	Flow Through Right Skewed Bridge	101
43.	Dimensionless Curves for Geometry V-b, Rough Boundaries	102
44.	Dimensionless Curves for Geometry VI Using F_n as Parameter, Rough Boundaries	104
45.	Dimensionless Curves for Geometry VII, Rough Boundaries	105
46.	Head Loss Coefficient for Geometry I-a, Smooth Boundaries, $L/b = 0.0$	108
47.	Head Loss Coefficient for Geometry I-b, Smooth Boundaries, $L/b = 0.25$	109
48.	Head Loss Coefficient for Geometry I-b, Smooth Boundaries, $L/b = 0.50$	110
49.	Head Loss Coefficient for Geometry I-b, Smooth Boundaries, $L/b = 0.75$	111
50.	Head Loss Coefficient for Geometry I-b, Smooth Boundaries, $L/b = 1.00$	112
51.	Summary of Head Loss Coefficient Curves for Geometries I-a and I-b, Smooth Boundaries	113
52.	Head Loss Coefficient Curves for Geometries I-a and I-b, Rough Boundaries	114
53.	Head Loss Coefficient Curves for Geometry V-b, Rough Boundaries	115
54.	Head Loss Coefficient Curves for Geometry VI, Rough Boundaries	116
55.	Head Loss Coefficient Curves for Geometry VII, Rough Boundaries	117
56.	Generalized Backwater Ratio Geometry I-a, Smooth Boundaries, $L/b = 0.0$	120

LIST OF FIGURES, continued

<u>Figure</u>		<u>Page</u>
57.	Generalized Backwater Ratio Geometry I-b, Smooth Boundaries $L/b = 0.25$	121
58.	Generalized Backwater Ratio Geometry I-b, Smooth Boundaries $L/b = 0.50$	122
59.	Generalized Backwater Ratio Geometry I-b, Smooth Boundaries $L/b = 0.75$	123
60.	Generalized Backwater Ratio Geometry I-b, Smooth Boundaries $L/b = 1.00$	124
61.	Summary of Backwater Ratio Curves for Geometries I-a and I-b, Smooth Boundaries	125
62.	Generalized Backwater Ratio Geometries I-a and I-b, Rough Boundaries	126
63.	Generalized Backwater Ratio Geometry V-b, Rough Boundaries	127
64.	Generalized Backwater Ratio Geometry VI, Rough Boundaries	128
65.	Generalized Backwater Ratio Geometry VII, Rough Boundaries	129

ABSTRACT

Eikeri, Oddvar, M.S.C.E. Purdue University, January 1964. "Hydraulics of Submerged Arch Bridges". Major Professor: Dr. J. W. Delleur.

This report is part of a general program sponsored by the State Highway Department of Indiana and the U. S. Bureau of Public Roads at Purdue University on the Hydraulics of River Flow Under Arch Bridges.

The project has been conducted since 1958 and several reports on different phases of the study have been submitted. In 1958 Mr. S. T. Husain^{1*} reported his work, "Preliminary Model Investigation of Hydraulic Characteristics of River Flow Under Arch Bridges". This was an investigation in a 12 foot long, 6 inches wide tilting flume with smooth boundaries which led to the building of a 64 foot by 5 foot by 2 foot all steel tilting flume. The construction of the 64 foot flume was undertaken by Mr. H. J. Owen² and the work was reported in his masters thesis entitled "Design and Construction of Hydraulic Flume and Back-water Effects of Semi-circular Constrictions in Smooth Rectangular Channel". Mr. A. A. Sooky³ derived an equation for the discharge through a sharp edged semi-circular constriction for the case of free surface flow through the opening. He also extended Mr. S. T. Husain's preliminary studies to include the effect of rough boundaries. The work of Husain, Sooky and Owen was summarized in a report entitled, "Hydraulics of River Flow Under Arch Bridges - A Progress Report",³

* Superscripts refer to references in the bibliography.

In January 1961 Mr. P. F. Biery⁴ presented a report on "Hydraulics of Single Span Arch Bridge Constrictions" as part of his work toward a Master's degree. Biery investigated the single span arch bridge with free surface flow through the constriction. The study did not include skew, eccentricity or entrance rounding. A backwater equation was presented together with a bridge design procedure for free surface flow through the opening.

The present report on "Hydraulics of Submerged Arch Bridges" covers the work done by the author from September 1962 to December 1963. This work was also conducted in the large 64 foot by 5 foot by 2 foot tilting steel flume in the Hydraulics Laboratory at Purdue University.

The existing instrumentation was improved. The measurement of flow velocity with the Prandtl tube was facilitated by the replacement of the usual fluid manometer by two pressure transducers and electric accessories. This gave a more sensitive reading of small velocities and a much faster response to small changes in the pressure differentials.

A theoretical discharge equation for orifice type flow through semi-circular bridge openings was developed. An equation for the head loss due to the bridge constriction was also derived. Model studies for submerged bridge constrictions were made both for smooth and rough channel boundaries. Models of two and three dimensions with and without skew, with one and two openings, but having no eccentricity or entrance rounding were investigated.

Through the theoretical and experimental analysis the following

results were obtained:

- a) A dimensionless relationship between discharge and backwater elevation.
- b) A semi-empirical expression to distinguish between the occurrence of free surface flow and orifice type flow through the bridge constriction.
- c) Two types of graphical presentation of the test results for each geometry. In one presentation, the discharge is shown as a function of the ratio of the backwater depth to the arch span, in the other the ratio of the backwater to the normal depth is shown as a function of the Froude number of the unconstricted flow and of the channel opening ratio.
- d) Empirical generalized backwater equations derived for the several geometries from the second presentation discussed under c.
- e) Graphs giving the value of the constriction head loss coefficient as a function of the channel opening ratio for different test geometries.

Finally, suggestions are made for further study of the submerged arch bridge constrictions.



FIG 1 TESTING FLUME, MODELS, AND INSTRUMENT CARRIAGE

CHAPTER I

Introduction

How many arch bridges are there in the entire United States? Although this figure is probably unknown, Indiana alone has about 900 arch bridges. By increasing the backwater upstream from the bridge site, many of these bridge constrictions cause additional flooding during high flows; people and valuable property are endangered. In recent years, the problem of minimizing the backwater effect due to bridge constriction has become increasingly important. The highway engineers are faced with a multisided problem; not only do they have to build bridges to convey a specified traffic volume and are safe with respect to flooding, but they also must find the most economic design possible. It is common knowledge to the highway engineer that a bridge crossing will interfere with the natural flow of the stream and will result in a rise of stage upstream from the bridge and in an increase in velocity through the bridge constriction. The engineers are also aware of alternatives of the inexpensive soil fill compared to a structural span. The optimum design, is the shortest span that will not cause damage due to stage increase during serious flood condition. In order to meet these requirements, exhaustive investigations were undertaken to study the hydraulic characteristics of the water flow through different bridge constrictions.

In 1958, a project was initiated in the Hydraulics Laboratory at Purdue University in order to study the hydraulics of stream flow under arch bridges. It is sponsored through the Joint Highway Research Project in cooperation with U. S. Bureau of Public Roads. Similar projects have also been conducted at many other universities throughout the United States to study different phases of the hydraulics connected with flow through bridge crossings.

The hydraulics of river flow through arch bridges is rather complicated, and its investigation involves many variables. The relationships between these variables cannot be handled completely by means of a theoretical analysis. Experimental models are necessary in order to investigate the problems, and even then only the simplest and most idealized conditions can be observed. In most cases the actual field conditions are so varied that each one could require a separate model study. The goal for this research is to obtain some empirical information about the hydraulic behavior under generalized conditions, and each field condition would then have to be given some special consideration.

The present report covers the investigation of the hydraulics of the submerged arch bridge constrictions of several geometries. The single-opening, two-dimensional, semi-circular arch constriction of infinitesimal length in the flow direction, without skew, eccentricity or entrance rounding was studied first. Submerged flow through this constriction was investigated in a smooth and in a rough channel with varying opening ratios and varying Froude numbers. The streamline pattern, the velocity distribution, and the resulting rise in

the backwater upstream of the bridge constriction, were studied. The coefficient of contraction, the coefficient of discharge, and the coefficient of velocity, were also investigated. The single span three-dimensional arch constriction (without skew, eccentricity or rounding) of several length simulates the most common bridge. About 480 out of 900 arch bridges in Indiana have approximately this geometry (I-b). Submerged flow through this type of constriction was investigated for smooth and for rough channel boundaries.

The skew bridges are next in importance since approximately 35 per cent of all arch bridges in Indiana are skewed. Among these bridges, the most common skew angles and the respective number of each structure in existence are: 15° - 14, 20° - 80, and 30° - 120. The most common thickness factor, L/b , is about 0.50 for all bridges. Models of Geometry V-b simulates the typical skewed arch bridge constriction.

After the one span bridges, two span bridges represent the next largest category. Having about 100 such bridges in Indiana; and representing about 11 per cent of all existing arch bridges in the state. Models of Geometry VI simulate two equal and symmetric spans without skew or rounding.

Geometry VII, represents two-dimensional arch segment constrictions. Some model tests had already been done by a previous investigator, T. P. Chang,⁵ but the data taken had not been analyzed. These experiments were complemented by additional testing and by the completion of the analysis of all the data of geometry VII.

CHAPTER II

REVIEW OF LITERATURE

There is no literature published to this date which is directly concerned with the hydraulic characteristics of submerged arch bridges. Therefore, papers on other submerged structures or on the fundamental aspects of the fluid mechanics of contracting and expanding flows were the only source of literature.

In 1952 A. M. Binnie⁶ presented a paper on "The Flow of Water under a Sluice-gate". By introducing the Froude number of the flow, Binnie simplifies relationship between conditions upstream and downstream from a sluice-gate. Well-known expressions are derived for alternate depth of flow, discharge, and force in the gate. A simple explanation is presented for the absence of waves on both sides of the gate. Coefficient of contraction C_c of the issuing flow is given as a review of experimental and theoretical investigations. Actually, Binnie does not mention C_c , but presents instead the gate opening required to produce a given Froude number. Although the paper presenting the problem uses the simplified one dimensional sluice opening, it is a good, clear compilation of the present knowledge of the subject.

P. Franke⁷ also studies the one-dimensional flow from a sluice gate in his paper of 1955 on "Jet Contraction in Flow under Sluice-gates in Rectangular Channels". His analysis is based on energy

considerations. He computes the downstream depth in the cases with and without energy losses taken into consideration. Values of the coefficient of contraction are given for different ratios of upstream depth to gate opening. All results are expressed in non-dimensional form.

In 1950, M. L. Albertson, R. A. Jensen, Y. B. Dai and H. Rouse⁸ published a paper on "Diffusion of Submerged Jets". This paper deals with the turbulence generated at the edge of a free air jet issuing from orifices and slots. Results are given of measurements of the distribution of the longitudinal velocity and turbulence characteristics. Of particular interest to bridge hydraulics is the discussion of H. R. Henry (1950)⁹ on this paper. Henry investigates the effect of boundary conditions which are different from those used in the main paper. These, for the case of the flow under a sluice gate, are the effect of the free surface, i.e. gravitational effect, and the presence of a solid boundary, i.e. the flume floor, instead of a plane of symmetry of a two-dimensional jet. As a hydraulic design conclusion, experimental discharge coefficients, C_d , for the flow under a sluice gate are given as a function of a dimensionless gate opening, h/B , using a dimensionless tailwater depth, t/B , or the orifice Froude number as a parameter. The experimental trend of the curves is verified by an approximate theoretical analysis.

In 1957 J. C. Gibbings and J. R. Dixon¹⁰ presented a paper on "Two-Dimensional Contracting Duct Flow". Although this paper is primarily for wind tunnel design dealing with flow through two-dimensional contracting channels of definite length, it presents a valuable potential flow study, and a detailed method of eliminating the adverse velocity

gradient along the channel walls.

Most of the literature reviewed so far has dealt with the one-dimensional opening in so far as they use a uniform "infinitely" wide slot as sluice gate opening. But the submerged arch bridge constriction is a two-dimensional opening case where the width of the opening varies with the height. This eliminates some of the simplifications made in the papers discussed above, and the present investigation has to rely more upon the experimental study. This is because it is not possible to develop a simple mathematical model of the flow patterns through two dimensional orifices subjected to the influence of gravity. However, the flow could in some respects be analyzed with the help of the orifice theories.

H. Rouse¹¹ discusses the characteristics of orifice flow and the variation of orifice coefficients with boundary geometry.

H. Rouse¹² and A. H. Abul-Fetouh¹² presented the paper "Characteristics of Irrotational Flow Through Axially Symmetric Orifices" in 1950. The authors conclude that use of the relaxation method has permitted a numerical determination of flow characteristics to be made with sufficient precision for the problem to be considered solved, though an exact solution of the orifice problem has not yet proved feasible. The coefficient of contraction was found to be practically identical with that evaluated by von Mises¹³ for two-dimensional flow from slots over the entire range of area ratio, and reasonable agreement was shown to exist between measurement and computation. Coordinates of the jet profiles were presented in tabular and graphical form and were found to differ appreciably from those previously adopted

from the two-dimensional case. A composite dimensionless chart was also provided showing the distribution of pressure along the boundary, center line, and across the efflux section for the various area ratios.

M. C. Chaturvedi¹⁴ a student of H. Rouse, presented in May 1963 a paper on "Flow Characteristics of Axisymmetric Expansions." He has studied the characteristics and dynamics of flow for four abrupt expansions. Certain general observations were done. Chaturvedi observed that the large scale properties of motion are not affected by viscous action. Thus, beyond the effect of viscosity on the conditions of stability, it has no influence on the pattern of separation and on the turbulence intensities. With regard to the dynamics of the flow, it was noted that the most significant feature of the separation is the turbulence production. Because of the complex nature of the phenomena, it was not possible to express the results and the details of the flow characteristics in simple mathematical terms. A simplified one-dimensional analysis of the variation of head loss was presented.

For the investigation of the three dimensional models under submergence, the problems become similar to those in the investigation of short culverts. Here, several investigations have been published and good sources were available in the literature searched.

The Highway Research Board Research Report 15-B on Culvert Hydraulics, published in 1953¹⁵, investigates the head-discharge relationship in short culverts. The existence of a transition zone between part-full phase and full-flow phase was also observed by the investigators.

Bulletin 126 from Highway Research Board in 1956¹⁶ presents a

study on Culvert-Flow Characteristics. The first part of the paper covers a series of typical water-surface profiles which can occur in a culvert; M. R. Garstens and A. R. Holt were the investigators. The second part was presented by R. E. Schiller, Jr. and treated the effect of various types of inlets on flow through short model circular pipe culverts.

In 1959, Hunter Rouse and D. E. Metzler¹⁷ presented a paper "Hydraulics of Box Culverts". The various graphs and experimental evidence were based upon an extensive study on box-culvert characteristics. But the generality of the approach in the presentation of the non-dimensional curves makes much of the material applicable in a qualitative sense to pipe culverts and submerged arch bridge flow as well.

G. E. Myers, J. J. Schauer and R. H. Eustis¹⁸ presented in March 1963 a paper on "Plane Turbulent Wall Jet Flow Development and Friction Factor." They investigated the jet development, the velocity profiles, and the wall shearing stress in a two-dimensional, incompressible, turbulent wall jet. The maximum velocity decay, jet thickness, and shearing stress were predicted analytically by momentum - integral methods. Experimental data concerning velocity profiles, velocity decay, and jet thickness agreed well with those of previous investigators. The wall shearing stress was measured by a hot-film technique and the results help to resolve a wide divergence between experimental values of other investigators. All their tests were conducted with air blowing through a nozzle.

CHAPTER III

THEORETICAL ANALYSIS

Figures 2 and 3 show the centerline profile and the plan view respectively of a typical flow through a submerged arch bridge opening. In figure 2 the approaching water surface is shown to have a profile of an M_1 curve as defined by Ven Te Chow¹⁹, Y_0 or Y_n is the normal depth of the unobstructed channel flow, Y_1 is the depth at the section of maximum backwater, Y_2 is the downstream depth taken in the deadwater flow portion of the channel (see figure 3). The plan view of the channel constriction flow in figure 3 shows the streamlines of the flow entering the opening. The velocity upstream of the constriction is low and the streamlines follow the walls very closely. The eddies sketched on the upstream side of the opening moves in a vertical plane in a screw motion towards the opening. A particle in the corner would not remain in this region but due to these eddies it moves towards the opening. The eddies downstream of the constriction, shown on both sides of the jet, are in the horizontal plane and are less active. Particles could often remain there for longer periods of time.

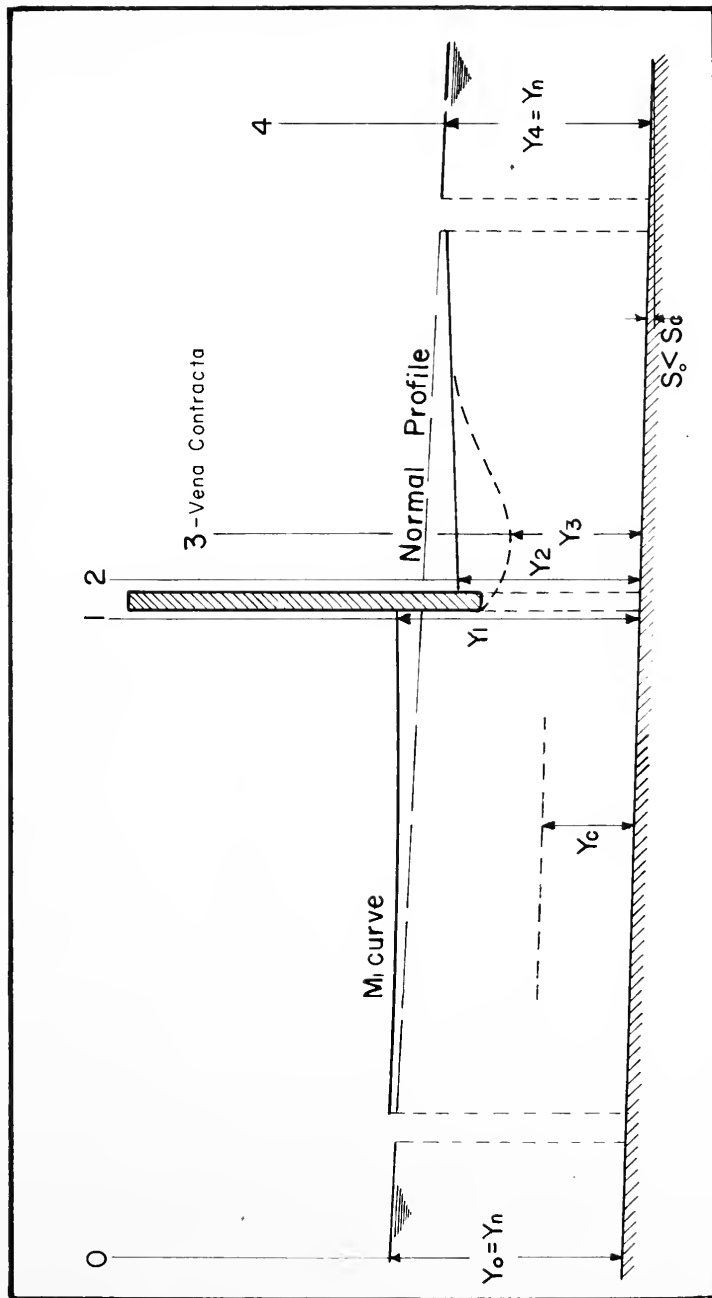


Fig 2 Center Line Surface Profile Near Submerged Constriction

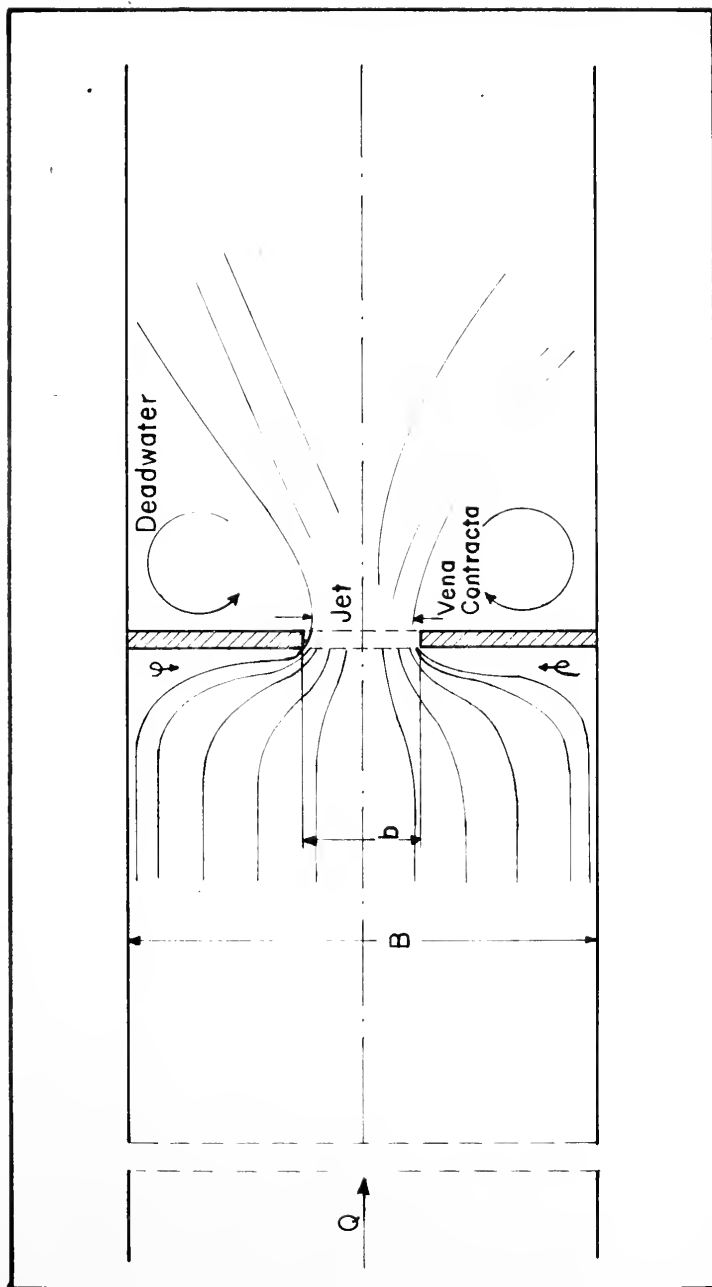


Fig 3 Plan View of Flow Through a Submerged Constriction

Dimensional Considerations

A dimensional analysis was used for the design of the experiment and for the presentation and interpretation of the results. The variables which govern such an analysis are of three kinds: the fluid properties, the kinematic and dynamic variables and the dimensions defining the constriction geometry.

The variables are:

(a) Fluid Properties

- 1) ν , the kinematic viscosity of the fluid
- 2) ρ , density of the fluid

(b) Kinematic and Dynamic Flow Variables

- 1) g , acceleration of gravity
- 2) Y_1 , maximum water depth upstream of the constriction
- 3) Y_n , the normal depth of flow in the approach channel
- 4) V_n , the velocity of flow at normal depth
- 5) n , Manning's roughness coefficient of the approach channel
- 6) Δh , the maximum water surface drop across the constriction

$$(\Delta h = Y_1 - Y_2)$$

(c) Properties of the Constriction Geometry (see figures 2, 4, and 24 for definition of symbols).

- 1) A_{n1} , the total normal depth flow area at section 1.
- 2) A_{n2} the normal depth flow area in the opening of the constriction (see Fig. 4). $A_{n2} = A_0$ for submerged bridges.

- 3) L/b , thickness factor, where L is the length of bridge in direction of flow, b is the width of opening at the bottom.
- 4) bL_d/A_{n2} , distance factor where L_d is the distance between two parallel identical bridges.
- 5) ϕ_1 , wing wall angle
- 6) ϕ_2 , skew angle
- 7) β , segment factor defined by $\beta = d/r$ where d is the distance between the channel bottom and the center of the circular segment.
- 8) N , number of spans
- 9) e , eccentricity defined by $e = 1 - c/a$, where c and a are the width on either sides of the bridge openings.

From the above list of variables,

$$Y_1 = f_1 (Y_n, V_n, n, \Delta h, V, p, g, A_{n1}, A_{n2}, L/b, \frac{bL_d}{A_{n2}}, \phi_1, \phi_2, e, \beta, N) \quad (1)$$

Buckingham's theorem states that in a physical problem including n quantities in which there are m dimensions, the quantities may be arranged into $(n - m)$ dimensionless parameters. With the mass, length and time system of units, the $n - m$ or 14 dimensionless parameters are as follows:

$$\frac{Y_1}{Y_n} = f_2 \left(\frac{V_n^2}{Y_n^3}, \frac{V_n Y_n}{\nu}, \frac{n}{Y_n^{1/6}}, \frac{A_{n1}}{Y_n^2}, \frac{A_{n2}}{Y_n^2}, \frac{\Delta h}{Y_n}, \frac{L}{b}, \frac{bL_d}{A_{n2}}, \phi_1, \phi_2, e, \beta, N \right) \quad (2)$$

where $\frac{V^2}{Y_n g}$ is the square of the Froude number F_n and $\frac{V Y_n}{\nu}$ is the Reynolds number R . It is known that:

- 1) Viscous forces play a negligible role in open channel flow. So the term R can be neglected.
- 2) The backwater superelevation upstream is not materially affected by the shape of the downstream water surface, and the term $\frac{\Delta h}{Y_n}$ can be neglected.

Furthermore, by combining the ratios A_{n2}/Y_n^2 and A_{n1}/Y_n^2 into $A_{n2}/A_{n1} = M'$, and letting n be constant, which means that the boundary roughness in the flume is kept the same, then the above equation simplifies to:

$$\frac{Y_1}{Y_n} = f \left(F_n, M', \frac{L}{b}, \frac{b L_d}{A_{n2}}, \phi_1, \phi_2, e, \beta, N \right) \quad (3)$$

Of the nine variables only two, the Froude number and the contraction ratio describe the flow field. The other seven variables in the dimensionless analysis describe the different model geometries that could be tested separately. For a definition of the separate geometries see section on Definition of Test Geometries in Chapter V.

Definition of Channel Opening Ratio and Channel Width Ratio

In an earlier investigation on the hydraulics of arch bridges P. F. Biery⁴ defined the channel openings ratio (M'). Referring to figure 4, the channel opening ratio is defined as that portion of the total normal depth flow which can pass through the bridge waterway without contraction. This is equivalent to the ratio A_{n2}/A_{n1} obtained from the dimensional analysis.

$$M' = q/Q = A_{n2}/A_{n1}$$

For the submerged case where orifice flow occurs, the normal depth for the flow is close to or exceeds the height of the model openings. So for all practical purposes the area, A_o , of the bridge opening can be used instead of A_{n2} , under said conditions. And M' may be defined for submerged bridges as

$$M' = q/Q = A_o/A_{n1}$$

Beside the Froude number (F_n) and the channel opening ratio (M'), the channel width ratio (M) is perhaps the most significant variable in the problem. The channel width ratio is defined as the ratio of the model opening width at the bottom, b , to the width of the channel, B .

$$M = b/B$$

Both M and M' are ratios related to the geometry of the constrictions, while the Froude number represents the effect of gravity upon the state of flow.

Orifice Flow

A distinction between the occurrence of free surface flow and orifice flow is essential, and some means is needed for predicting when the different types of flows occur.

Orifice flow will occur when the head over the crown of the arch exceeds the velocity head plus the head loss in the orifice type opening.

Putting this statement into an equation gives, for the limiting case:

$$\frac{v_3^2}{2g} + \left(\frac{1}{C_v^2} - 1 \right) \frac{v_3^2}{2g} = Y_1 - r \quad (4)$$

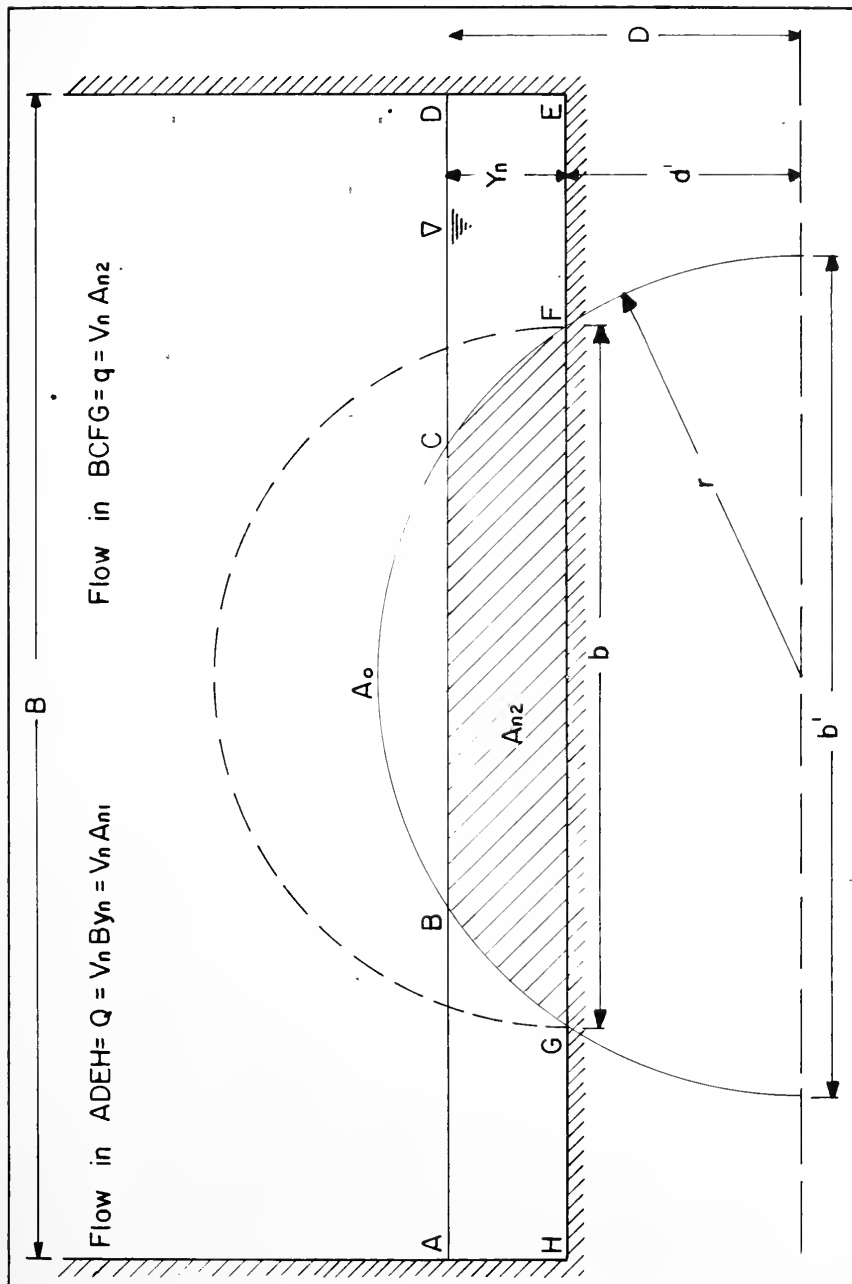


Fig 4 Definition Sketch for the Channel Opening Ratio

where $\left(\frac{1}{C_v^2} - 1 \right) \frac{V_3^2}{2g}$ is the orifice head loss.

$$\text{Then } \frac{1}{C_v^2} \frac{V_3^2}{2g} = Y_1 - r$$

and from the continuity equation:

$$V_1 B Y_1 = V_3 A_3 = V_3 C_c A_o$$

where A_o is the opening area of the model.

$$\text{Then } \frac{1}{C_v^2} \frac{V_1^2}{2g} \frac{B^2 Y_1^2}{C_c^2 A_o^2} = Y_1 - r \quad (5)$$

$$\text{rearranging (5): } \frac{V_1^2}{2g Y_1} = \left(1 - \frac{r}{Y_1} \right) C_d^2 \left(\frac{A_o}{A_1} \right)^2$$

$$\text{Hence } F_1^2 = 2 C_d^2 \left(1 - \frac{r}{Y_1} \right) \left(\frac{A_o}{A_1} \right)^2 \quad (6)$$

and there will be submergence when:

$$F_1^2 < 2 C_d^2 \left(1 - \frac{r}{Y_1} \right) \left(\frac{A_o}{A_1} \right)^2 \quad (7)$$

An average experimental value of C_d is 0.57. (See Chapter VII)

The Equation of Discharge for Orifice Flow

With reference to Figure 5 and neglecting the velocity of approach, the discharge was calculated as follows:

$$Q_t = \int V dA \quad (8)$$

$$\text{where } V = C_d \sqrt{2g (Y_1 - h)}$$

and
$$A = 2 \int_{h=0}^{h=r} \sqrt{r^2 - h^2} \, dh$$

hence
$$Q = 2 \int_0^r \sqrt{Cd^2 \, 2g \, (Y_1 - h)} \sqrt{r^2 - h^2} \, dh$$

$$= 2 \, Cd \sqrt{2g} \int_0^r (Y_1 - h)^{\frac{1}{2}} (r^2 - h^2)^{\frac{1}{2}} \, dh$$

An approximate solution to the above integral is found by expanding each term of the integrand into a binomial series, multiplying the two series and integrating term by term. The result, using the 5 leading terms, is

$$Q = 0.4019 \, C_d \sqrt{2g} \, Y_1^{\frac{1}{2}} b^2 \left[1 - 0.2136 \left(\frac{r}{Y_1} \right) - 0.03216 \left(\frac{r}{Y_1} \right)^2 - 0.0112 \left(\frac{r}{Y_1} \right)^3 - 0.005344 \left(\frac{r}{Y_1} \right)^4 \dots \right] \quad (10)$$

or
$$Q = C_1 \, Y_1^{\frac{1}{2}} \, b^2 \, T$$

where

$$C_1 = 0.4019 \sqrt{2g} \quad C_d = 3.22 \, C_d$$

and

$$T = 1 - 0.2136 \left(\frac{r}{Y_1} \right) - 0.03216 \left(\frac{r}{Y_1} \right)^2 - 0.0112 \left(\frac{r}{Y_1} \right)^3 - 0.005344 \left(\frac{r}{Y_1} \right)^4 \dots$$

The above equation is valid as long as the constriction is submerged, which means for $Y_1 > r$.

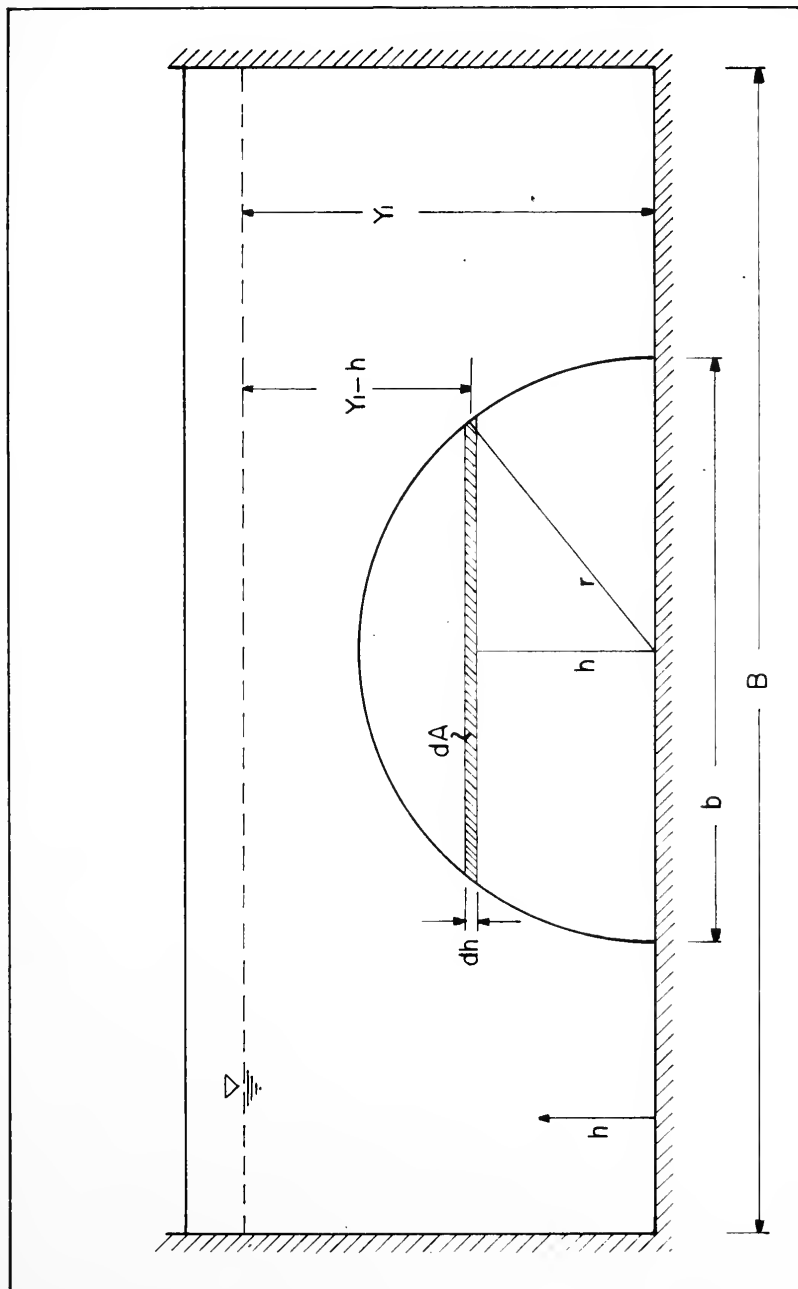


Fig 5 Definition Sketch for Orifice Flow Calculation

Backwater Ratio Equation for Submerged Inlet with Orifice Flow

The backwater ratio is defined as the ratio of the maximum center-line depth to the normal depth of flow. See Figure 2.

An expression for the backwater ratio may be obtained from the theoretical discharge equation for orifice flow. The equation for the discharge through the constriction was found to be:

$$Q = C_1 Y_1^{\frac{1}{2}} b^2 T \quad (11)$$

The discharge in the approach channel is:

$$Q = V_n A_n = F_n \sqrt{g} B Y_n^{3/2} \quad (12)$$

Equating the two discharge equations 11 and 12 :

$$C_1 Y_1^{\frac{1}{2}} b^2 T = F_n \sqrt{g} Y_n^{3/2} B \quad (13)$$

and

$$C_1 = \left(\frac{Y_n}{Y_1} \right)^{\frac{1}{2}} \frac{F_n B Y_n}{b^2 T} = \left(\frac{Y_n}{Y_1} \right)^{\frac{1}{2}} \left(\frac{B}{b} \cdot \frac{Y_n}{b} \right) F_n \frac{1}{T} \quad (14)$$

but

$$\frac{B}{b} \cdot \frac{Y_n}{b} = \frac{A_n}{k A_o} = \frac{1}{k M'}$$

where $k = \frac{8}{\pi}$

Now rearranging the equation (14) :

$$\frac{Y_1}{Y_n} = \left(\frac{1}{k M'} F_n \cdot \frac{1}{C_1} \cdot \frac{1}{T} \right)^2 \quad (15)$$

or in general a relation of the following form would be expected

$$\frac{Y_1}{Y_n} = C \left(\frac{F_n}{M^*} \right)^2 \quad (16)$$

It has been found empirically that, instead of equation (16), the experimental results can conveniently be represented by a function of the form:

$$\frac{h_1^*}{Y_n} = \frac{Y_1}{Y_n} - 1 = f \left(\frac{F_n}{M^*} \right)^2$$

where h_1^* is the backwater superelevation.

Experimental results for the orifice flow have yielded the following relation (see Chapter VII)

$$\frac{Y_1}{Y_n} = 1 + 1.18 \left[\left(\frac{F_n}{M^*} \right)^2 \right]^{0.90} \quad (17)$$

or

$$\frac{Y_1}{Y_n} = 1 + 1.18 \left(\frac{F_n}{M^*} \right)^{1.60} \quad (18)$$

The experimental result for the backwater ratio equation for free surface was developed by P. F. Biery^L and found to yield the relation

$$\frac{Y_1}{Y_n} = 1 + 0.47 \left[\left(\frac{F_n}{M^*} \right)^{2/3} \right]^{3.39} \quad (19)$$

or

$$\frac{Y_1}{Y_n} = 1 + 0.47 \left(\frac{F_n}{M^*} \right)^{2.26} \quad (20)$$

Dimensionless Equation for Orifice Type Flow

When the approach velocity to the constriction is neglected, orifice type flow is a good approximation to the flow condition

existing through a fully submerged arch bridge. In all the tests performed on the submerged bridge openings the approach velocity was very low relative to the velocity in the discharge jet, and the assumption appears to be safe. The rate of flow through a submerged semi-circle type bridge opening can thus be written as follows (ref. Figures 2 and 5):

$$Q = C_d \frac{1}{2} \frac{\pi d^2}{4} \sqrt{2g Y_1} \quad (21)$$

where

Q = discharge through the opening

d = diameter of the opening

and

Y_1 = the depth of the backwater

C_d = coefficient of discharge for type of inlet

Now rearranging equation (21):

$$\frac{Q^2}{g d^4} = \frac{C_d^2 \pi^2}{32} Y_1 \quad (22)$$

By dividing by d , and taking the square root of both sides of (22), the following dimensionless equation is obtained

$$\frac{Q}{g^{\frac{1}{2}} d^{5/2}} = \frac{C_d \pi}{\sqrt{32}} \left(\frac{Y_1}{d} \right)^{\frac{1}{2}} \quad (23)$$

where $\frac{C_d \pi}{\sqrt{32}}$ is a constant.

The previous equation may be written in the general form

$$\frac{Q}{g^{1/2} d^{5/2}} = f \left(\frac{Y_1}{d} \right) \quad (24)$$

Which is used in plotting experimental results

Head Loss Due to Bridge Constriction

An equation for the head loss due to the constriction effect may be derived from an energy equation written between the section, 1, of maximum depth and section 4 where the flow has regained its normal depth. With reference to Figure 2.

$$S_o L_{1-4} + Y_1 + \alpha_1 \frac{V_1^2}{2g} = Y_4 + \alpha_4 \frac{V_4^2}{2g} + E_{1-4} \quad (28)$$

where S_o = slope of channel bottom

L_{1-4} = distance between sections 1 and 4

Y_1 and Y_4 = water depth of sections 1 and 4 respectively

V_1 and V_4 = mean velocity at sections 1 and 4

α_1 and α_4 are the respective kinetic energy coefficients

hence $S_o L_{1-4}$ = the difference in bottom elevation between the two sections

and E_{1-4} = the total head loss between sections 1 and 4.

The energy loss between sections 1 and 4 may be considered to be made up of two parts:

- (a) The head loss that would exist if uniform flow existed between these sections, which would be equal to the change in elevation between these two sections as in

uniform flow the gravity forces exactly balance the resistance forces.

- (b) The additional head loss due to the non-uniformity of the flow: namely the combined effect of the contraction, separation and expansion of the flow as it passes through the constriction. The total head loss may be written as:

$$E_{1-4} = h_{f1} + h_{f2} \quad (29)$$

where h_{f1} is the head loss in the unobstructed channel and hence equation 29 becomes

$$E_{1-4} = S_o L_{1-4} + h_{f2}$$

It has been suggested by C. Izzard (24) that h_f can be expressed as a function of the velocity head in the opening

$$h_f = K \frac{V_o^2}{2g} \quad (31)$$

where

$$V_o = \frac{Q}{A_o}$$

K is the additional head loss coefficient due to the bridge constriction. Now equation 28 simplifies to:

$$Y_1 - Y_4 = \alpha_4 \frac{V_4^2}{2g} - \alpha_1 \frac{V_1^2}{2g} + K \frac{V_o^2}{2g} \quad (32)$$

setting $Y_1 - Y_4 = h_1^*$ and rewritten equation 32 gives

$$h_1^* = K \frac{V_o^2}{2g} + \left[\alpha_4 \left(\frac{V_4}{V_o} \right)^2 - \alpha_1 \left(\frac{V_1}{V_o} \right)^2 \right] \frac{V_o^2}{2g} \quad (33)$$

α_4 and α_1 can be assumed to be equal, and by using the relationship

between the velocities and areas, equation. 33 can be written:

$$h_1^* = K \frac{V_o^2}{2g} + \alpha \left[\left(\frac{A_o}{A_4} \right)^2 - \left(\frac{A_o}{A_1} \right)^2 \right] \frac{V_o^2}{2g} \quad (34)$$

Divide by $\frac{V_o^2}{2g}$ and solve equation 34 w.r.t. K gives an equation for the additional head loss coefficient due to the bridge constriction, for submerged conditions.

$$K = \frac{h_1^*}{V_o^2/2g} - \alpha \left[\left(\frac{A_o}{A_4} \right)^2 - \left(\frac{A_o}{A_1} \right)^2 \right] \quad (35)$$

The ratio $\frac{A_o}{A_4}$ is the same as $\frac{A_o}{A_n}$ (ref. figure 2) and hence equal to the channel opening ratio M' .

CHAPTER IV

EXPERIMENTAL APPARATUS

Flume

All tests were performed in a tilting flume 5 feet wide, 2 feet deep and 64 feet long. The flume was made of welded steel plates coated with an epoxy resin paint. Six screw jacks, three on each side, placed underneath the flume made it possible to set the flume bed to any desired slope with an accuracy of ± 0.000025 feet/feet. Each pair of jacks had a different gear ratio and was placed in such a way that 96 turns of a common drive shaft, connected to an electric motor, would raise the flume 1, 2, and 3 inches respectively, the upstream pair of jacks raising 1 inch. The electric motor was operated by three switch buttons - raise, lower and stop. A revolution counter, calibrated to indicate the slope, made it possible to adjust the flume to the proper slope within minutes. Figure 6 shows a plan view of the jacks and gears and Figure 7 shows jack detail.

At the upstream end the flume was hinged to a forebay consisting of an 8 foot by 10 foot headbox lined with sheet metal. To assure a smooth flow condition from the headbox into the flume, the box was equipped with a stone baffle, several screens and a smooth elliptical transition into the flume.

At the discharge end of the flume an adjustable weir type tailgate provided control of the depth of the flow. It could be raised

or lowered by means of a calibrated wheel (4 turns per inch).

Figure 8 shows tailgate construction. A catchment box eliminated any splash as the flume discharged the water over the tailgate and into the sump. For a more complete description of the testing flume see reference 2. Figure 9 shows apparatus arrangement.

Water Supply and Measurement System

A recirculating sump provided the water to the flume by means of two centrifugal pumps of capacity 2000 GPM and 300 GPM. These fed the headbox through a 6 inch and a 3 inch pipeline. The flow was measured by two venturi meters connected to a 30 inch manometer filled with mercury, (Sp. Gr. 13.6) for the 6 inch line from the 2000 GPM pump, and to a 60 inch manometer filled with tetrabromoethane (Sp. Gr. 2.95), for the 3 inch line and 300 GPM pump.

The calibration of the venturi meters were done by means of a concrete side channel and a large weighing tank. The flow through the pipelines was controlled by gate valves. Calibration charts were made for both venturi meters. (Figures 10 and 11 calibration charts for 6" and 3" pipes). The manometers were placed close to the flow controlling valves so their deflections were easily visible when adjusting the valves.

To eliminate undesirable surface waves which reflected back and forth in the upper part of the flume, a skimming board was placed at the entrance in the flume.

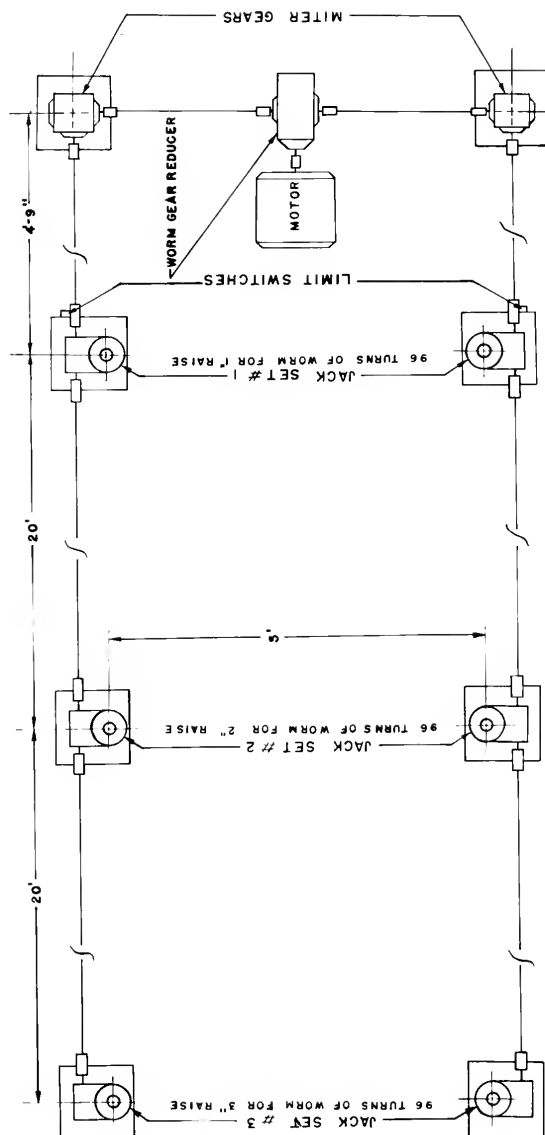


FIG 6 PLAN VIEW OF JACKS AND GEARS

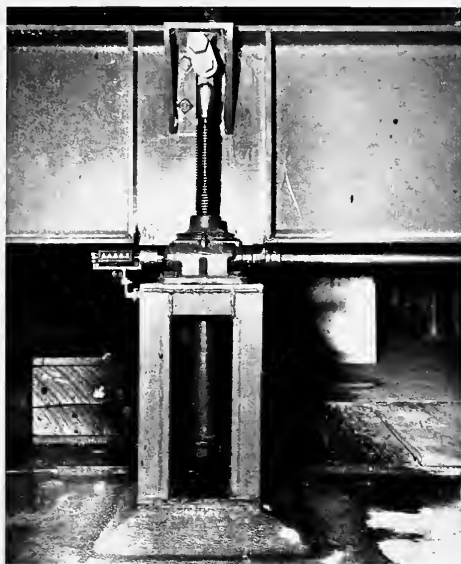


FIG 7 JACK DETAIL



FIG 8 TAIL GATE CONSTRUCTION

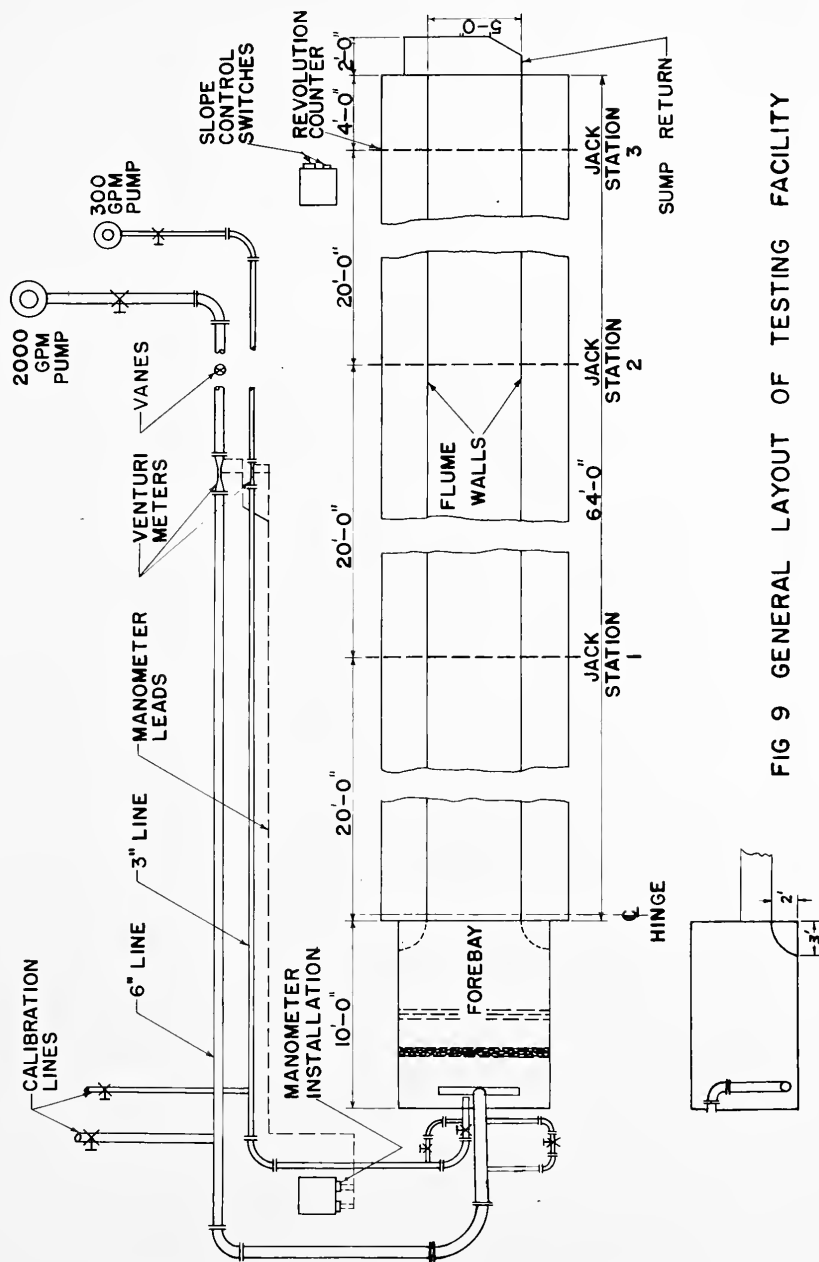


FIG 9 GENERAL LAYOUT OF TESTING FACILITY

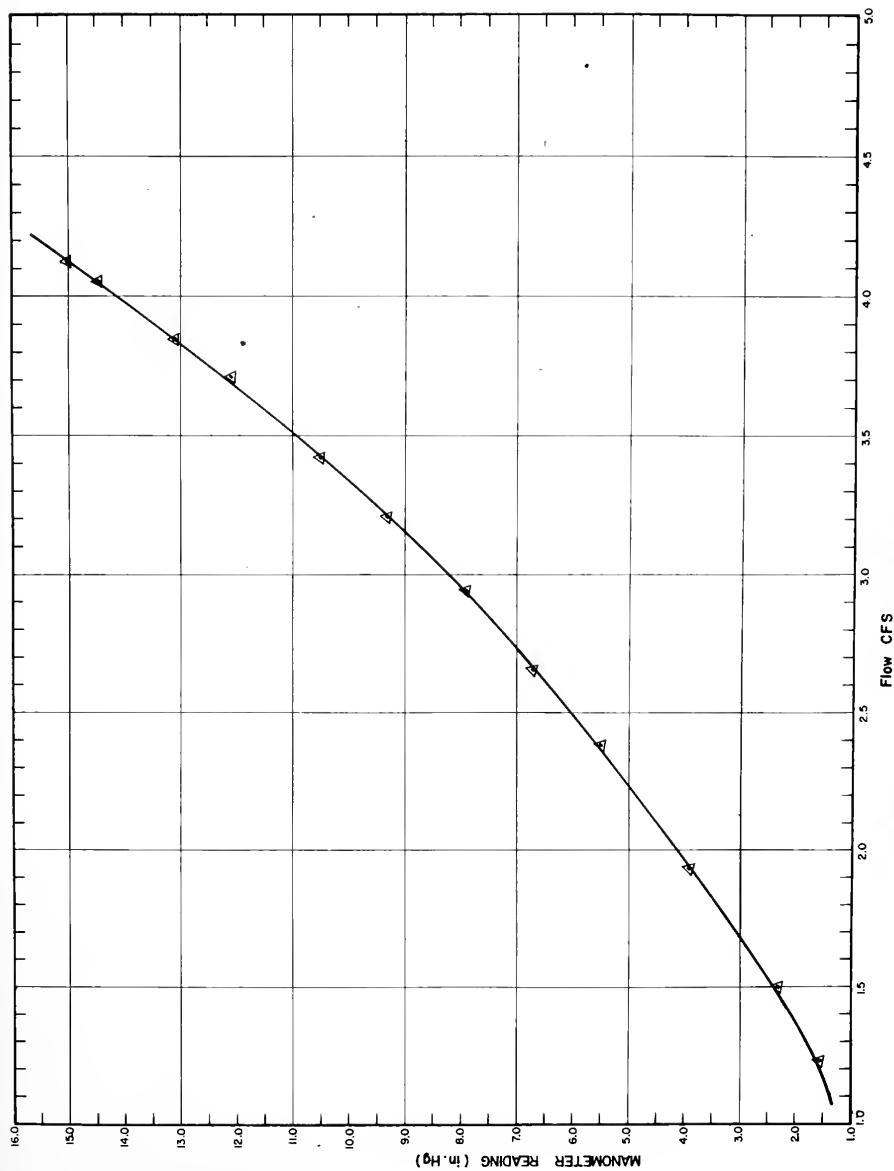
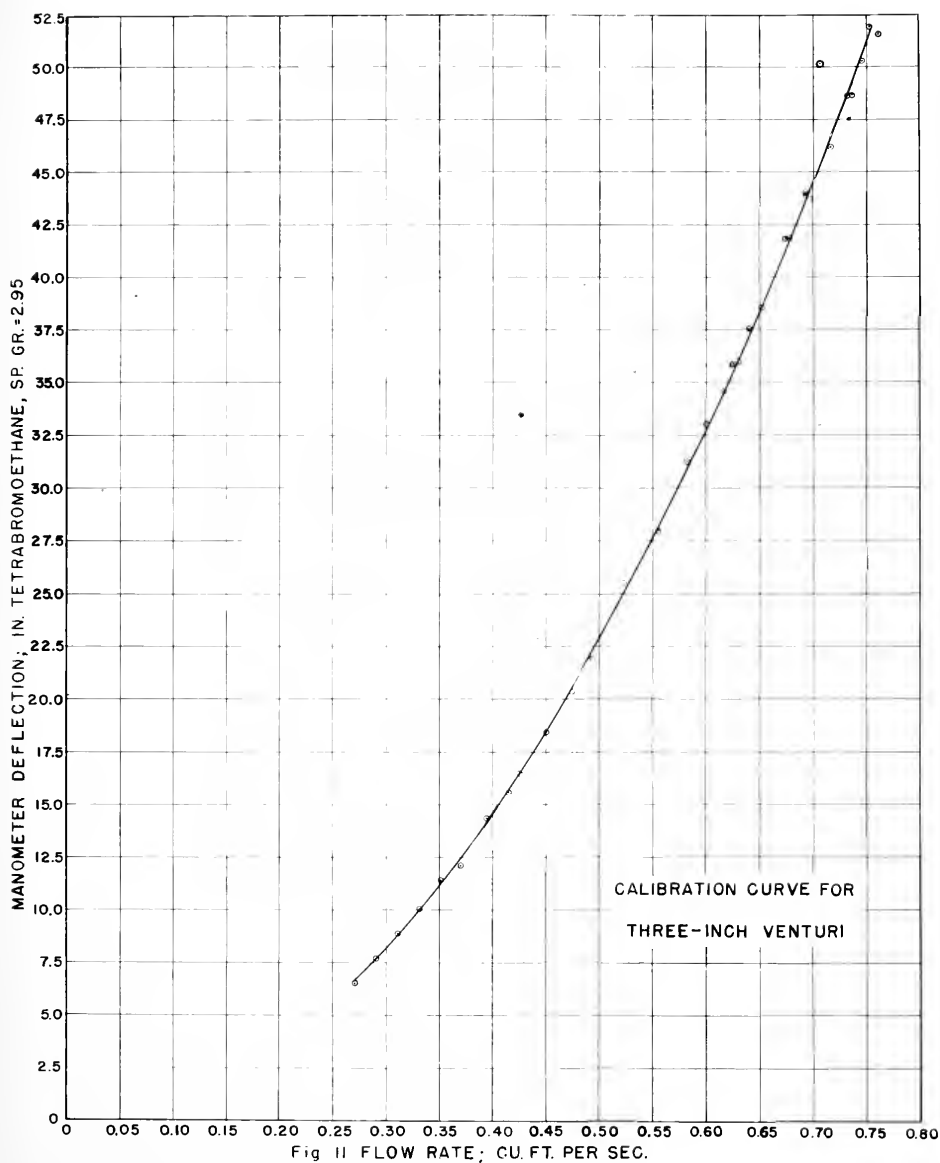


FIG. 10 CALIBRATION CURVE FOR 6" VENTURIMETER



Test Station

To be able to change models while the water was running, to put the models into the flow at the particular station - at a particular angle - was essential in order to secure uniform conditions at the testing section in the flume. This problem was solved by the use of two 1" x 1" x 18" angle irons. They were bolted to the sidewalls of the flume in such a way that they easily could be removed when calibration of the normal flow depth had to be done. Figure 12 shows the test section with a model in place. Each angle iron had two holes where bolts leading through the model could be fastened.

To change models, the four bolts holding the model were loosened and the model was lifted out. The new model was slid down behind the angle irons into a perfect position at the test station and the bolts were tightened to hold it in place.

Measuring Equipment

Instrument Carriage

An aluminum instrument carriage, mounted on two stainless steel guide rails running the length of the flume, was installed so that the bottom of the flume could serve as a reference plane. The four wheels of the carriage were grooved to give a precision fit on the rails. One of the wheels had a set screw to keep the carriage from moving when an experiment was conducted. A surveyors tape was mounted along the whole length of the flume and an indicating point on the carriage served as a reference point for all longitudinal measurements. Another surveyors tape was installed in the transverse direction of

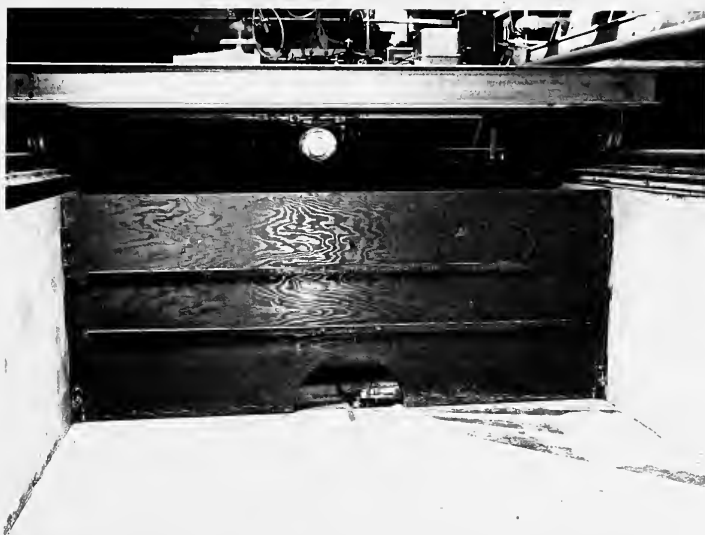


FIG. 12a TEST SECTION



FIG. 12b TEST SECTION DETAIL

the flume on a grooved rail of the instrument carriage. This rail served as a guide for the slide on which a point gage and a Prandtl tube were mounted. This slide also had an indicating point serving as reference point for transverse measurements. By means of these two tapes any point in the flume could be located in the horizontal plane. The instrument carriage was also equipped with a florescent lamp, several electrical outlets and a wide $3/4$ inch plywood strip on one side to serve as a desk for notekeeping etc. The carriage could easily be moved to any location along the flume and locked in a specific position with an accuracy of 0.005 ft. (Figure 13 shows a top view of the carriage.)

Point Gage

All water surface elevation measurements were obtained by means of an electric indicating point gage. It was mounted on the instrument carriage slide. This could be positioned with an accuracy of ± 0.002 ft. in the transverse direction of the flume. The staff of the pointgage was marked in millimeters and was equipped with a vernier which allowed a reading accuracy of ± 0.05 mm in the vertical direction. The accuracy of the water surface elevation measurements varied between 0.1 mm to 2.0 mm depending on the smoothness of the free surface.

The procedure used when the free surface was not smooth was to observe the time intervals of the blinking light of the point gage. The light is on when the measuring point is at or below the water surface. When the light was blinking on and off with equal time intervals, that is the measuring point was in and out of the water

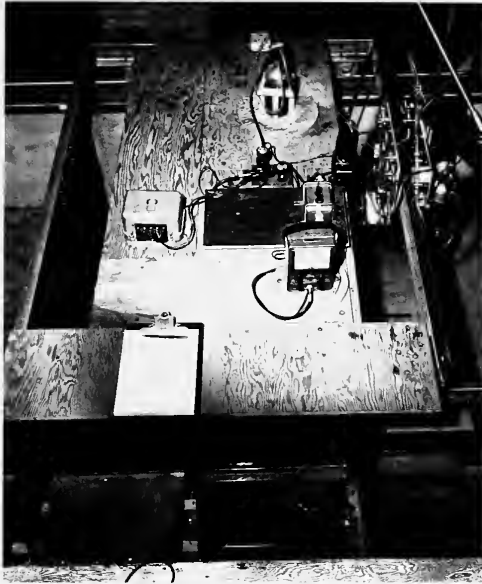


FIG. 13 TOP VIEW OF INSTRUMENT CARRIAGE

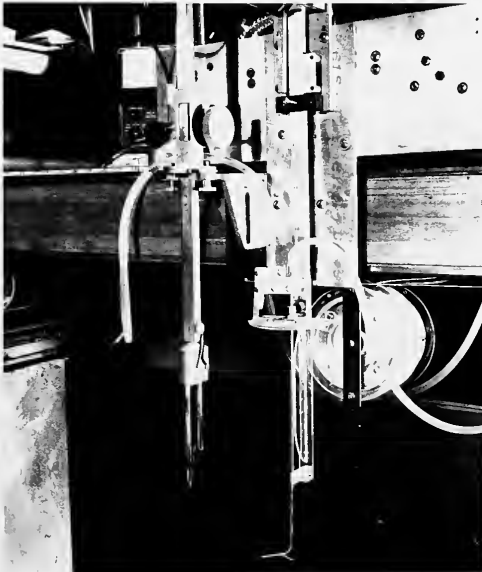


FIG. 14 POINT GAGE AND PRANDTL TUBE

for an equal duration, the reading of the vernier was recorded.

Prandtl Tube

The flow velocity measurements were obtained by means of a $1/8"$ O.D. Prandtl tube of standard design. The Prandtl tube was mounted on a vertical staff which was marked in 0.2 cm and had a vernier allowing a vertical positioning within ± 0.01 cm of accuracy. A set screw prevented the position to change during test measurements. The support of the Prandtl tube permitted, in addition to vertical and traverse motions, a rotation so that the horizontal portion of the probe could be aligned according to the direction of the flow indicated by a freely swinging stiffened tuft attached to the tube. Figure 14 shows point gage and Prandtl tube. The amount of rotation was measured as an angle by means of an indicator sliding along a fixed protractor.

Since the tip of the Prandtl tube could be aligned with the streamline direction in the horizontal plane only, the question arose as to the reliability of the measured velocity whenever it had a vertical component. In order to establish the directional sensitivity of the prandtl tube, a series of velocity measurements were taken varying the angle, γ , between tip of the Prandtl tube and the direction of a uniform flow. It was established that the velocity reading was within about 3% accuracy when the tip of the Prandtl tube was directed within 17° of the flow direction. Figure 15 shows graph of directional sensitivity of Prandtl tube.

Variable-Reluctance Pressure Transducers

The small magnitude of the pressure differentials to be measured

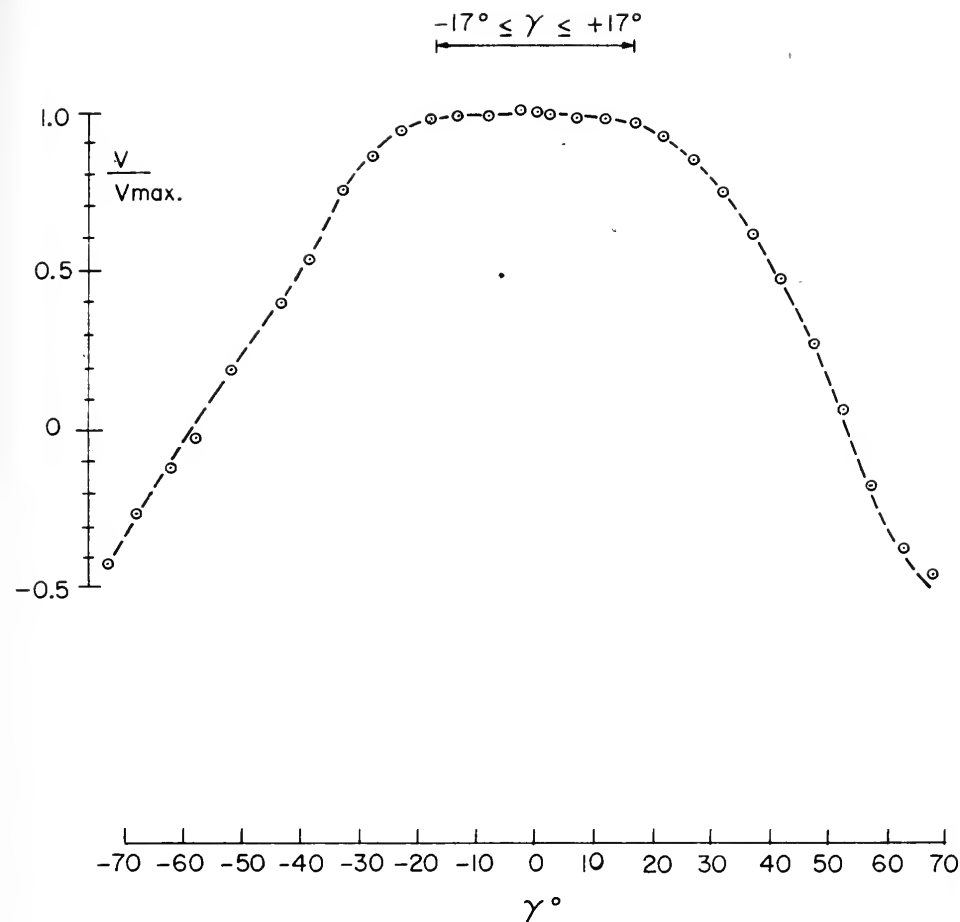


FIGURE 15 ACCURACY OF VELOCITY READINGS AS
A FUNCTION OF ANGLE OF ATTACK

with the Pradtl tube made it necessary to employ a Variable-Reluctance Differential Pressure Transducer (model P7D, Pace Eng. Comp.) instead of the conventional liquid manometer. In the low velocity regions a pressure transducer having a range of ± 0.1 psid. was used. In the higher velocity regions - as in the discharge jet of the models - a range at ± 0.5 psid. was needed.

The range of the pressure transducer was varied by changing diaphragm (membrane) in the pressure cell. Figure 16 shows sketch of velocity pressure transducer system. The thickness of the diaphragm governs the pressure range; thicker diaphragm are used for larger differential pressure ranges. The leads from the static and stagnation points on the Prandtl tube, filled with Meriam No. D-2930 fluid of controlled specific weight (sp. gr. 1.00) and low surface tension, were connected to each side of the transducer diaphragm. In order to prevent fluctuation of the flow to influence the pressure differential and hence the voltmeter reading, the leads contained coiled lengths of tubing - giving reservoir action. Shorter pieces of leads with much smaller diameter were also introduced to help dampen the pressure fluctuations.

The principle of operation of the diaphragm type variable-reluctance pressure transducer is as follows:

A diaphragm of magnetically-permeable material, supported between two symmetrical E core inductance assemblies, Figure 17, completed a magnetic circuit with each E core. The diagram deflected when there was a difference in pressure between the two input lines. This increased the gap in the magnetic flux path of one core, and decreased the gap equally in the other.

The magnetic reluctance varied with the gap, determining the

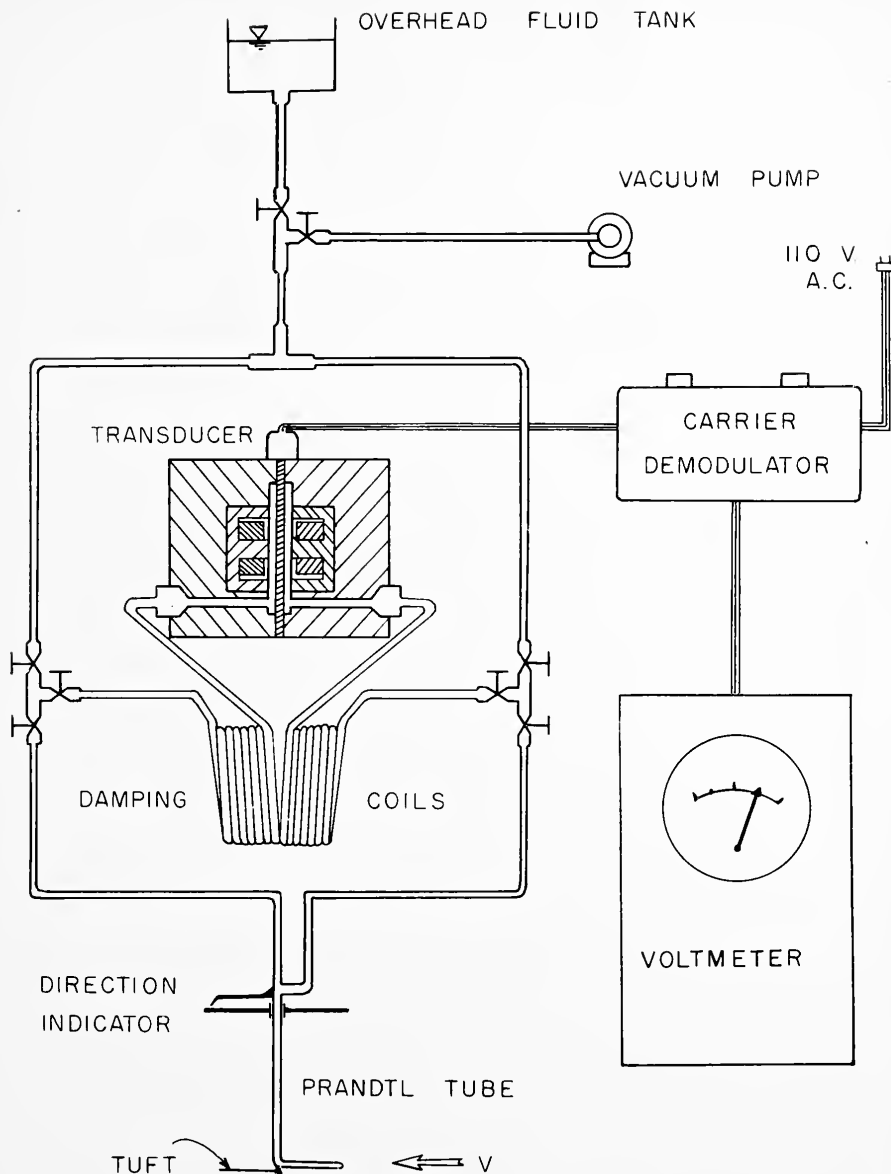


FIGURE 16 VELOCITY TRANSDUCER SYSTEM

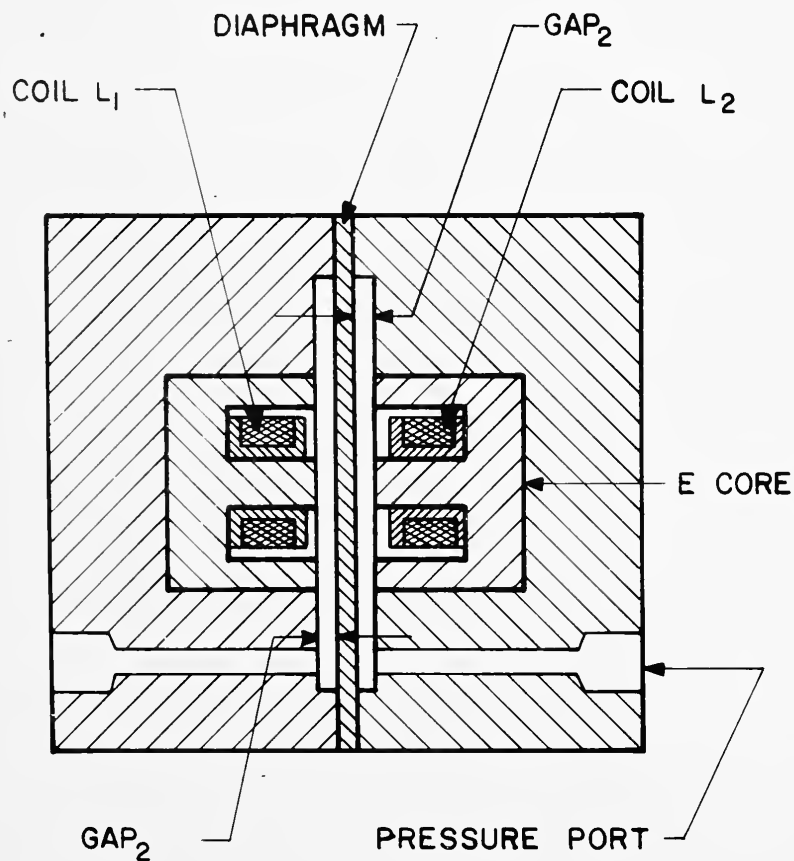


FIG.17 DIAPHRAGM-TYPE VARIABLE-RELUCTANCE
PRESSURE TRANSDUCER

inductance value, so that the over-all effect of diaphragm motion resulted in a change in inductance of two coils L_1 and L_2 . The inductance ratio L_1/L_2 was conveniently measured in a bridge circuit

which produced an output voltage proportional to the pressure difference.

Between the Pressure Transducer and the voltmeter a Carrier-Demodulator (model CD10, Pace Eng. Comp.) provided a carrier excitation of 3000 cps. (Figure 18 Carrier-Demodulator). It was operated from the 115V60Cy line. The span control knob provided a scale adjustment and the zero control knob set the voltage output corresponding to zero pressure difference.

A Junior Volt Ohmyst Voltmeter (model WV-77A, RCA) was used. This also had zero setting and five scale adjustments besides a + and - volt selector switch. The voltmeter was placed on a rotating disk to obtain a flexible position for the reader, who had to read the instrument from several different positions during calibrations and testing.

Three diaphragms were available which could be used for pressure differential measurements up to 0.1, 0.5 and 1.0 psi. A diagram was prepared for the selection of the proper diaphragm for a given velocity range. The velocity is related to the pressure differential by the equation

$$V = \sqrt{2g \Delta p / r}$$

where Δp is the pressure differential measured between the dynamic and static openings of the Prandtl tube. The pressure differential was plotted vs. the velocity on Figure 19, where the range of the several diaphragms were indicated.

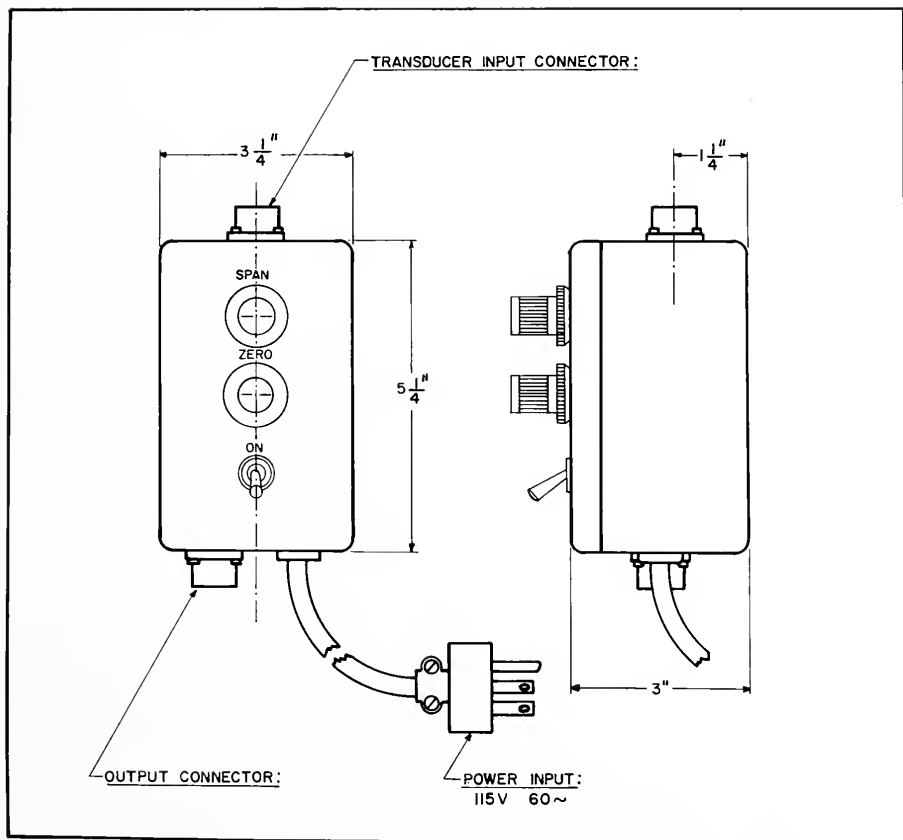


FIG 18 CARRIER — DEMODULATOR

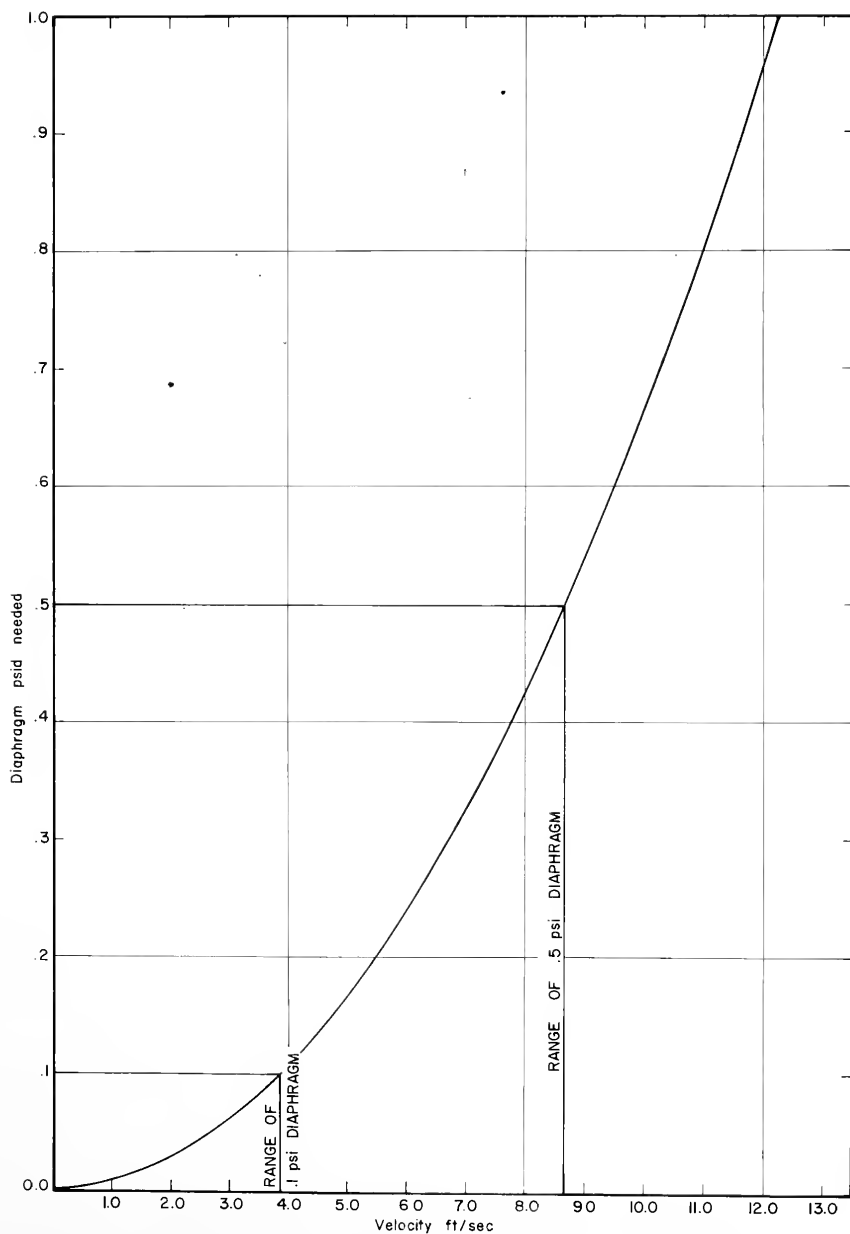


FIG 19 DIAGRAM FOR SELECTION OF DIAPHRAGM IN TRANSDUCER

Calibration of Velocity Probe

By using the relation between the dynamic and static head

$\frac{V^2}{2g} = h$ (where V is velocity in fps., h is feet of water and g is the acceleration of gravity) a static calibration could be performed.

Two reservoirs were connected to the stagnation and static openings of the Prandtl tube respectively. The reservoirs were connected through a valve. A datum level was measured by an electric point gage when the connecting valve was open, and the voltmeter needle was adjusted to the zero mark. The pressure was then equal on both sides of the diaphragm in the pressure transducer. The valve connecting the reservoirs was closed and distilled water was added to increase the level in the reservoir connected to the stagnation opening. The water level was recorded for even increments in the voltmeter reading. Figures 20 and 21 show the calibration setup. By means of a least square subroutine of an electronic computer (see Appendix C) the relation between the output voltage and velocity was determined from the measured pairs. This relation was found to be a constant, C , and the velocity was found from the expression

$$V \text{ (fps.)} = C\sqrt{\text{Volt.}}$$

A new calibration test had to be made each time the diaphragm was changed. Repeated calibrations without changing the diaphragm gave the same calibration curve. Typical calibration curves for probe are shown in Figure 22 where velocity versus voltage are plotted. During the experiments it was necessary to measure both high and low velocities. To omit the timeconsuming process of calibration, two individual pressure transducers were used with a range of 0.5 psid.

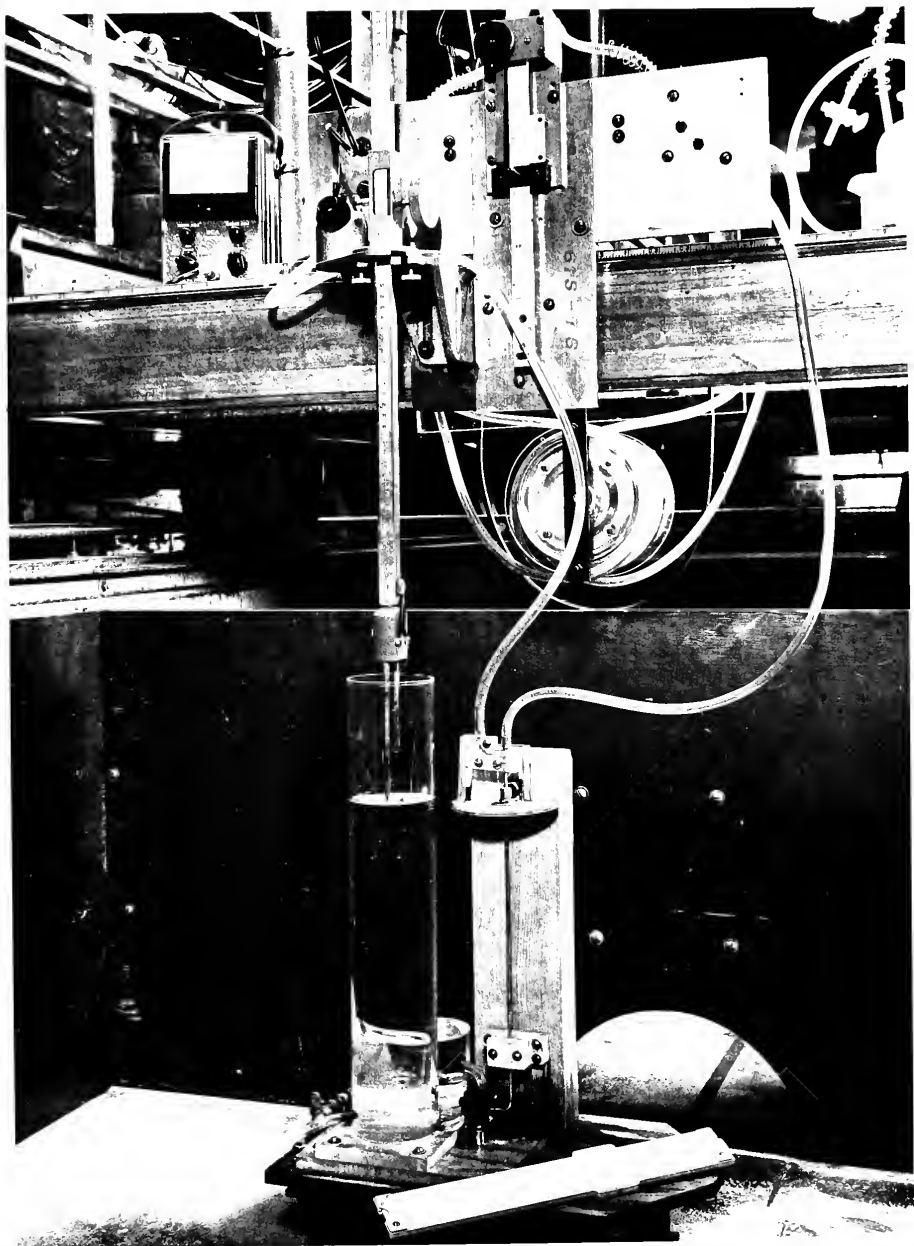


FIG 20 CALIBRATION APPARATUS FOR PRANDTL TUBE

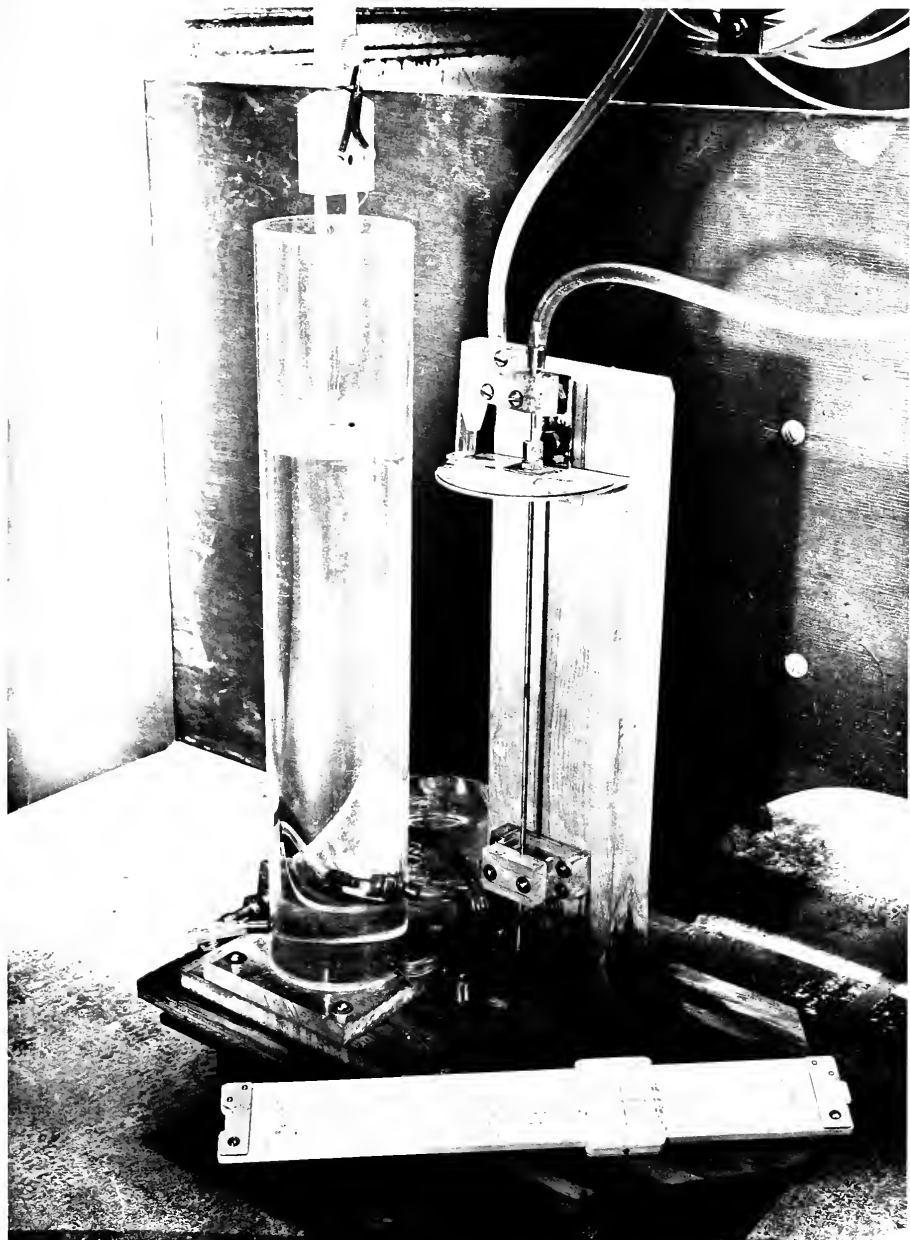


FIG 21 DETAIL OF CALIBRATION APPARATUS

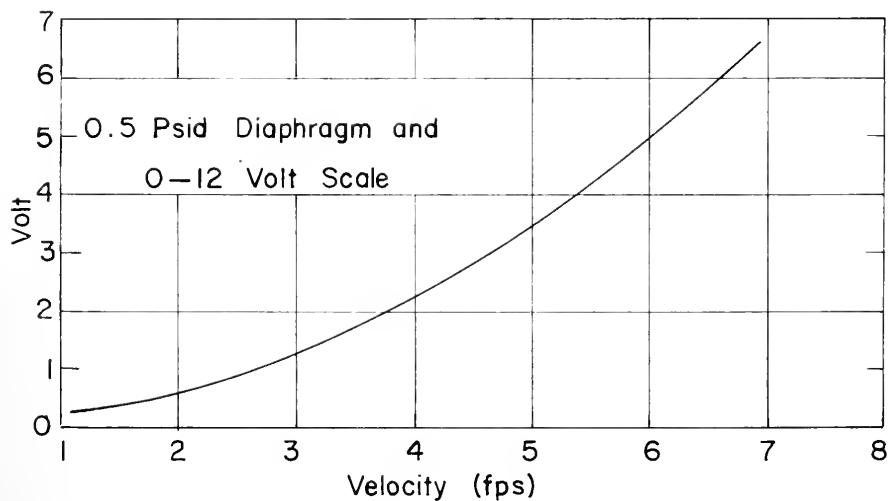
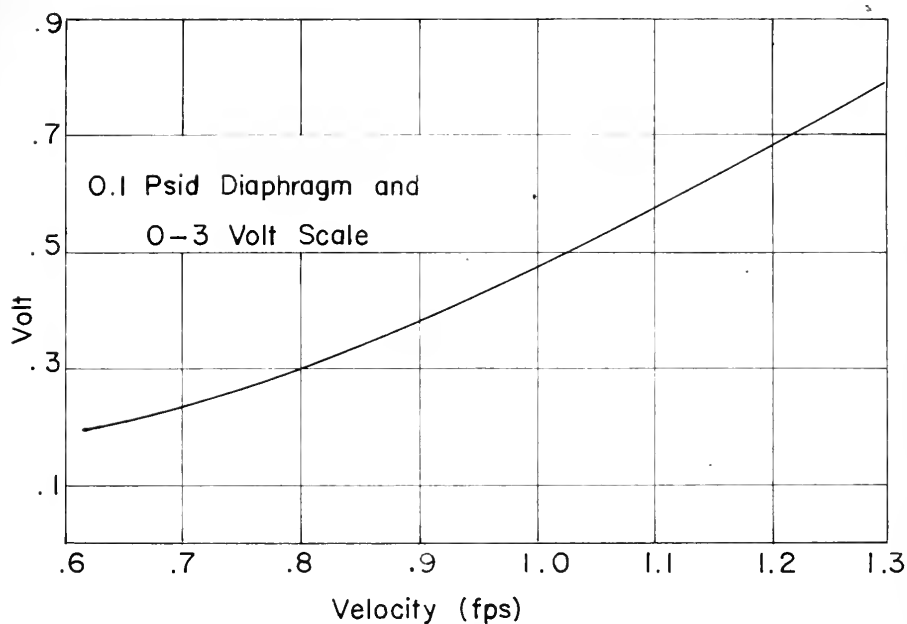


Fig 22 Typical Calibration Curves for Probe

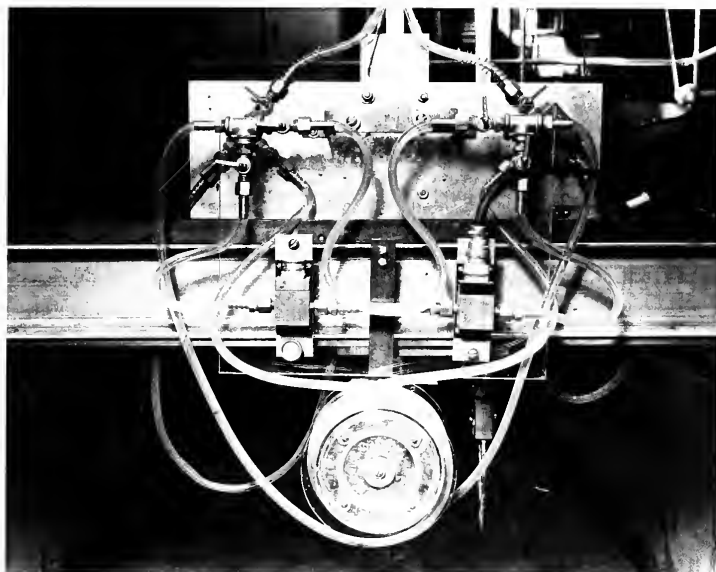
and 0.1 psid. respectively. They were mounted on a lucite plate in such a way that one could switch from one to the other in a matter of seconds. The lucite plate was mounted on the slide of the instrument carriage as shown in Figure 23, which also shows the change in position of the valves as one or the other pressure transducer was in use.

Procedure for Measuring of the Velocity

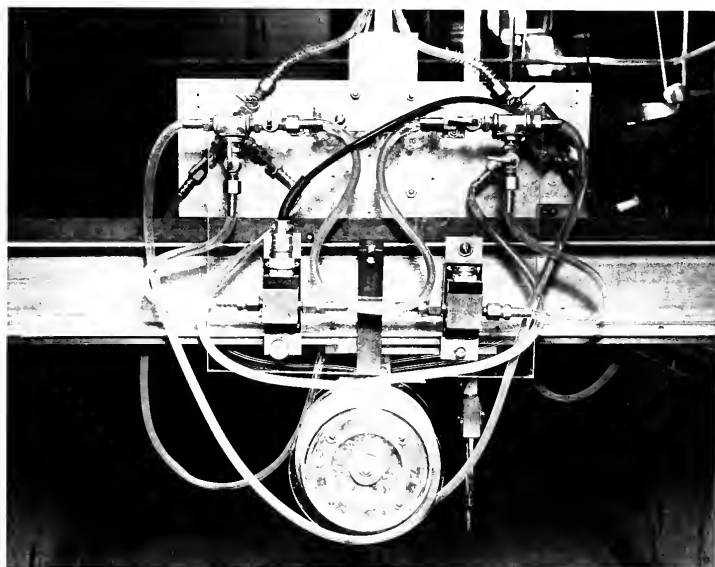
After checking that no air was trapped in the pressure leads, equal pressure was applied on both sides of the diaphragm by connecting both leads to the same reservoir. Then the voltmeter needle was adjusted to zero on the proper scale needed for the expected velocity range in the experiment. The valves to the equal pressure reservoir were closed, the Prandtl tube was inserted into the flow and the cap covering the stagnation and static openings was removed. Now the valves connecting the stagnation and static pressure tubes with the pressure transducer were opened to introduce the pressure difference upon the diaphragm and thus make a change in the output voltage. The Prandtl tube was placed in the desired position and the voltmeter reading was recorded.

After the test measurements were taken, the instruments were again checked against the equal pressure reservoir to see that the voltmeter read zero for the same pressure on both sides of the diaphragm.

The calibration apparatus and the technique of the use of the pressure transducer for velocity measurement were developed by A. A. Sooky as part of another research project.



RIGHT CELL CONNECTED FOR HIGH VELOCITY MEASUREMENT



LEFT CELL CONNECTED FOR LOW VELOCITY MEASUREMENT

FIG. 23 PRESSURE CELLS

CHAPTER V

DEFINITION OF TEST GEOMETRIES - SELECTION OF TESTS

Nine independent variables were considered in the dimensional analysis to determine the dependent variable Y_1/Y_n . Of these nine variables, seven describe different types of constriction geometries, the other two, the Froude number and the contraction ratio describe the flow field and the amount of contraction. These seven geometric variables were used to define seven types of geometries that were tested separately. These types of geometries are defined below.

Geometry I-aTwo-Dimensional Semicircle Arch Bridge Constrictions:

(Figure 24) The characteristics of this type of geometry are the following:

- a) Since the model is two-dimensional, $\frac{L}{b} = 0$
- b) Single bridge case, $L_d = 0$ and $\frac{bL_d}{A_{n2}} = 0$
- c) No wingwalls, according to definition of ϕ_1 , $\phi_1 = 90^\circ$
- d) None-skew case, according to definition of ϕ_2 , $\phi_2 = 0^\circ$
- e) Semicircular case, $d = 0$ and $\beta = \frac{d'}{r} = 0$
- f) One span case, $N = 1$
- g) No eccentricity, $e = 0$

h) Froude number, $F_n = \frac{V_n}{(gy_n)^{\frac{1}{2}}}$ designated as an independent variable.

i) Constriction opening ratio M' , designated as an independent channel opening ratio M'

Hence, seven independent descriptive variables, $\frac{L}{b}$, $\frac{bL_d}{A_{n2}}$, e , ϕ_1 , ϕ_2 , β and N in the dimensionless equation: (3).. $\frac{Y_1}{Y_n} = f(F_n, M', \frac{L}{b}, \frac{bL_d}{A_{n2}}, \phi_1, \phi_2, e, \beta, N)$ are designated as constants and we get the relation:

$$\frac{Y_1}{Y_n} = f(F_n, M')$$

Geometry I-b

Three-Dimensional Semicircular Arch Bridges:

This geometry differs from the previous one only in that L is varied, thus the parameter $\frac{L}{b}$ describing the length of the model in the direction of the flow is a variable and the dimensionless equation (3) for this case becomes

$$\frac{Y_1}{Y_n} = f(F_n, M', \frac{L}{b})$$

Geometry II

Dual Parallel Three-Dimensional Arch Bridge Constrictions:

This geometry consists of two identical bridges of geometry I-b, placed at a distance L_d apart, measured center to center. One new variable, L_d , is introduced, which is characterized by the parameter

$\frac{bL_d}{A_{n2}}$ (Note: For submerged bridge constrictions, $A_{n2} = A_0$, see Chapter

III). Equation (3) simplifies for this case to:

$$\frac{Y_1}{Y_n} = f \left(F_n, M', \frac{L}{b}, \frac{bL_d}{A_{n2}} \right)$$

However, in order to simplify the testing, the length ratio $\frac{L}{b}$ was limited to the case of $\frac{L}{b} = 0.25$, so that this quantity was a constant for the tests, and equation (3) reduces to:

$$\frac{Y_1}{Y_n} = f \left(F_n, M', \frac{bL_d}{A_{n2}} \right)$$

Geometry III

Three-Dimensional Arch Bridge Constriction with Wingwalls:

The geometric characteristics were as follows:

- | | |
|---|------------------------|
| a) $\frac{L}{b} = 0.25$ | e) $\beta = 0$ |
| b) $\frac{bL_d}{A_{n2}} = 0$ | f) $N = 1$ |
| c) ϕ_1 is a variable $\phi_1 = 90^\circ, 60^\circ, 45^\circ, \text{ or } 30^\circ$ | g) $e = 0$ |
| d) $\phi_2 = 0^\circ$ | h) F_n is a variable |
| i) M' is a variable | |

Hence, equation (3) can be simplified to:

$$\frac{Y_1}{Y_n} = f \left(F_n, M', \phi_1 \right)$$

Geometry IVTwo-Dimensional Semicircular Arch Bridge Constrictions with Eccentricity:

The geometric characteristics were as follows:

- | | | |
|------------------------------|-----------------------|------------------------|
| a) $\frac{L}{b} = 0$ | d) $\phi_2 = 0^\circ$ | g) e is a variable |
| b) $\frac{bL_d}{A_{n2}} = 0$ | e) $\beta = 0$ | h) F_n is a variable |
| c) $\phi_1 = 90^\circ$ | f) $N = 1$ | i) M' is a variable |

And the equation (3) can be reduced to:

$$\frac{Y_1}{Y_n} = f(F_n, M', e)$$

Geometry V-aTwo-Dimensional Semicircular Arch Bridge Constrictions With Skew:

The geometric characteristics were as follows:

- | | | |
|------------------------------|---------------------------|------------------------|
| a) $\frac{L}{b} = 0$ | d) ϕ_2 is a variable | g) $e = 0$ |
| b) $\frac{bL_d}{A_{n2}} = 0$ | e) $\beta = 0$ | h) F_n is a variable |
| c) $\phi_1 = 90^\circ$ | f) $N = 1$ | i) M' is a variable |

And the equation (3) can be reduced to:

$$\frac{Y_1}{Y_n} = f(F_n, M', \phi_2)$$

Geometry V-bThree-Dimensional Semicircular Arch Bridge Constrictions With Skew:

This geometry is the same as the previous one, except that the length of the constriction is allowed to vary, the parameter $\frac{L}{b}$ is thus a variable and the dimensionless equation (3) can be simplified to:

$$\frac{Y_1}{Y_n} = f(F_n, M', \phi_2, \frac{L}{b})$$

Geometry VIThree-Dimensional Two-Span Semicircular Arch Bridge Constrictions:

The geometric characteristics were as follows:

- | | |
|------------------------------|----------------------------|
| a) $\frac{L}{b} = 0.50$ | f) $N = 2$, Two-span case |
| b) $\frac{bL_d}{A_{n2}} = 0$ | g) $e = 0$ |
| c) $\phi_1 = 90^\circ$ | h) F_n is a variable |
| d) $\phi_2 = 0^\circ$ | i) M' is a variable |
| e) $\beta = 0$ | j) $p = \frac{b}{10}$ |

The equation (3) can be reduced to:

$$\frac{Y_1}{Y_n} = f(F_n, M')$$

Geometry VIITwo-Dimensional Segment Arch Bridge Constrictions:

The geometric characteristics were as follows:

- | | |
|------------------------------|--------------------------|
| a) $\frac{L}{b} = 0$ | e) β is a variable |
| b) $\frac{bL_d}{A_{n2}} = 0$ | f) $N = 1$ |
| c) $\phi_1 = 90^\circ$ | g) $e = 0$ |
| d) $\phi_2 = 0^\circ$ | h) F_n is a variable |
| i) M' is a variable | |

Hence, equation (3) reduces to:

$$\frac{Y_1}{Y_n} = f(F_n, M', \beta)$$

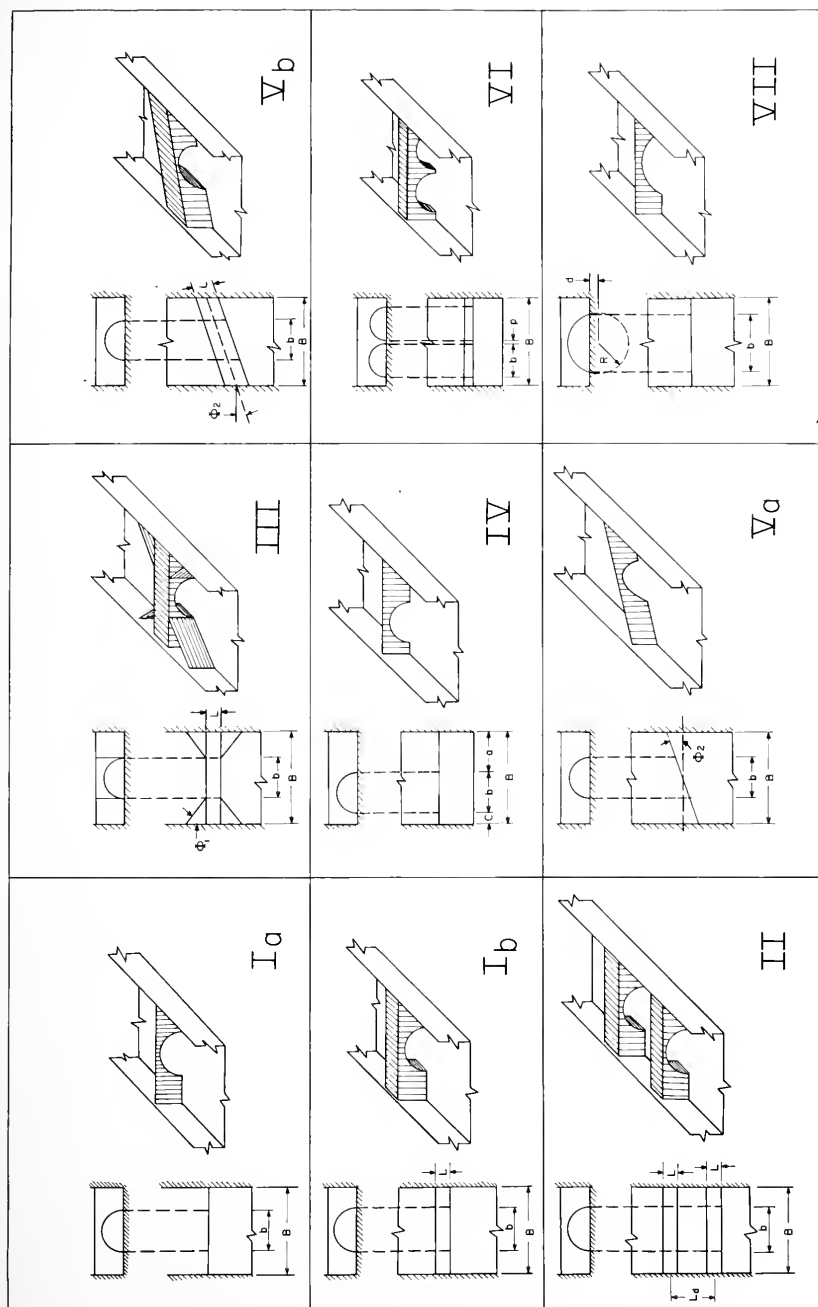


FIGURE 24 DEFINITION SKETCHES OF TEST GEOMETRIES

Submerged Test Geometries:

The test geometries defined and sketched in the previous section give an overall picture of the variety of models that were considered in the arch bridge testing program. Only five of these geometries were tested for submergence. (See Introduction, for background of model selection)

Geometry I-a was selected to be tested first. This two-dimensional geometry was the simplest possible arch model. It was tested in the smooth channel to give some basic information on the velocity distribution and on the coefficients of contraction, of velocity and of discharge. It also served as a guide for further investigation on the more complicated constrictions.

The three dimensional geometry I-b was the next step. These models were also tested in the smooth boundary channel and the results are presented in non-dimensional form. After the exploration of the test range was completed, and a suitable way of analyzing the data was found, the flume boundaries were changed from smooth to rough.

Roughness

The rough boundary was obtained by placing $\frac{1}{4}$ inch aluminum rods along the flume bottom and side walls. Along the bottom a layer of longitudinal bars were placed 12 inches on center and a top layer of transverse bars 6 inches on center. Along the side walls one layer of vertical bars 6 inches on center was placed $\frac{1}{4}$ inch from the wall. The bottom layer of bars were tied together with wire. The vertical bars were tied at the bottom to the transverse bars and clamped to

the walls above the free surface. Figure 1 shows the roughness bars placed in the flume. The roughness was calibrated and Mannings roughness coefficient, n , was found. The average Mannings $n = 0.0238$, as found by Biery (4), was verified and used for the rough boundaries. For a more detailed description of the rough boundary pattern and the calibration calculations done, see reference (20). "Roughness spacing in Rigid Open Channels".

Geometries I-a and I-b were tested for the rough boundary condition. The results indicated that a similar procedure could be followed in testing of other geometries. A suitable range for the relative length, $\frac{L}{b}$, was decided upon for the future models. The channel width ratio, M , had to be chosen so that submergence could be obtained for the available flow. All these variables were selected from the data obtained from the testing of geometries I-a and I-b, and by observation of the submerged flow behavior.

Besides the four models made for geometry I-a and twelve models made for geometry I-b, six models were made for geometry V-a, three models for geometry VI and four models for geometry VII. Figure 25 shows the models that were tested under submerged conditions. The tables (I - VII) show the tests performed on each geometry for submergence.

Construction of Models

The two dimensional models were made from $3/4$ " thick marine plywood and painted to keep them from rotting. Due to the high pressure exerted by the backwater, the models were stiffened by mounting two angle irons on the downstream face of each model as shown in

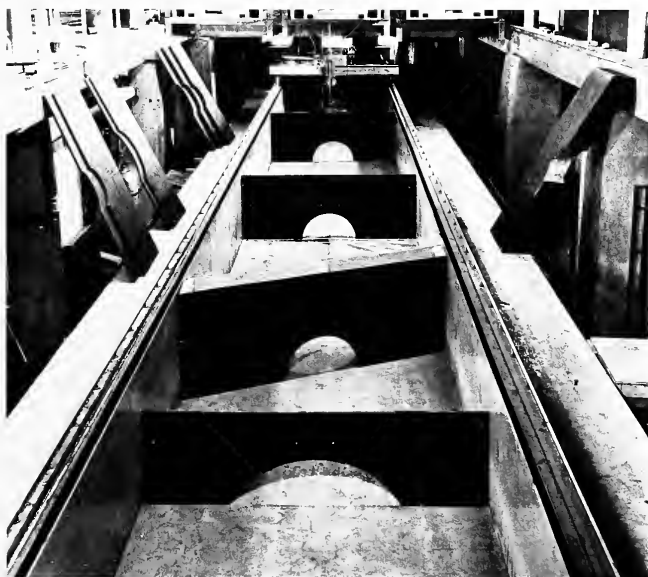


FIG. 25 TESTING MODELS

Figure 12, detail at test section. Holes for fastening purposes were made along the vertical sides of the model.

The three dimensional models were made from $3/8$ " thick exterior plywood. These models were braced from the inside by 2" x 4" studs. The plywood pieces making up a model were glued together to prevent leakage of water into the model. The three-dimensional openings were lined with sheet metal. A special DAP Architectural Grade Caulking compound that could adhere readily to both wood and sheet metal was used as seal around the model openings. The models were also painted to prevent the plywood from rotting.

Selection of Variables

The 29 selected models were to be tested in the 64 foot long flume, first with smooth and then with rough boundaries. The large number of variables involved made it necessary to establish a systematic procedure for selecting the quantities allowed to vary and those held constant in the several tests so that the possible range of the variables could be covered uniformly and completely. This was of concern because the range of discharges and slopes for which submergence could be attained was very limited and each test was time consuming. The procedure followed to solve this problem was based on the theoretical analysis and on the testing of simple geometries. The theoretical analysis had resulted in a dimensionless equation (24), that could be interpreted to prevent the grouping of the data. The testing of simple geometries also gave the possible range of the key variables: discharge, slope and opening ratio.

Preliminary test runs had given information about the channel opening ratios, $M = b/B$, which could be submerged with the available flow in the laboratory. Testing of the simple geometry I-a with the selected channel opening ratios gave the flow rates necessary for each model to have submergence. Now, by interpreting the dimensionless equation (24) the ordinates of the plotting points on the graphs could be computed for the several flow rates of the respective channel opening ratios chosen. A table was made containing these ordinates for five discharges' and the opening width representing the five channel widths ratios to be investigated. The dimensionless ordinate axis was found to be:

$$\frac{Q}{g^{1/2} b^{5/2}}$$

by substituting the different values of Q (cfs) and b (ft), g being constant, the following table was obtained for the ordinate values for the five channel opening ratios, M ,"

Q	$\frac{Q}{g^{1/2} b^{5/2}}$				
	$M' = 0.15$	$M' = 0.20$	$M' = 0.25$	$M' = 0.275$	$M' = 0.30$
2.0	0.7095	0.353	0.202	0.159	0.128
2.5	0.885	0.441	0.2525	0.199	0.160
3.0	1.062	0.529	0.303	0.238	0.192
3.5	-	-	0.354	0.278	0.224
4.0	-	-	0.405	0.318	0.256

By choosing flow rates in the test runs that give different ordinate values in the table, grouping of data in the graphs can be prevented. As an example it can be seen from the table that, to give a complete uniform coverage for plotting of a curve it is not necessary to make more than about 4 test runs if they are carefully selected. When using the table, it should be kept in mind that it would not be possible to make all 21 test runs listed in the table for all geometries even if desired. This is because some test geometries may be overtopped and some will not obtain submergence, depending on the value chosen for the Froude number. The seven tables that follow this section show the test runs made for the different geometries. The conditions selected in Table I through VII were chosen in part from the table developed in this section. Further limitations were imposed as to number of test runs after the data taken for the limiting curves were calculated and plotted. From the spacing of these curves, the decision was made as to the number of additional runs desired. If the limiting curves were closely spaced, runs were made to establish how the other curves were spaced between the limiting ones.

Table I - Smooth Boundary Tests

$$n = 0.0110$$

Geometry I-a

Flow Rate cfs.	Froude Number Fn			Channel Width Ratio (b/B)			
	0.10	0.15	0.20	0.20	0.25	0.275	0.30
2.0	X			X	X	X	X
2.0		X		X	*	*	*
2.0			X	X	*	*	*
2.5	X			O	X	X	X
2.5		X		X	X	X	X
2.5			X	X	X	X	X
3.0	X			O	X	X	X
3.0		X		O	X	X	X
3.0			X	O	X	X	X
3.5							
3.5		X		O	X	X	X
3.5			X	O	X	X	X

X Regular test measurements obtained

O The flow overtopped the model and channel walls

* Submergence was not possible for these flow conditions

Table II - Smooth Boundary Test

$$n = 0.0110$$

Geometry I-b

Flow Rate cfs.	Froude Number Fn			Channel Width Ratio b/B											
	.10	.15	.20	0.20				0.25				0.30			
				Thickness Factor L/b											
				.25	.50	.75	1.0	.25	.50	.75	1.0	.25	.50	.75	1.00
2.0	X			X	X	X	X	X	X	X	X	X	X	X	X
2.0		X _i		*	*	*	*	*	*	*	*	*	*	*	*
2.0			X _i	*	*	*	*	*	*	*	*	*	*	*	*
2.5	X			O	O	O	O	X	X	X	X				
2.5		X		X	X	X	X	X	X	X	X	X	X	X	X
2.5			X				X	X			X	X	X	X	X
3.0	X _i			O	O	O	O								
3.0		X		O	O	O	O	X	X	X	X	X	X	X	X
3.0			X	O	O	O	O				X				
3.5	X _i			O	O	O	O	O	O	O	O				
3.5		X		O	O	O	O	X	X	X	X	X	X	X	X
3.5			X	O	O	O	O			X	X				
4.0	X _i			O	O	O	O	O	O	O	O				
4.0		X		O	O	O	O	O	O	O	O			X	X
4.0			X _i	O	O	O	O								

X Regular test measurements obtained

O The flow overtopped the model and channel walls

* Submergence was not possible for these flow conditions

 X_i Experimental condition investigated

Table III - Rough Boundary Tests

$$n = 0.0238$$

Geometry I-a

Flow Rate cfs.	Froude Number Fn			Channel Width Ratio (b/B)			
	0.10	.015	0.20	0.20	0.25	0.275	0.30
2.0	X			X	X	X	X
2.0		X _i			*	*	*
2.0			X	X	*	*	*
2.5							
2.5		X		X	X	X	X
2.5			X	X	X	X	X
3.5							
3.5		X		O	X		
3.5			X	O			

X Regular test measurements obtained

O The flow overtopped the model and channel walls

* Sumbergence was not possible for these flow conditions

X_i Experimental condition investigated

Table IV - Rough Boundary Tests

$$n = 0.0238$$

Geometry I-b

Flow Rate cfs.	Froude Number Fn			Channel Width Ratio (b/B)											
	.10	.15	.20	0.20				0.25				0.30			
				.25	.50	.75	1.0	.25	.50	.75	1.0	.25	.50	.75	1.0
2.0	X			X			X	X			X			X	
2.0		X_1						*	*	*	*	*	*	*	*
2.0			X	X	X		X	*	*	*	*	*	*	*	*
2.5	X_1			O	O	O	O								
2.5		X		X		X	X	X		X	X	X	X	X	
2.5			X	X			X	X			X			X	
3.5	X_1			O	O	O	O	O	O	O	O				
3.5		X		O	O	O	O	X	X		X				
3.5			X_1	O	O	O	O								

X Regular test measurements obtained

O The flow overtopped the model and channel walls

* Submergence was not possible for these flow conditions

 X_1 Experimental condition investigated

Table V - Rough Boundary Tests

$$n = 0.0238$$

Geometry V-b

Flow Rate cfs.	Froude Number			Thickness Factor $L/b = 0.50$ Channel Width Ratio (b/B)					
	.10	Fn		0.20			0.30		
		.15	.20	Angle of Skew ϕ					
				15°	22½°	30°	15°	22½°	30°
2.0	X			X	X	X	X	X	X
2.0		X		X	X	X	*	*	*
2.0			X	X	X	X	*	*	*
3.0	X			X		X	X		X
3.0		X		X		X	X		X
3.0			X	X		X	X		X

X Regular test measurements obtained

O The flow overtopped the model and channel walls

* Submergence was not possible for these flow conditions

Table VI - Rough Boundary Tests

$$n = 0.0238$$

Geometry VI

Flow Rate cfs.	Froude Number Fn			Thickness Factor $L/b = 0.50$ Channel Width Ratio b/B		
	.10	.15	.20	.15	.20	.25
2.0	X			X	X	X
2.0		X		X	X	*
2.0			X	X	X	*
2.5	X			X	X	X
2.5		X		X	X	X
2.5			X	X	X	*
3.0	X			X	X	X
3.0		X		X	X	X
3.0			X	X	X	X

X Regular test measurements obtained

O The flow overtopped the model and channel walls

* Submergence was not possible for these flow conditions

Table VII - Rough Boundary Tests

$$n = 0.0238$$

Geometry VII

Flow Rate cfs.	Froude Number Fn					Channel Width Ratio b/B					
	.1	.2	.3	.4	.5	$\beta = .0$	$\beta = .3$ ^{0.35}	$\beta = .5$	$\beta = .0$	$\beta = .3$ ^{0.50}	$\beta = .5$
1.0	X					*			X	*	*
2.0	X					*	X			*	*
2.0		X				*	X			*	*
2.0			X			*	X			*	*
2.0				X		*				*	*
2.0					X	*				*	*
2.5	X					X				*	
2.5			X			*	X			*	*
2.75				X		*	X			*	*
3.0	X										X
3.0		X				X				*	X
3.85	X							O	X		
3.85		X						O	*	X	
3.85			X			X		O	*	*	X
3.85				X		X		O	*	*	X
3.85					X	X		O	*	*	X

X Regular test measurements obtained

O The flow overtopped the model and channel walls

* Sumbervence was not possible for these flow conditions

CHAPTER VI

TESTING PROCEDURE AND DATA PROCESSING

Test Setups for Submerged Flow Conditions

In the previous chapter the geometries to be tested were described and the selection of variables were made. To set up a test-condition where uniform flow exists with a pre-determined discharge and Froude number in the unobstructed channel can be a rather time-consuming process when it is based upon a trial and error method. P. F. Biery (4) had developed a systematic procedure to obtain the uniform flow in the flume after a Froude number and a flow rate had been selected. A similar procedure was adopted for the present investigation.

Nomographic Charts

A nomographic chart was prepared which relates the Froude number F_n , the normal depth Y_n , the discharge Q , the tailgate elevation Y_t , the channel slope S , and the slope control reading. The relationships used are:

$$F_n = \frac{Q}{BY_n \sqrt{gY_n}} \quad (25)$$

Manning's formula

$$V = \frac{1.486}{n} R^{2/3} S^{1/2} \quad (26)$$

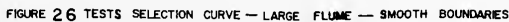
Francis weir formula

$$Q = K B \left[(H + H_v)^{3/2} - H_v^{3/2} \right] \quad (27)$$

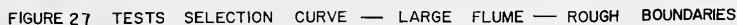
The curves relating these variables are shown in Figures 26 and 27 for smooth and rough boundaries respectively. The calculations were made using the 1620 IBM computer. The program is given together with the derivation of the relationships in Appendix C.

To use the monographic chart one enters the left side with a selected Froude number and discharge and read the normal depth. Now, with Q and Y_n fixed, the slope is found. With Q and slope fixed, the tailgate setting Y_t is read. The slope-revolution calibration curve is projected onto the nomograph and the setting of the revolution counter can be read directly from the charts. Arrows drawn on the charts demonstrate the path to follow for the selection of a particular test condition. The use of these charts helped to set the normal depth flow within 30 minutes even when corrections had to be made. The normal depth was always checked along the centerline and minor adjustments made of the tailgate to ensure uniform flow in the flume.

After the test conditions were determined and set by means of the chart of fig. 26,, the angle irons were fastened at the test section and the model was placed behind them to the correct position and bolted to the angle irons. The backwater rose behind the model until equilibrium was obtained between the upstream and downstream flow. The time required to obtain equilibrium varied between 10 to 30 minutes depending on the opening of the model, the Froude number and the rate of flow used.







FROUDE NO. IFn

Figure 28 shows an upstream and a downstream view of a typical test run after the backwater has come to equilibrium. At this stage, surface elevation, streamlines, velocities and flow patterns were observed and recorded. All depths were measured relative to the bottom. The electronic point gage was used to measure the backwater. Dye was injected by means of a syringe having an 18" long needle, in order to study the streamline paths and flow behavior as presented in Figures 3 and 38. The Prandtl tube connected to the pressure diaphragm was used for all velocity readings (see section on measuring equipment, Chapter IV).

Data Processing

The data obtained from the test runs were processed on the IBM 1620, IBM 7090 and LGP 30 computers. By using the computers, valuable time was saved, and more reliable answers were obtained than could be expected from manual calculations. An outline of the computer programs is presented in Appendix C.

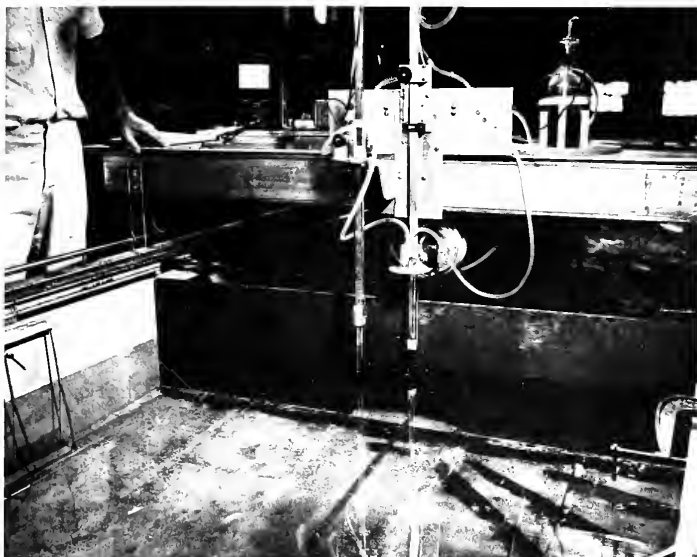


FIG. 28 UPSTREAM AND DOWNSTREAM VIEWS OF
TYPICAL TEST RUN

CHAPTER VII

RESULTS AND THEIR ANALYSIS

In this chapter the results of the processed data are presented and analyzed. Due to the large amount of data taken, the test runs will not be treated separately but in groups according to the geometries. The results from each group of tests are presented in dimensionless graphs and an explanation is given as to each graphs significance.

The terms free outflow, fully submerged and partly submerged outflow are frequently used in this chapter and are defined as follows. Free outflow exists when the jet discharging from the downstream face of the bridge opening is surrounded, except for the channel bottom, only by air and a hydraulic jump occurs further downstream. Fully submerged outflow exists when the jet discharges into a stream that has a depth equal to or greater than the downstream height of the bridge opening. A partly submerged outflow is the case when the jet discharges into a stream that has a depth less than the height of the bridge opening and no downstream jump occurs.

The coefficients of contraction, of discharge and of velocity are presented for geometry I-a with free jet outflow. For the same flow conditions, the velocity distribution over the cross section at vena contracta is presented in form of isovelocity curves covering the cross section. A velocity comparison at different elevations

in the vena contracta is also given some special attention.

The backwater depths obtained for the different geometries are presented first in terms of the discharge and with the Froude number as a parameter, and second as a function of the ratio of the Froude number to the channel opening ratio.

The presentation of the data can be broken into two major categories - the smooth boundary ($n = 0.0110$) and the rough boundary ($n = 0.0238$). Comparisons are made between findings from the two boundary conditions. Pictures of typical directions of the discharge jet for different flow conditions are presented together with a discussion of other observations and analysis made.

Geometry I-a - Smooth Boundaries

Coefficients of Contraction, of Discharge and of Velocity for Free Jet Outflow

In order to investigate the coefficients of velocity, contraction and discharge for submerged bridge inlets 67 test runs were made (see Table I - VII). The coefficients are defined as follows:
Coefficient of contraction, C_c , is the ratio of jet area at vena contracta A_v to the area of the orifice A_o .

$$C_c = \frac{A_v}{A_o}$$

Coefficient of discharge, C_d , is the ratio of the actual discharge Q_a , obtained from the Venturimeter reading, to the theoretical Q_t , as calculated by formula (10)

$$C_d = \frac{Q_a}{Q_t}$$



Coefficient of velocity is the ratio of actual velocity V_a to the theoretical velocity V_t

$$C_v = \frac{V_a}{V_t}$$

It is customary to combine the three coefficients as follows:

From continuity equation the following can be written:

$$\frac{Q_a}{Q_t} = \frac{A_v}{A_o} \frac{V_a}{V_t}$$

from which it follows that:

$$C_d = C_c C_v$$

To find the coefficient of contraction the vena contracta had to be located and the cross-sectional area measured. This was done by means of the electronic pointgauge.

A sufficient number of readings were taken at the vena contracta to plot the cross sectional area on graph paper. By use of a planimeter the area A_v was obtained and the coefficient of contraction could be calculated, as the area of the model opening was known. The coefficient of contraction was plotted versus the ratio b/Y_1 of the model opening width to the backwater depth using the channel width ratio b/B , as parameter (see Figure 29).

To obtain values for the calculation of the coefficient of discharge C_d , a theoretical discharge equation was developed. The development of this equation (10) was presented in the theoretical analysis in Chapter III. A detailed presentation of the numerical calculations involved is given in Appendix B. The actual rate of flow through the constriction was obtained from the manometer readings

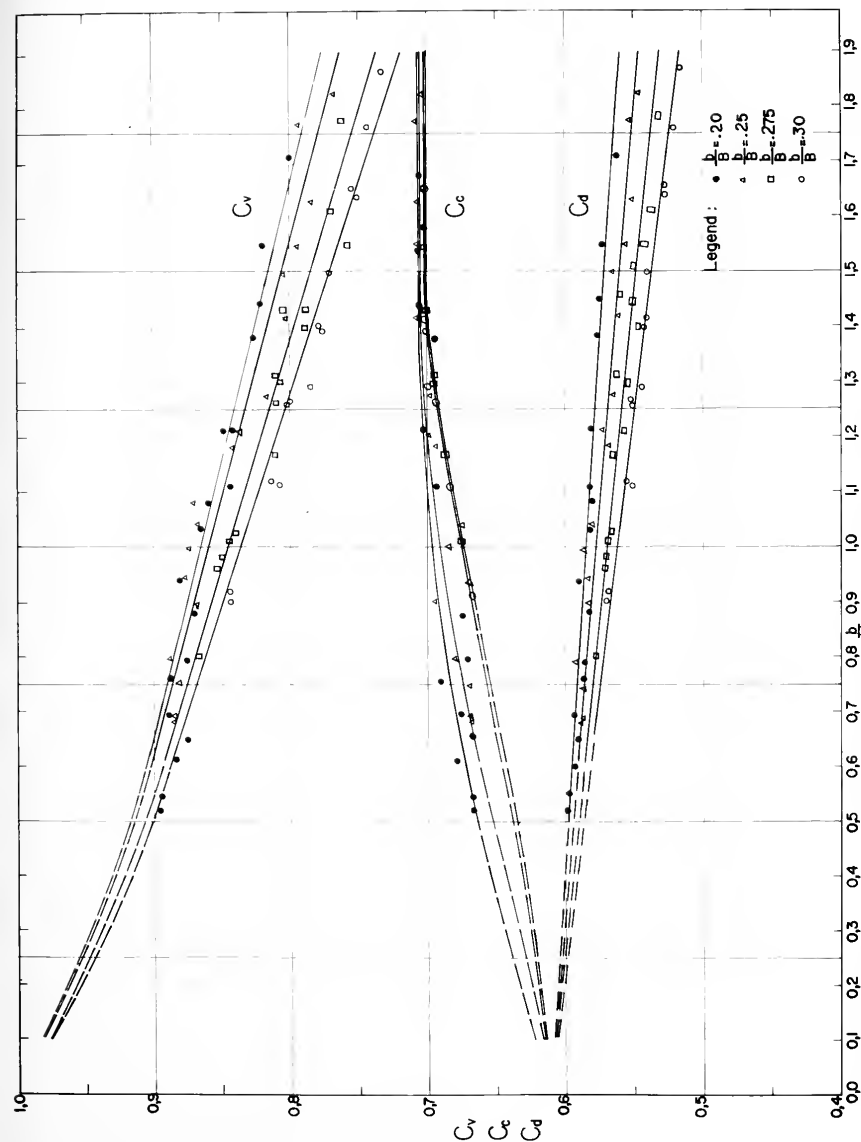


FIGURE 2.9 COEFFICIENTS OF VELOCITY, CONTRACTION & DISCHARGE - SUBMERGED INLET BUT UNSUBMERGED DISCHARGE JET.



and the venturi meter calibration curves. Curves were plotted for the coefficient of discharge C_d versus the ratio b/Y_1 and the channel width ratio was again used as parameter (see Figure 29). The coefficient of velocity was then found from the relationship between the three coefficients, $C_d = C_c C_v$ and plotted versus b/Y_1 in Figure 29.

The C_d curves seem to converge toward the value 0.61 as the $\frac{b}{Y_1}$ ratio tends to zero. The curves are closely spaced straight lines and the C_d values decrease with increasing channel width ratios. The C_c curves also tend towards the 0.61 value as the $\frac{b}{Y_1}$ ratio decreases. Values of C_c decrease for increasing channel width ratios. For increasing C_c values, within the test range, the C_c curves tend to increase toward the value 0.71 and then stabilize at this value. The C_v curves have the same relative spacing as the C_c and C_d curves as to the $\frac{b}{Y_1}$ ratio but tend toward the value 1.0 as a limiting value when the $\frac{b}{Y_1}$ ratio decreases toward zero.

These findings check well with the typical value 0.611 found from the theory of free streamlines. Streeter²¹ shows this for a two dimensional ideal orifice where he applies complex variables to the "Schwarz - Christoffel Transformation" and gets the ideal discharge coefficient

$$C_d = \frac{2b}{2b + \frac{4b}{\pi}} = \frac{\pi}{2 + \pi} = 0.611$$

Nearly a century ago Kirchhoff²² showed that the contraction coefficient for irrotational efflux from a plane orifice, under idealized conditions, would have the magnitude $\frac{\pi}{\pi + 2} = 0.611$.

Von Mises ¹³ determined tables of the C_c coefficient for several boundary characteristics which show the same trend as those found in this investigation. The test data are recorded in test runs 1 - 67 shown in Tables (VIII - XV). The calculated values to find C_c , C_d , and C_v are found in Table (XXX).

Velocity Distribution at Vena Contracta for Free Jet Outflow

Extensive velocity measurements were taken in the jet downstream of constriction at the vena contracta in order to observe the velocity distribution. The Prandtl tube together with the pressure transducer were used. The readings were taken in a grid system to obtain full coverage over the cross section. The borderline of the area at the cross-section was also measured and plotted on graph paper together with the velocity grid values. From this the isovelocity curves were drawn. Figure 30 shows one of the typical isovelocity curves drawn from such grid measurements. Figure 31 shows the result obtained by following the individual isovelocity curves in the water cross-section itself. This was done by moving the Prandtl tube through the cross-section and mapping the path for the individual isovelocity curves obtained by means of the horizontal and vertical traversing devices. The data of Figures 30 and 31 correspond to discharges 3.75 cfs and 2.62 cfs, normal depth Froude number 0.142 and 0.103 and opening ratios 0.30 and 0.30 respectively.

In Figure 32 the values of the velocities are plotted at different depths and a mean velocity curve is drawn. The data for Figure 32 are the same as those for Figure 31. Figure 32 shows the velocity variation over the opening width at different depth. A similar



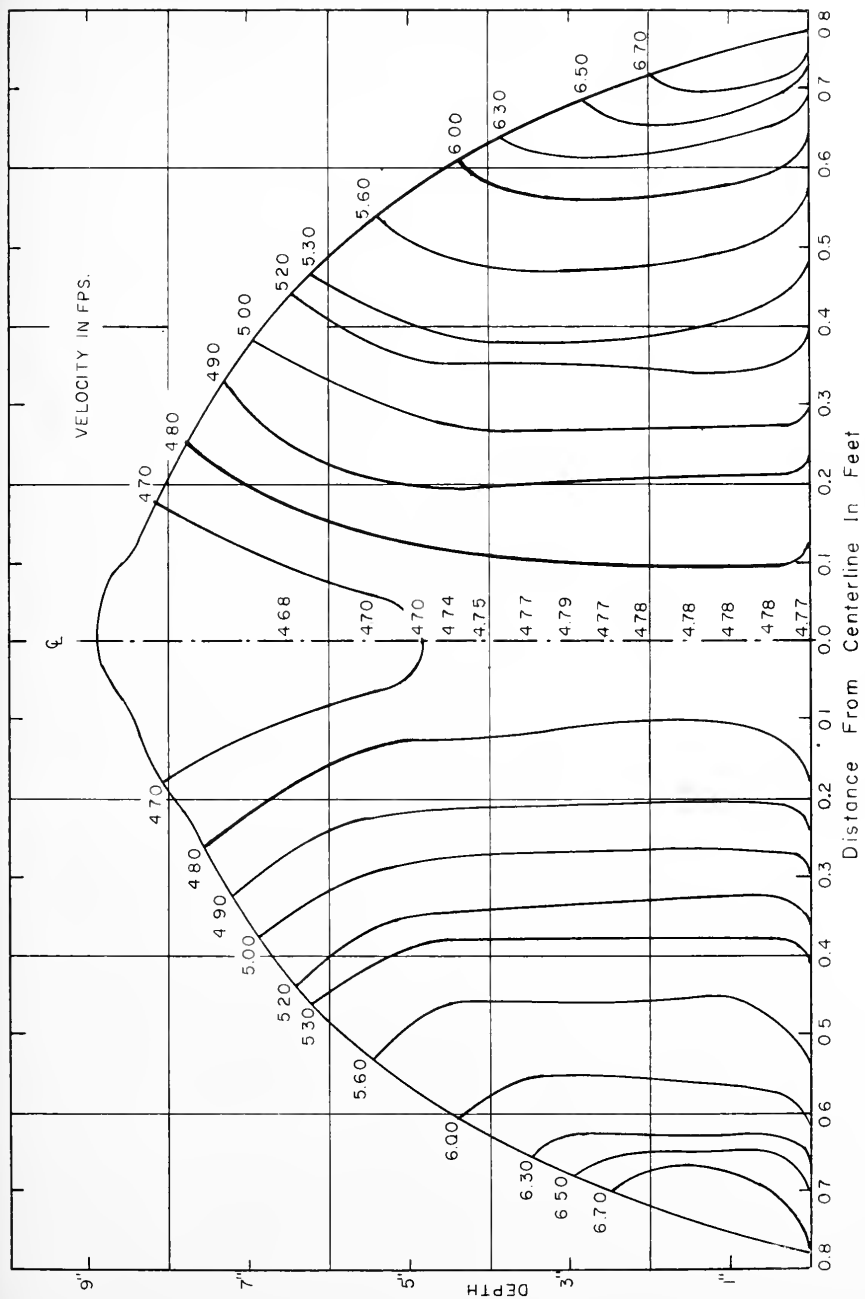


FIG. 30 ISOVELOCITY CURVES AT VENA CONTRACTA

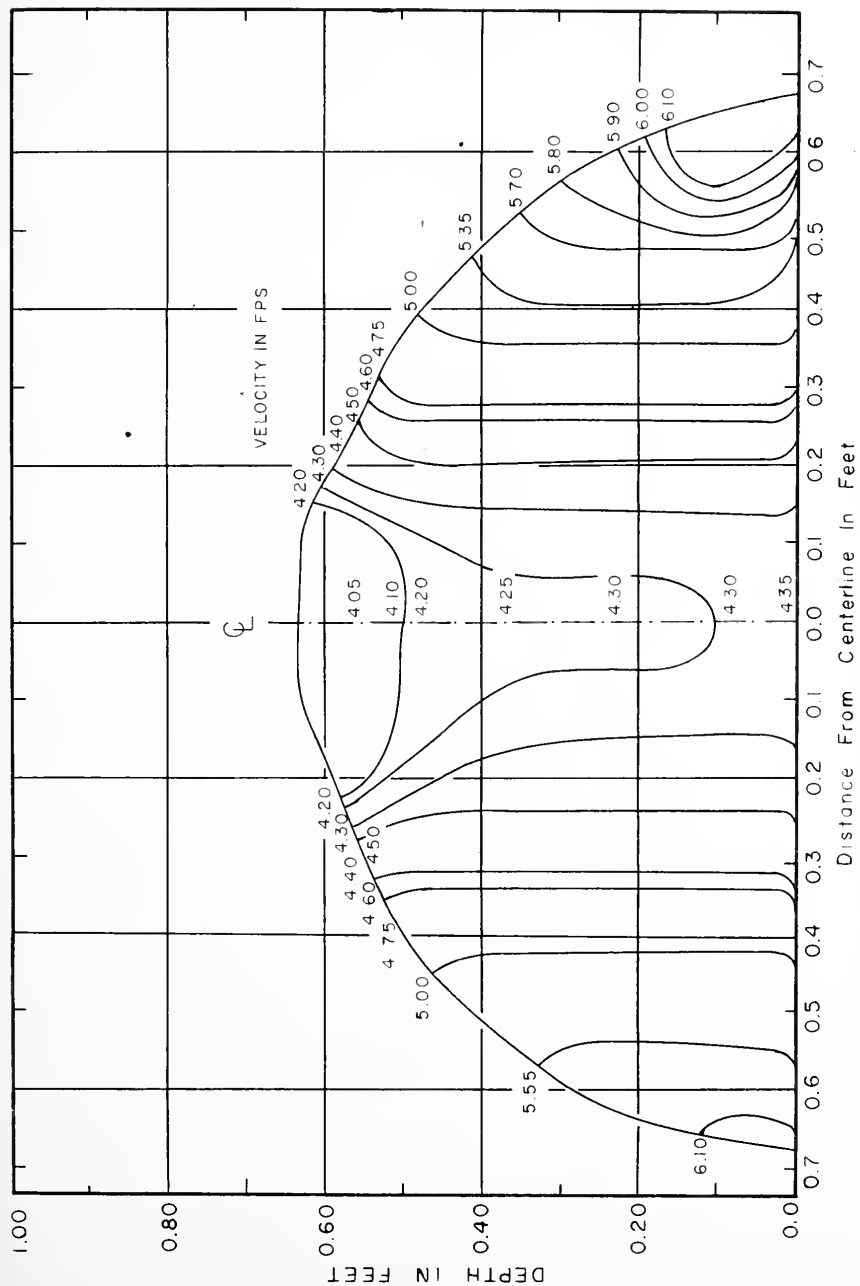


FIG. 31 ISOVELOCITY CURVES FOR CROSS SECTION AT VENA CONTRACTA



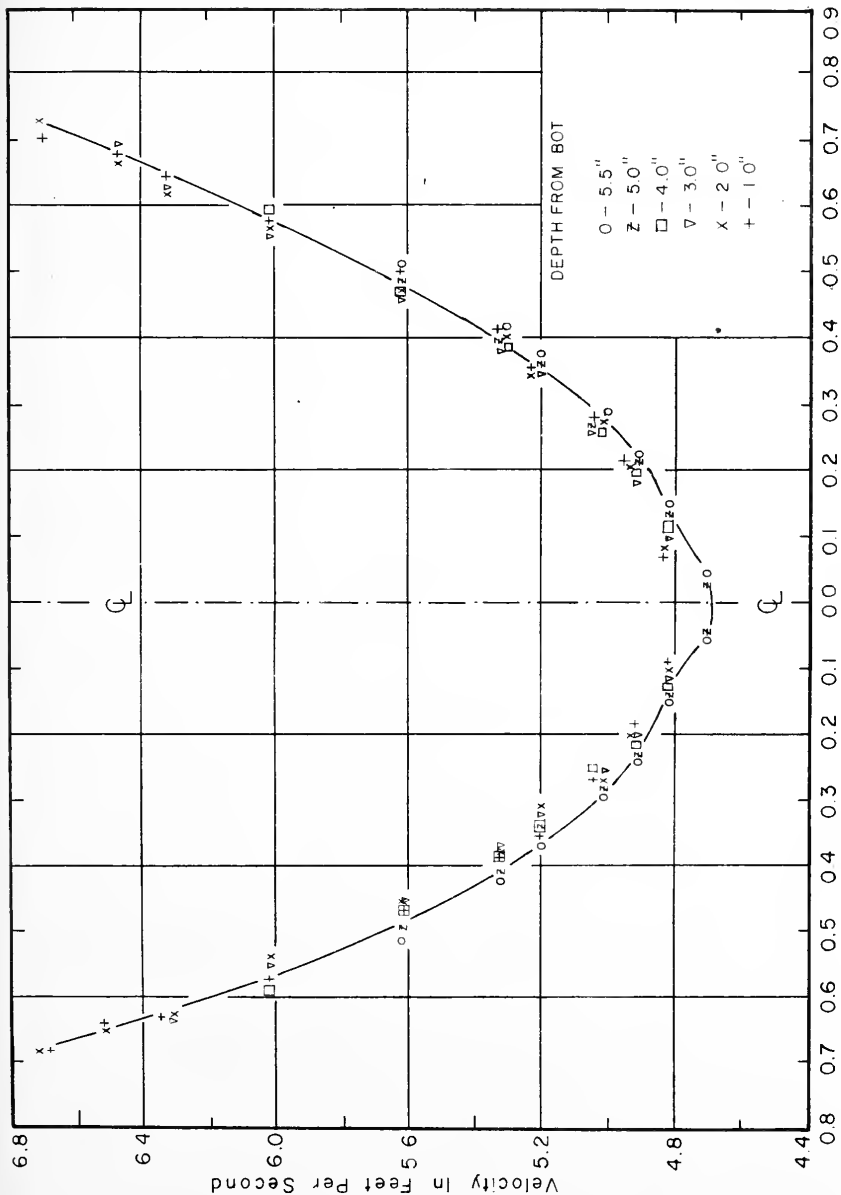


FIG. 32 VELOCITY DISTRIBUTION AT VENA CONTRACTA



study was made for other flow conditions as recorded in Tables XXVIII and XXIX. All the recorded values when plotted, show the same characteristic velocity distribution as shown in Figures 30, 31, and 32.

The Generalized Backwater Equation -

Outflow Fully and Partly Submerged

From the theoretical analysis done in Chapter III it is expected that the general relation between the backwater and normal depth is of the form

$$\frac{Y_1}{Y_n} = C \left[\left(\frac{F_n}{M'} \right)^2 \right]^\gamma \quad (36)$$

where C is a coefficient that would take into account the effects of the approach velocity, discharge coefficient, non-hydrostatic pressure distribution, non-uniform velocity distribution and other empirically determined factors. In a logarithmic plot of Y_1/Y_n versus $(F_n/M')^2$, the slope of the line is γ . A total of 33 tests were made on geometry I-a and processed on the IBM 1620 computer to obtain plotting values of $(Y_1/Y_n - 1)$ versus $(F_n/M')^2$. The value $(Y_1/Y_n - 1)$ was used in order to expand the scale of the graph. The graph is shown on Figure 33. From this graph the values γ and C were found to be 0.90 and 1.18 respectively, and equation (36) can be written for the submerged conditions of geometry I-a in the following way:

$$\frac{Y_1}{Y_n} = 1 + 1.18 \left[\left(\frac{F_n}{M'} \right)^2 \right]^{0.90} \quad (17)$$

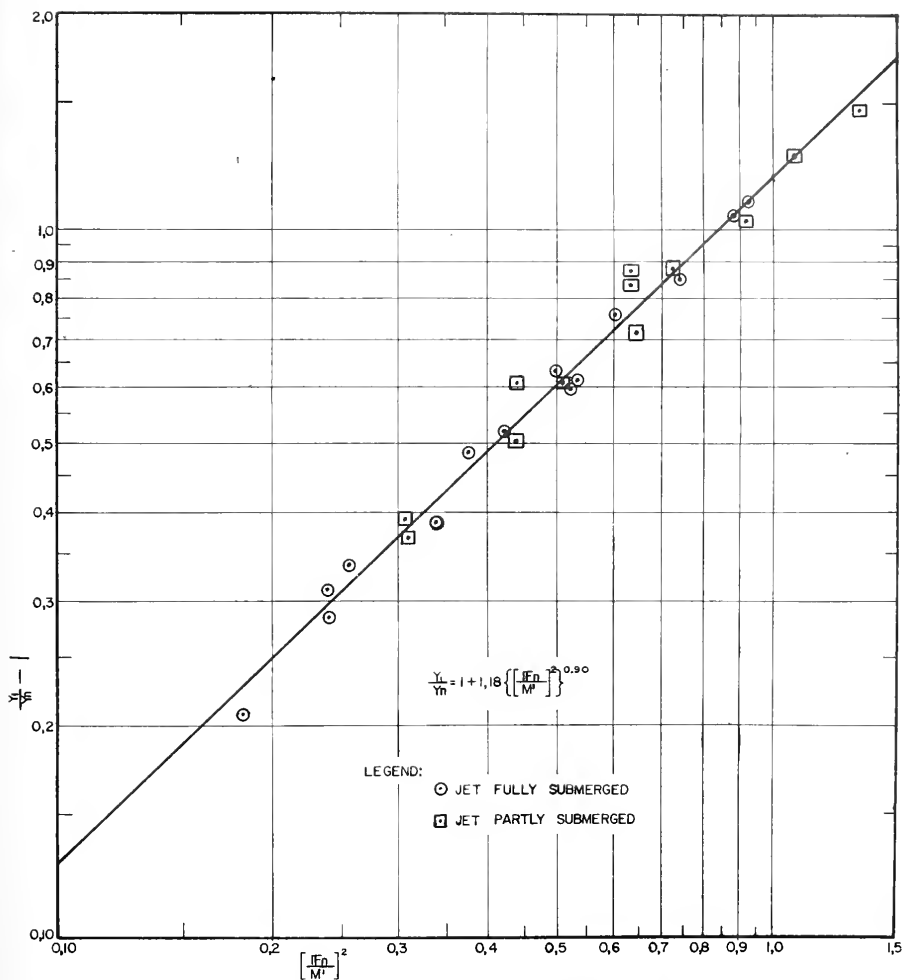


FIGURE 33 GENERALIZED BACKWATER RATIO FOR SUBMERGED INLET. GEOMETRY Ia

or

$$\frac{Y_1}{Y_n} = 1 + 1.18 \left(\frac{F_n}{M'} \right)^{1.80} \quad (18)$$

The test data taken to obtain this generalized backwater equation (18) are recorded in test runs 102-134 which are located in Tables XVI and XVII. The calculated values from the data are presented in Table XXX.

A general backwater equation was not obtainable for the free jet outflow. This is because the Froude numbers for test runs 1 - 67 are all in the range of 0.550 - 0.587 which results in one group of numbers and a line could not be defined. The calculation of the Froude numbers on the computer are shown in Appendix C and the results are listed in Table XXX.

Discharge Coefficient for Free, Submerged and Partly Submerged Outflow

A graph was made of the discharge coefficient, C_d , versus the channel opening ratio, M' , for the submerged smooth bridge opening, Geometry I-1a (Figure 34). The curves obtained are for the submerged discharge jet except for the two upper most curves which are for partly submerged jets. These curves are similar to those estimated by P. F. Biery (4) for the unsubmerged case and for channel opening ratios of 0.29 and up. The present values for the submerged case were obtained for the range of M' between 0.10 and 0.35. Figure 34 shows the C_d versus M' curves for submerged and partly submerged flow as well as Biery's discharge coefficient curves for the unsubmerged case which have been superposed for the purpose of comparison. The

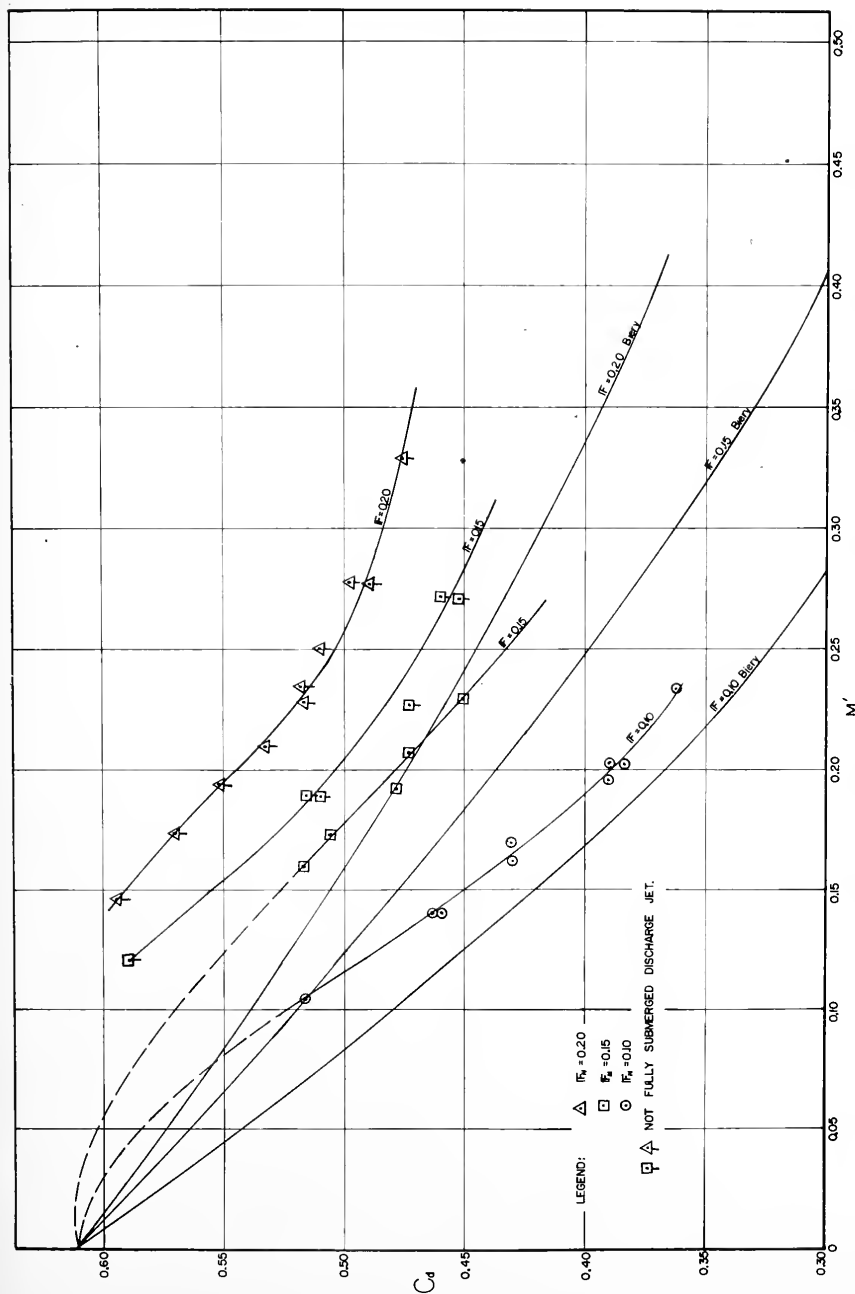


FIG. 34 DISCHARGE COEFFICIENT VS CHANNEL OPENING RATIO, SMOOTH BOUNDARIES, GEOMETRY I_d



test data taken to obtain the curves in Figure 34 are recorded in test runs 102 to 134 which are located in Tables XVI and XVII. The calculated values are presented in Table XXX.

The values of the discharge coefficient are summarized in Figure 35. For the submerged jet, two sets of curves are given, one uses the Froude number as a parameter, the other uses the ratio $Y_n / \frac{b}{2}$ of the normal depth to the arch radius. The free jet discharge coefficient curves previously presented in Figure 29 have been reproduced here for completeness. The calculations are shown in Table XXX.

Geometry I-b - Smooth Boundaries

As can be seen from the definition of test geometries, the geometry I-a is a special case of geometry I-b. By setting the variable $\frac{L}{b}$ equal to zero in the definition of geometry I-b, the geometry I-a is obtained. Geometry I-a therefore represents the limiting case of geometry I-b, and can be treated together with I-b.

In the theoretical analysis made in Chapter III the dimensionless relation

$$\frac{Q}{g^{1/2} b^{5/2}} = f \left(\frac{Y_1}{b} \right)$$

was developed for the orifice type flow through a submerged arch constriction. A total of 92 test runs were conducted for submerged conditions in the smooth channel. Three sets of dimensionless curves were plotted. To save space and make it easier to compare the curves, they were all plotted in one figure. The $\frac{L}{b}$ ratio is used as parameter, and the Froude number is constant for each set of curves.

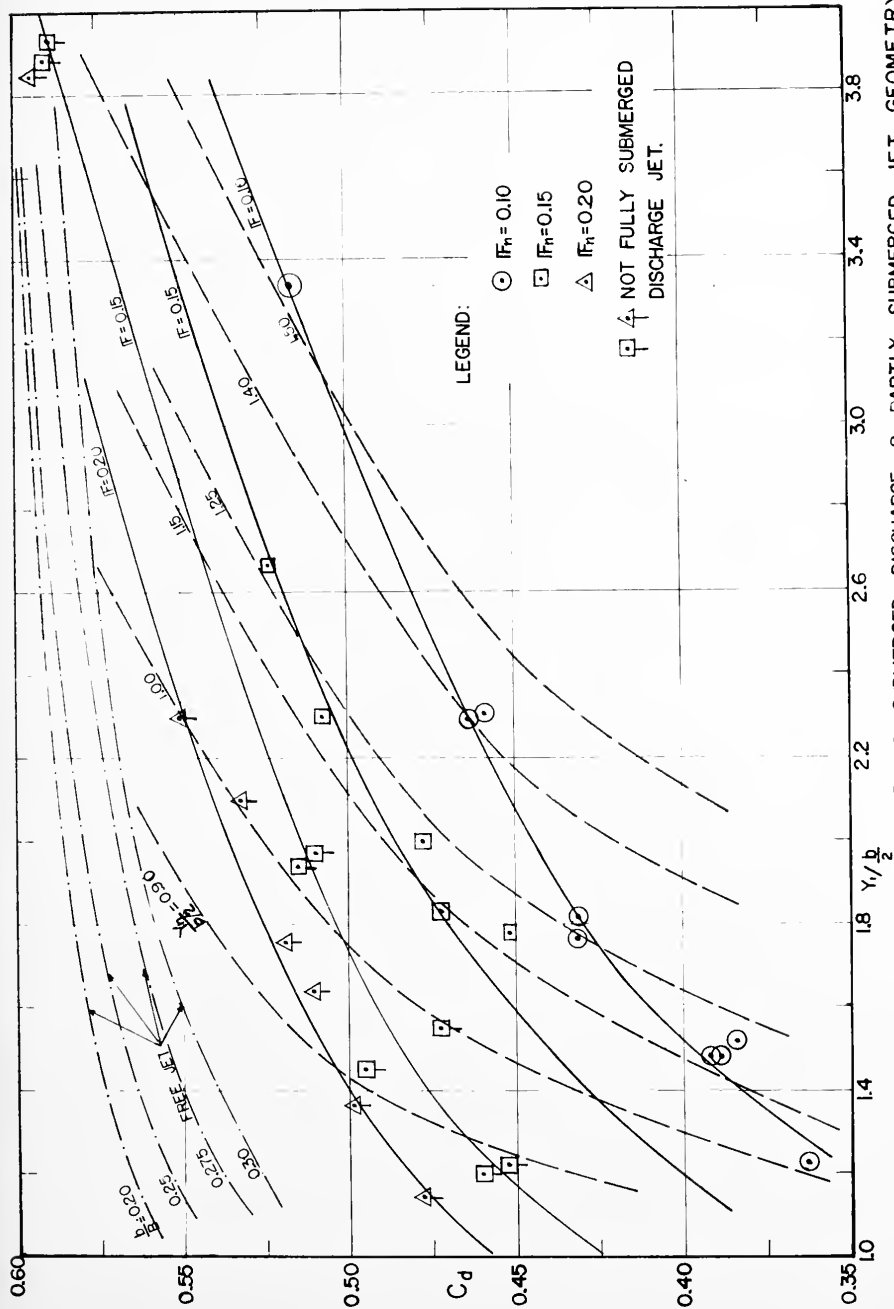


FIGURE 35 DISCHARGE COEFFICIENT FOR FREE & SUBMERGED DISCHARGE & PARTLY SUBMERGED JET. GEOMETRY I & O

To be able to show all three sets of curves clearly on one graph, the vertical coordinate axis was broken into three parts each starting from zero. The curves are shown in Figure 36. For higher Froude numbers the curves get closer spaced. This means that the L/b ratio becomes insignificant for all practical purposes when the Froude number reaches a value of about 0.20 for the smooth ($n = 0.0110$) boundary case of geometry I-b. The data from the 92 test runs are listed in run number 101 - 192 and recorded in Tables XVI - XXI. The calculated values of the plotted points are shown in Tables XXX and XXXI.

Geometries I-a and I-b - Rough Boundaries

After the roughness was installed and calibrated for Mannings n , test selection curves were computed and plotted as shown in Figure 27. An average Mannings n of 0.0238 was found and used for the rough boundary condition.

Geometries I-a and I-b were again treated together. A total of 38 test runs were made in order to plot the dimensionless curves shown in Figure 37. These three sets of curves were also based on the dimensionless equation (24) developed in Chapter III. Due to the previous experience with Geometries I-a and I-b in the smooth boundary test runs, a better test selection was possible for the rough boundary tests with respect to grouping of the points in the graphs. The data are recorded in test runs 193 - 231 and can be found in Tables XXI - XXIII. The calculated values from the data are listed in Table XXXI.



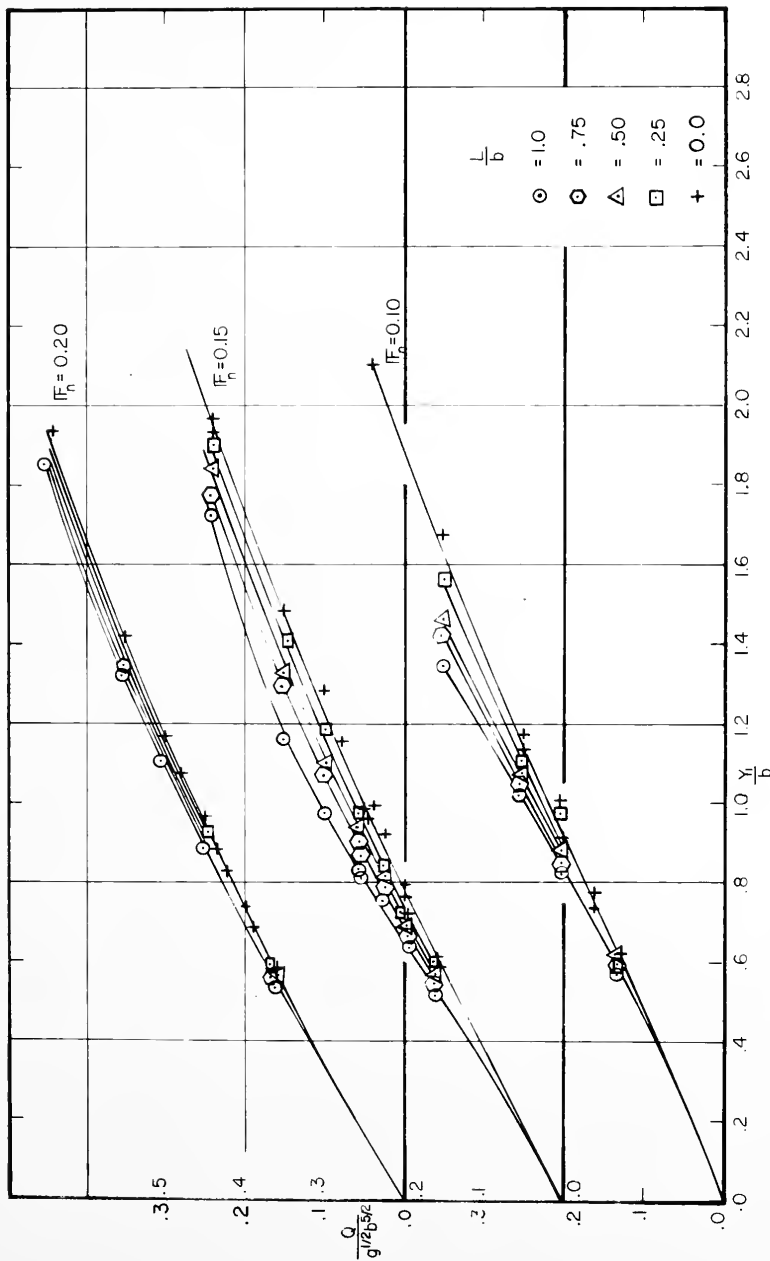


FIG 36 DIMENSIONLESS CURVES FOR GEOMETRIES Ia AND Ib. SMOOTH BOUNDARIES



The investigation shows that the width of the constriction in the direction of flow, L , influences the backwater to a certain degree when the Froude number is low. The wider the bridge in the direction of flow the lower is the backwater depth obtained. For a Froude number of 0.15 the backwater ratio for an L/b ratio of 1.0 was as much as 30% lower than for a L/b ratio of 0.00. For the more practical cases where the Y_1/b ratio is in the order of about 0.50 to 1.00, a lowering of about 10 - 20% in the backwater ratio is usual when the L/b ratio is increased from 0.00 to 1.00. Flow through three dimensional arch bridges is very similar in behavior to the flow through short culverts. For short culverts, the flow characteristics are relatively independent of the slope and the factors that involve the length are comparatively unimportant. The control section for square edge openings, such as investigated here, is at the inlet.

Separation of flow around the opening, at the inlet section, was frequently observed. The flow contracted towards vena contracta section in the first part of the barrel expanded in a spiral motion as shown in Figure 38 and ended in a slug flow at the submerged outlet. Figure 39 shows the case where slug flow occurs at the exit of the barrel. Figure 40 presents the free jet case for geometry I-a with rough boundaries and the same flow.

Vortex action was also often observed. This air-vortex occurs from the surface right above the crest of the inlet and introduces air through the opening. This decreases the water area of the opening and hence the flow through the constriction, and as a result the backwater increases.



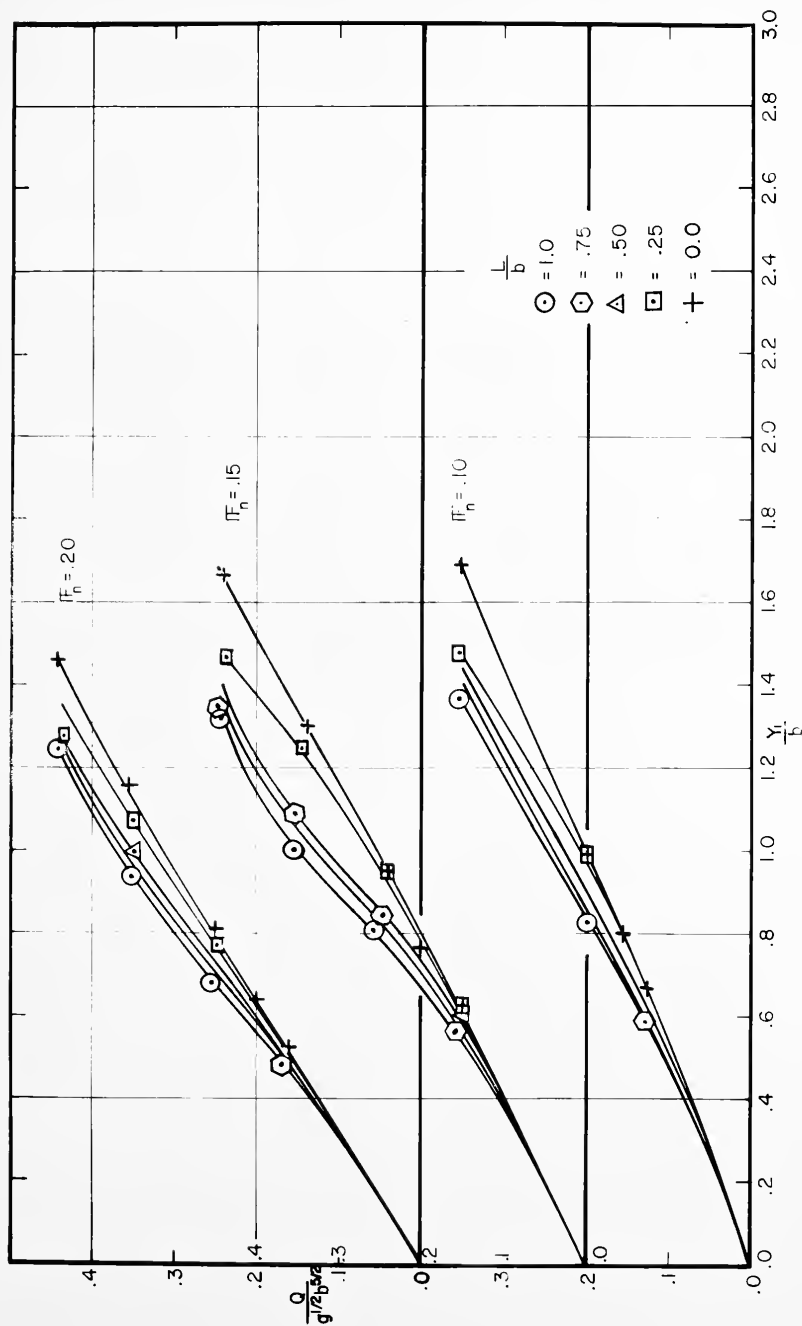


FIG 37 DIMENSIONLESS CURVES FOR GEOMETRIES Ia AND Ib. ROUGH BOUNDARIES

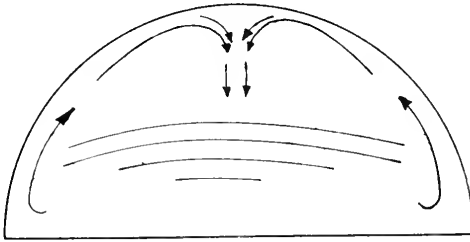


Fig 38a Spiral Motion in Barrel Section Downstream of Vena Contracta

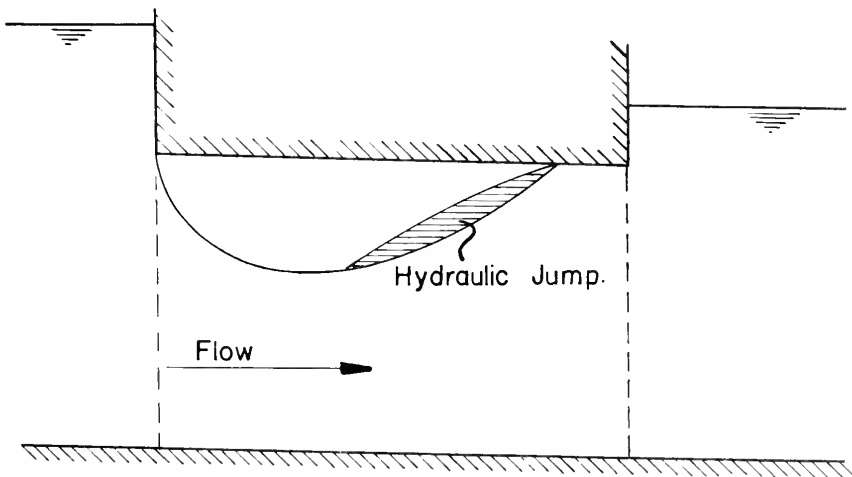


Fig 38b Typical Flow Condition Through Constriction

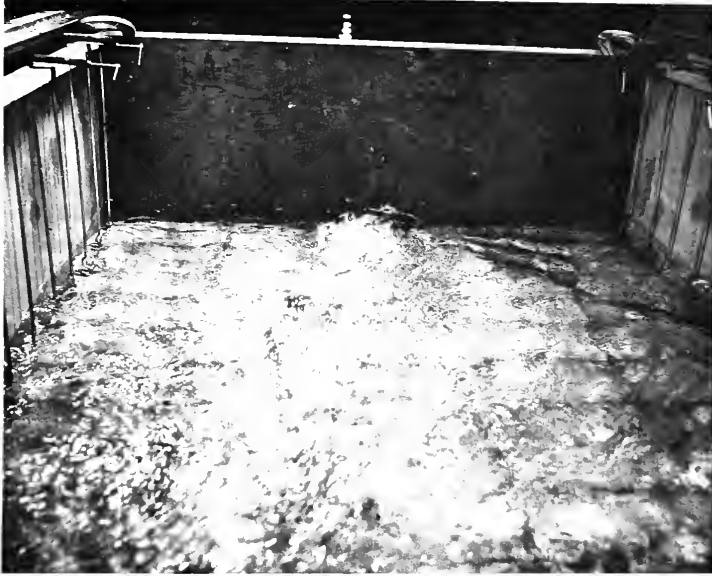


FIG. 39 SLUG FLOW AT BARREL EXIT



FIG. 40 FREE DISCHARGE JET

An important effect upon the separation phenomena, that controls the change of flow from a sluice type to full conduit flow, is the existence of a negative pressure in the barrel. This is caused by the relative magnitudes of air inflow from the outlet and from the vortex action over the inlet. The outflow of air due to entrainment at the air-water surface also has an effect upon the separation phenomena, the more air entrained the less separation will occur and the barrel will tend towards full conduit flow.

Comparison Between Smooth and Rough Boundary Tests

A comparison between the limiting curves of Figures 36 and 37 for the smooth and rough boundary conditions respectively are made in Figure 41. These curves show that a rough boundary condition is of advantage for higher Froude numbers ($F_n > 0.15$), as could be expected from observing the flow behavior. For higher Froude numbers the approach velocities will increase and consequently give a higher turbulence level due to the natural roughness. This will improve the ability of the barrel to produce full conduit flow, because it increases the air entrainment in the barrel at the air-water surface and hence reduces the separation at the inlet. To further help the air entrainment, a roughening of the inlet surface would be desirable. It appears that by increasing the upstream approach flow turbulence or introducing a higher turbulence in the inlet section, a more desirable flow capacity is obtained through the constriction and hence lower backwater depth. In other words, the experiments show that for structures flowing full such as culverts the aim should not be to design approach channels of highly engineered smooth boundaries and perhaps precise alignment, but rather to con-

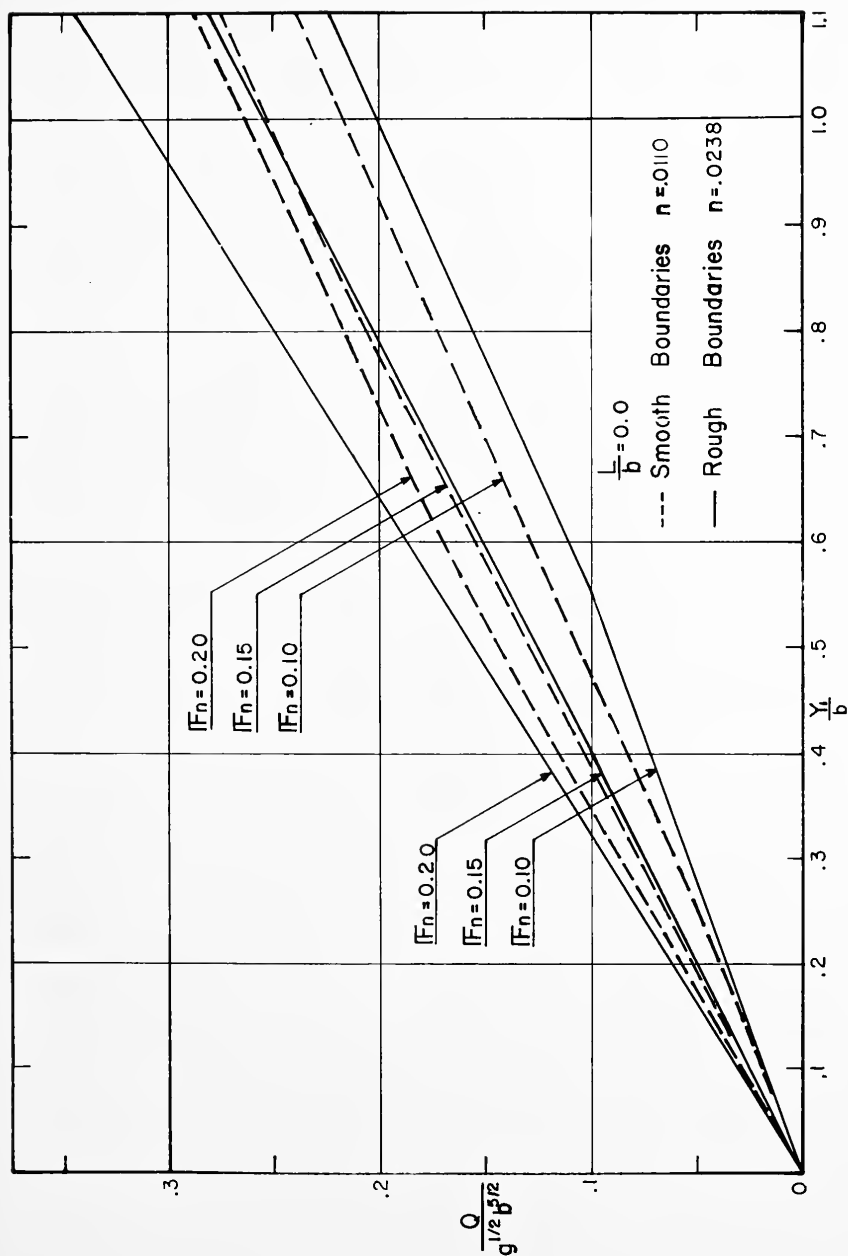


Fig 41 Comparison of Dimensionless Curves for Geometry Ia for Smooth and Rough Boundaries



centrate on high approach velocities and agitating the turbulence in the flow. This way more air entrainment is obtained and hence more security of getting a full conduit flow through the constriction.

The separation effect can also be greatly reduced by use of rounded inlet sections, tapered transition sections or equivalent inlet structures as shown by J. L. French²³. He also conducted experiments indicating that full conduit flow in corrugated barrels occurred at appreciably lower pool levels than in smooth wall barrels with the same inlet structure. These observations made by French shows the same trend as those made by the author in the present study of the flow behavior for submerged arch bridge constrictions.

To improve the flow through submerged constrictions or culverts the ability of the constriction to produce full flow must be perfected. From the above discussion of the observations it can be summarized that the following characteristics are of essence.

- 1) Reduction of separation effects through the inlet.
- 2) Changes in the geometry of the approach channel.
- 3) Increase in air entrainment at the inlet and in the barrel.
- 4) Reduction in vortex formation above the inlet.
- 5) Reduction in air inflow into the barrel from the constriction outlet.

The expected solutions to some of these essential characteristics were discussed above. It was not the scope of this study to investigate these suggested improvements, but further experimental work could with profit proceed in this direction.



Skewed Bridges - Geometry V-b

Rough Boundaries $n = 0.0238$

Figures 42 a and b show the flow at the outlet of a left and right skewed bridge. The discharge jet shoots to the side of the flume in a direction approximately perpendicular to the face of the bridge.

The test results are presented in the dimensionless performance curves in Figure 43, based on the theoretical equation (24) developed in Chapter III. Three sets of curves are plotted using the Froude number and the angle of skewness, ϕ_2 , as parameters. The width ratio, L/b , is kept constant at the value $L/b = 0.50$. The performance curves show that a variation in the angle of skew between $\phi_2 = 15^\circ$ and $\phi_2 = 30^\circ$ is a relative unimportant factor compared to the effect of a change in the Froude number. To be noted is also the better performance of these skewed bridge constrictions for low Froude numbers, ($F_n = 0.10$) compared to the $\phi_2 = 0.0$ constrictions of Geometry I-b. The explanation may be that the non-symmetry of the skewed bridge constriction generates more turbulence in the flow at the inlet and hence a flow condition closer to conduit flow, at a lower Froude number. As the Froude number increases and both Geometries, I-b and V-b, agitate about the same amount of turbulence in the flow, the difference in the performance curves decreases. The part of the curves having a Y_1/b ratio less than about 0.5 do not pertain to the submerged inlet cases, but are merely an expected trend of the curves for the free surface flow. A total of 24 test





FIG. 42a FLOW THROUGH LEFT SKEWED BRIDGE



FIG. 42b FLOW THROUGH RIGHT SKEWED BRIDGE



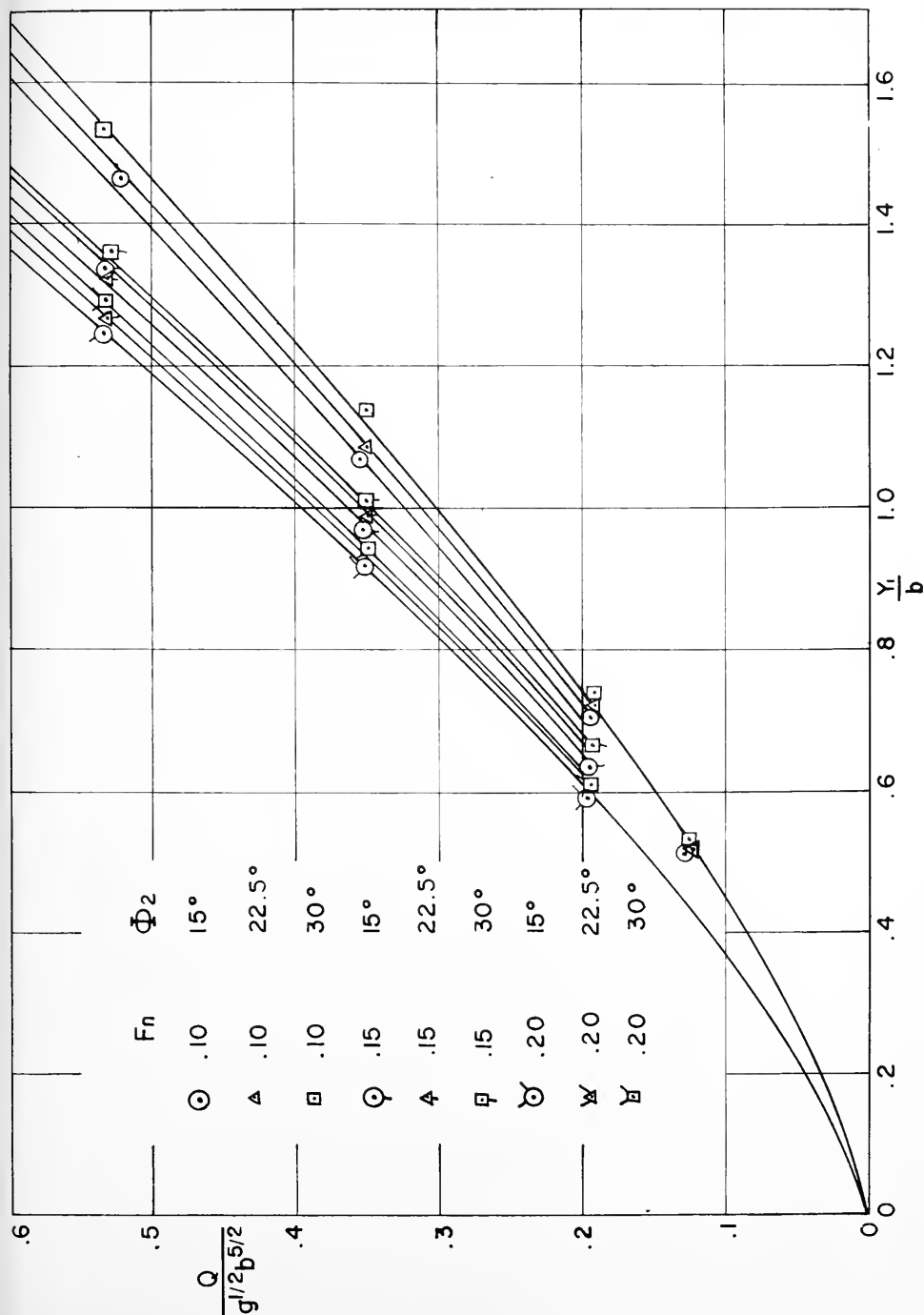


Fig.4.3 Dimensionless Curves for Geometry IIb. Rough Boundaries



runs were made on the skewed bridges. They are recorded in Tables XXIII and XXIV as test run number 232 to 255. The calculated data to plot the curves are listed in Table XXXI.

Geometry VI - Two Span Semicircular Arch Bridge Constriction

Rough Boundaries $n = 0.0238$

This Geometry represents about 11% of all existing arch bridges in the state of Indiana. The great majority of these bridge constrictions have a thickness factor, L/b , of about 0.50, which was chosen for the experimental models of Geometry VI.

The test results are presented in the dimensionless graphs shown in Figure 44. To be noted is that the opening width of the models, b , is the width of one of the openings. The performance of the models in Geometry VI is approximately the same as for Geometry I-b of same thickness factor.

A total of 27 test runs were made and the data taken are recorded in test runs no. (256 - 282) as shown in Tables XXIV - XXVI. The calculated values are presented in Table XXXI.

Geometry VII - Segment Arch Bridge

Rough Boundaries $n = 0.0238$

With reference to Figures 4 and 5, it is readily seen that the dimensionless relationship of the discharge as a function of the backwater depth and the width of the constriction holds true also for the segment arch openings. The curves shown in Figure 45 are based on this relationship as expressed in Equation (24), derived in Chapter III. A total of 22 test runs were done and recorded in



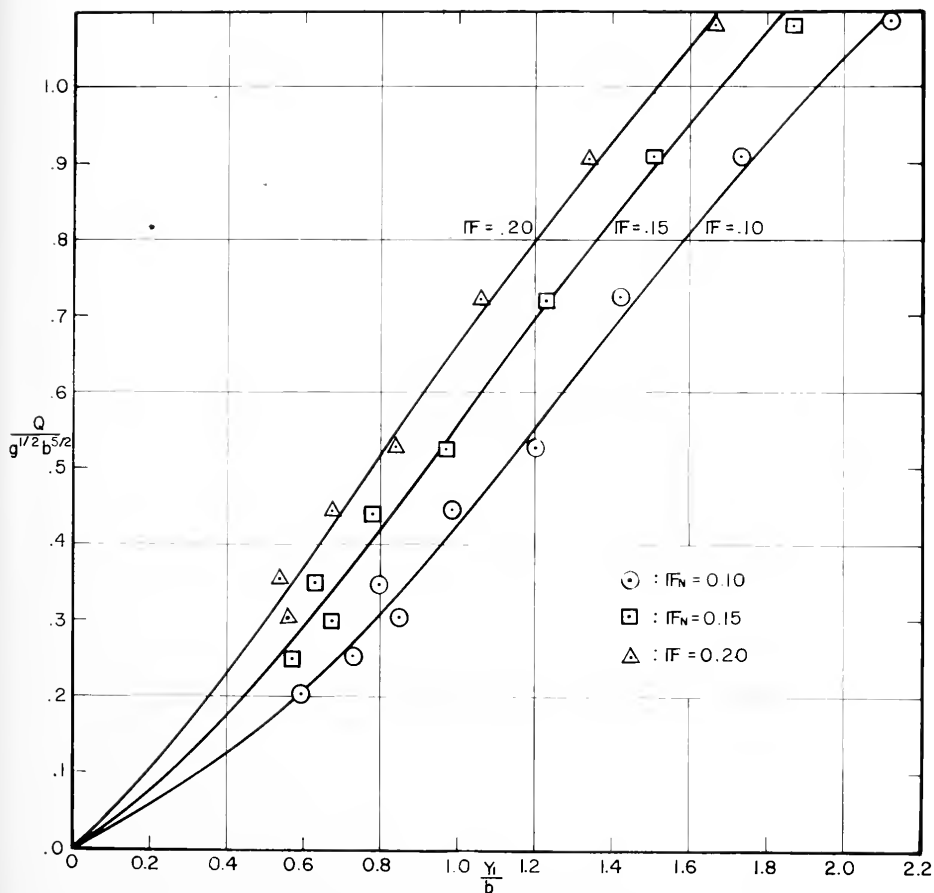


FIG 44 DIMENSIONLESS CURVES FOR GEOMETRY VI USING IF_n AS PARAMETER, ROUGH BOUNDARIES



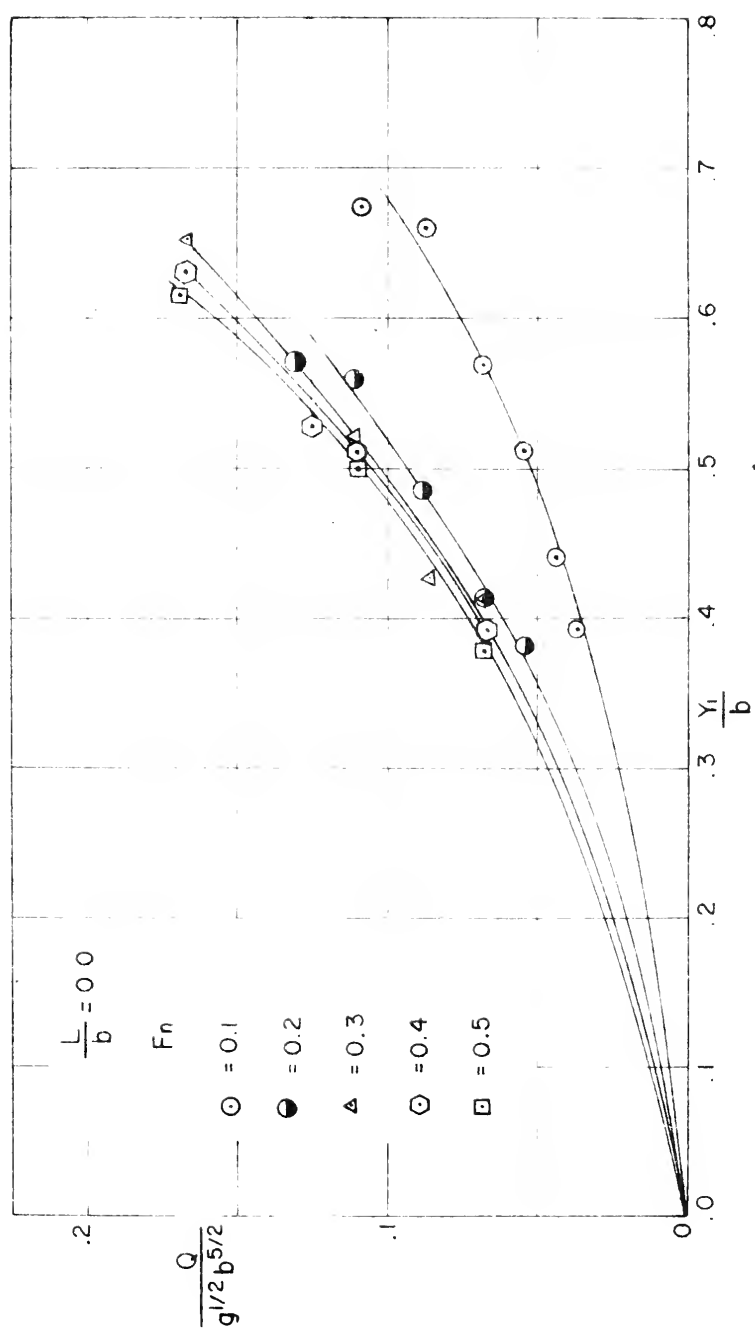


Fig. 4.5 Dimensionless Curves for Geometry VII

Rough Boundaries

Tables XXVI - XXVII. The calculated values are found in Table XXXI.

Figure 45 shows that the spacing between the curves become very small as the Froude number increases beyond 0.3. This means that the Froude number becomes insignificant as a parameter when the degree of turbulence increases beyond a certain value ($F_n > 0.3$).

Head Loss Considerations

In the theoretical analysis in Chapter III an expression for the additional head loss coefficient due to the bridge constriction was found, Equation (35).

$$K = \frac{h_1^*}{V_0^2/2g} - \alpha \left[\left(\frac{A_0}{A_y} \right)^2 - \left(\frac{A_0}{A_1} \right)^2 \right] \quad (35)$$

This equation, which holds for submerged bridge constrictions is similar to the one derived by Izzard²⁴ for free surface flow through a bridge constriction, and K varies primarily with

- a) The channel opening ratio M'
- b) Type and shape of bridge constriction such as inlet shape, wing wall angle ϕ_1 , skewness angle ϕ_2 and thickness factor, L/b
- c) Number of bridge spans, N
- d) Eccentricity of bridge opening, e
- e) Froude number F_n

Other variables of less effect may however have a cumulative effect upon the head loss coefficient depending on the problem at hand. The head loss coefficient K was computed on the IBM 7090 from Equation (35). The corresponding value of the channel opening ratio



M' was also computed, and by a least mean square routine the slope of the line of the plot K versus M' was found in arithmetic scale. A significant value such as L/b , ϕ_2 and N was used as parameters both for smooth and rough boundary tests. The plot of these curves are shown in Figures 46 to 55.

For the smooth boundaries a sufficient number of data was available to use the least square method on the computer. In the case of rough boundaries, however, the data available for each parameter were not always sufficient and some of the lines had to be fitted by eye.

The data used for the calculations are listed in runs 101 - 306 presented in Tables XVI - XXVII. The calculated values from the computer are listed in tables XXX and XXXI.



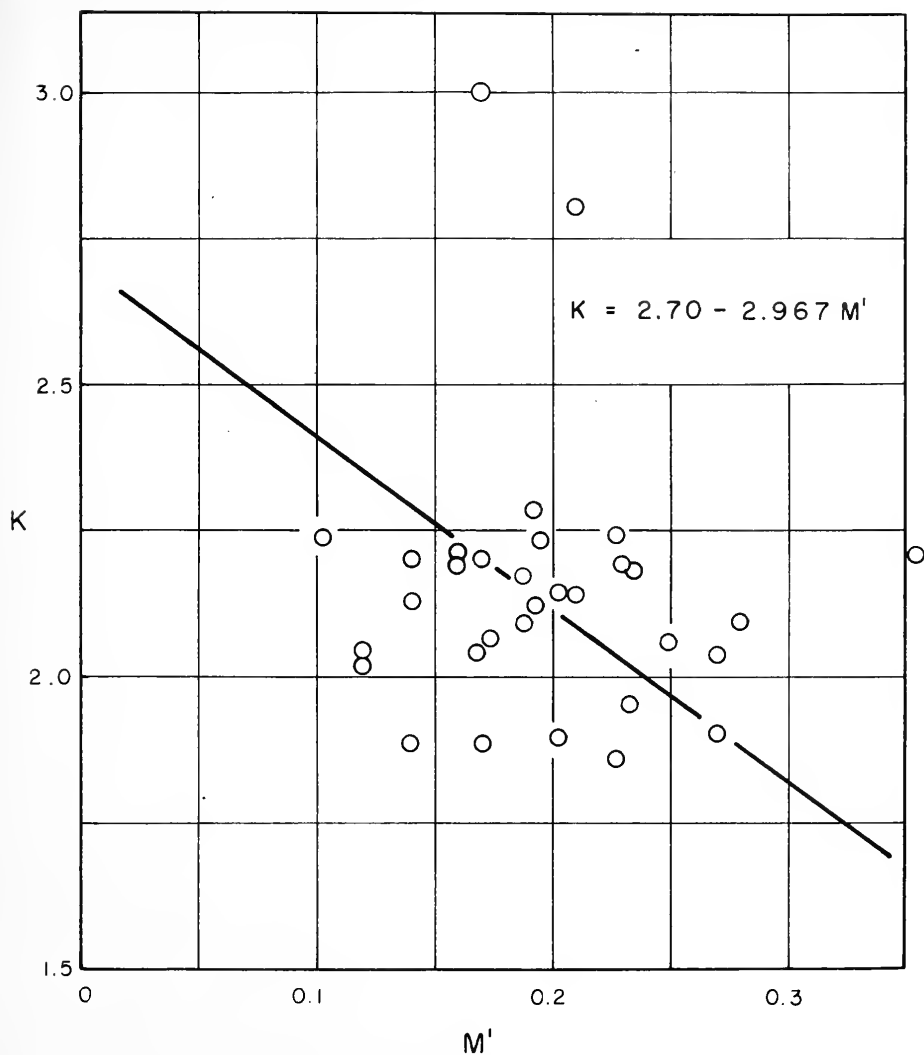
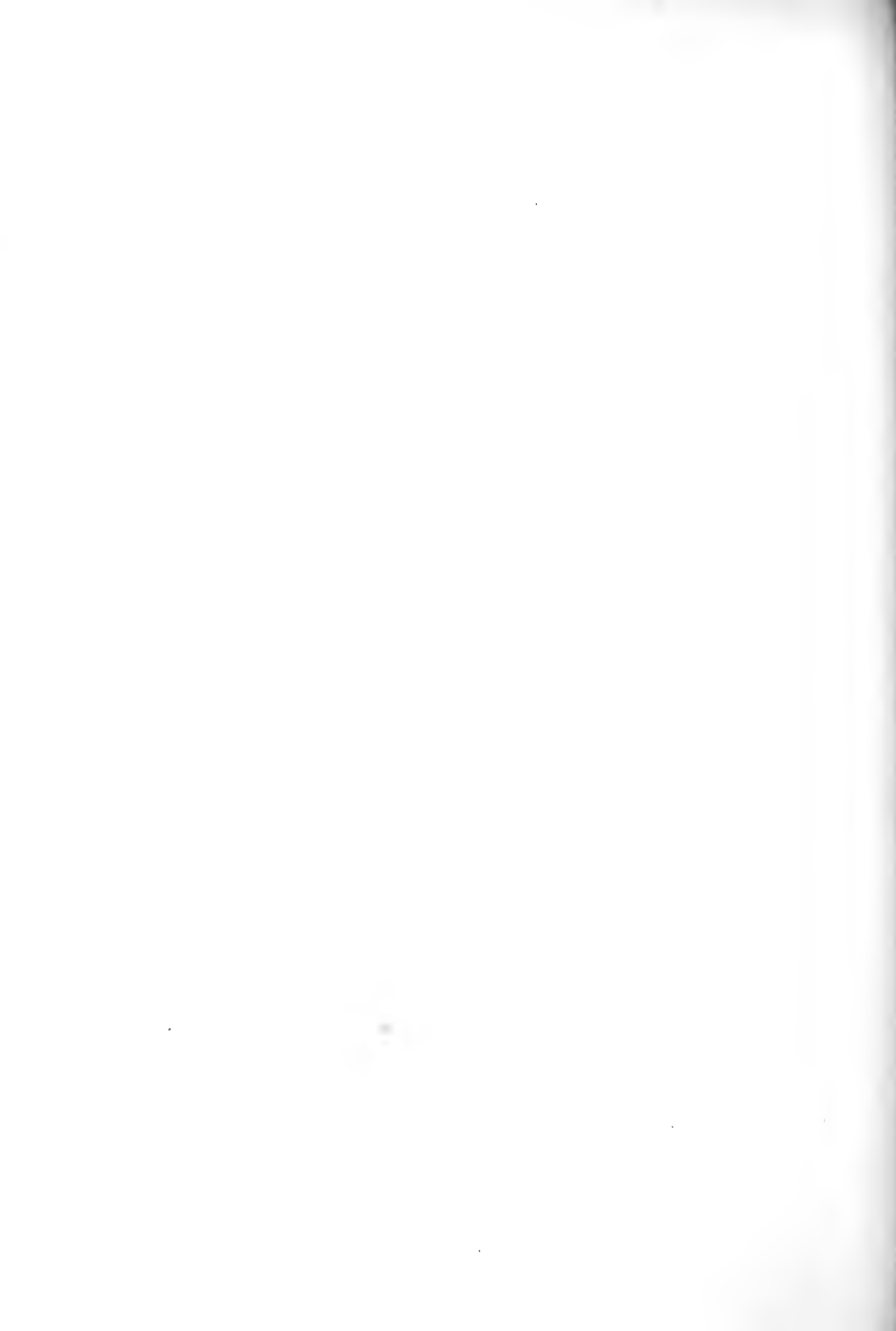


FIG. 46 HEAD LOSS COEFFICIENT FOR GEOMETRY
Ia SMOOTH BOUNDARIES, $\frac{L}{b} = 0.0$



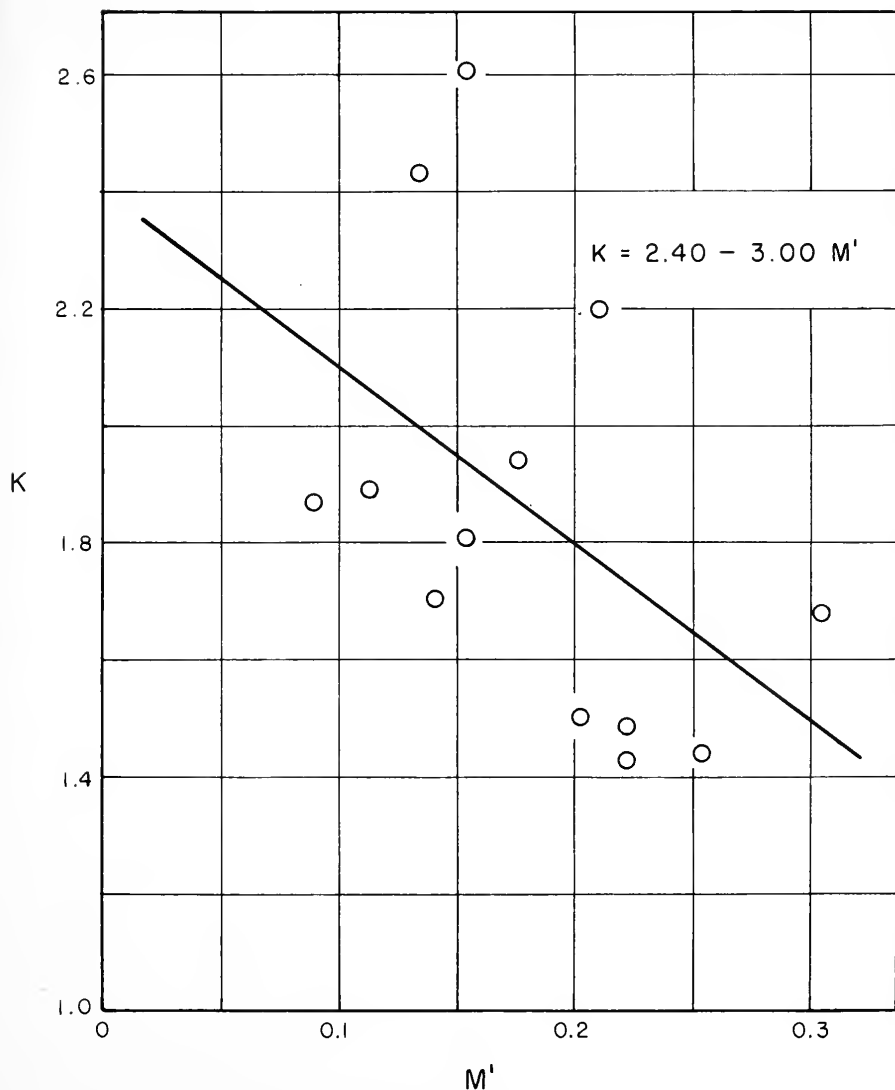


FIG. 47 HEAD LOSS COEFFICIENT FOR GEOMETRY

I_b SMOOTH BOUNDARIES, $\frac{L}{b} = 0.25$



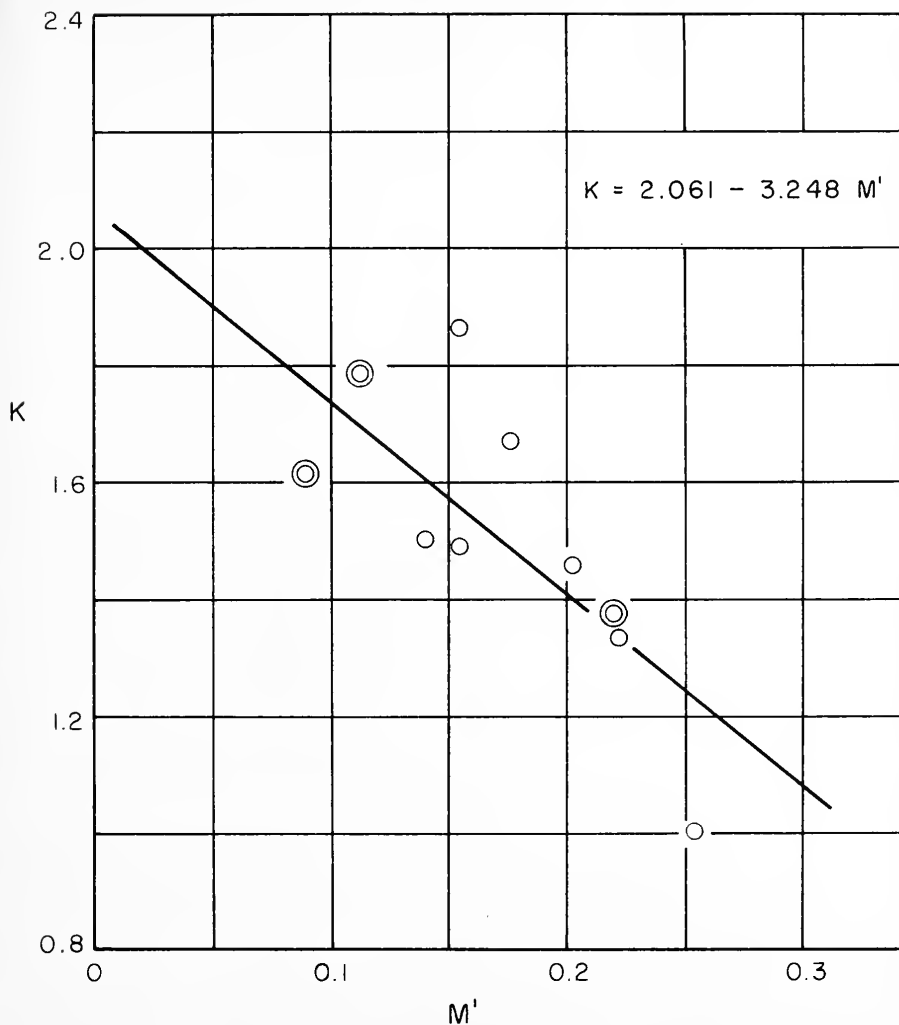


FIG. 48 HEAD LOSS COEFFICIENT FOR GEOMETRY

I_b SMOOTH BOUNDARIES, $\frac{L}{b} = 0.50$



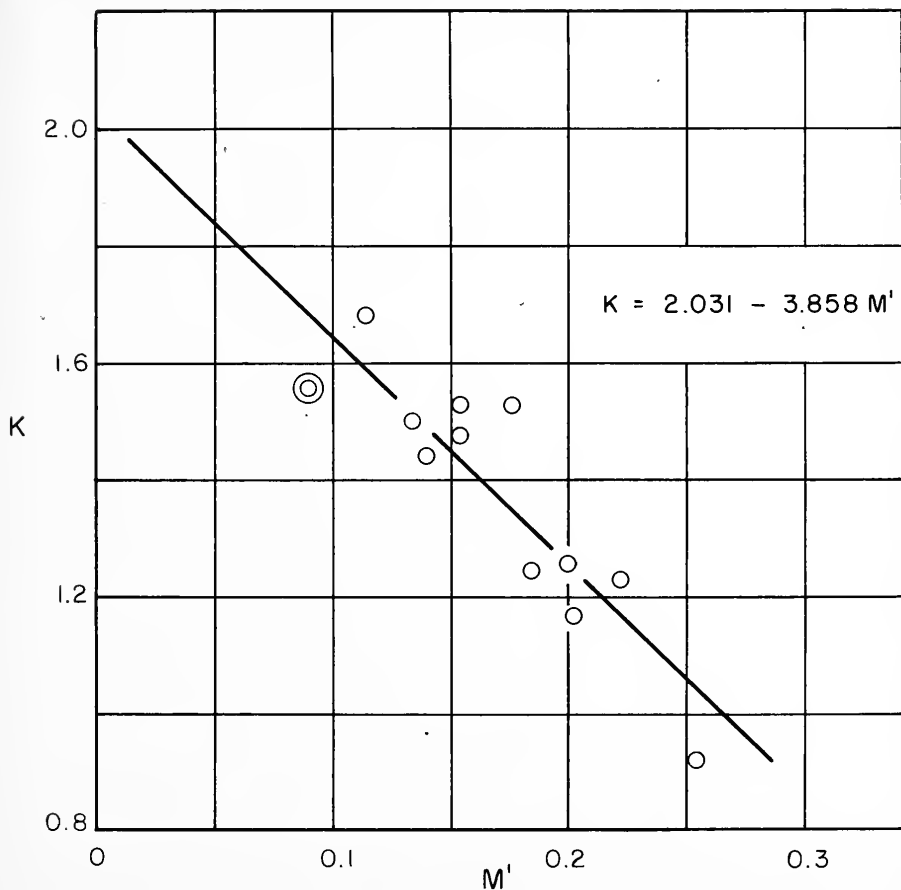


FIG. 49 HEAD LOSS COEFFICIENT FOR GEOMETRY

I_b SMOOTH BOUNDARIES, $\frac{L}{b} = 0.75$



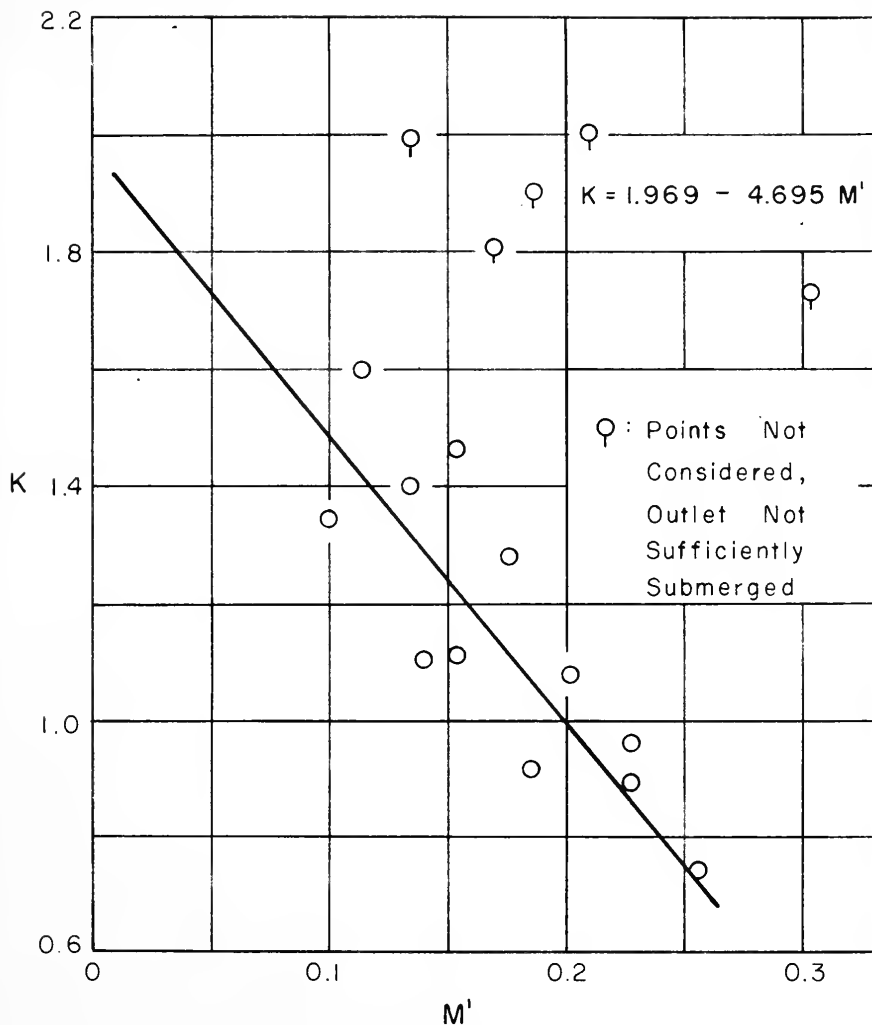


FIG. 50 HEAD LOSS COEFFICIENT FOR GEOMETRY

 I_b , SMOOTH BOUNDARIES, $\frac{L}{b} = 1.00$



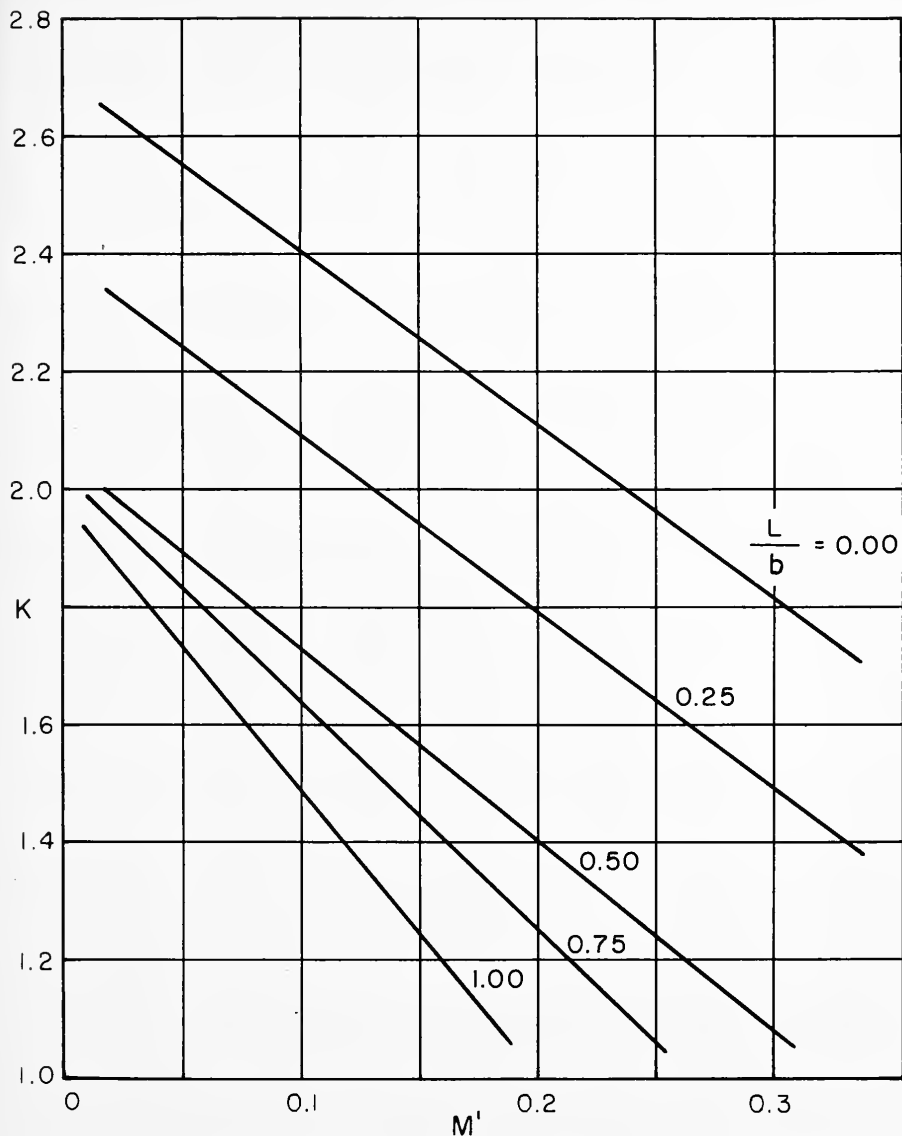


FIG. 51 SUMMARY OF HEAD LOSS COEFFICIENT CURVES FOR GEOMETRIES I_a , & I_b , SMOOTH BOUNDARIES



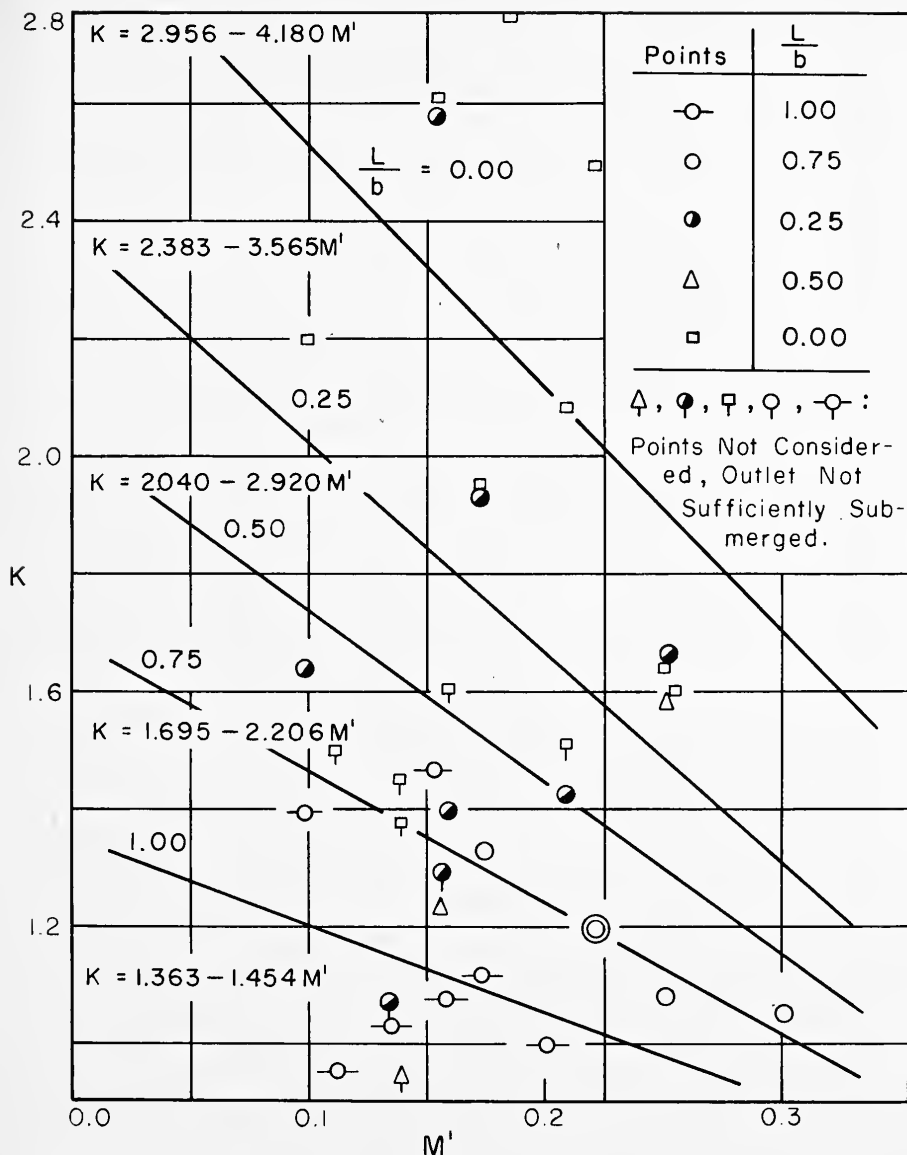


FIG. 52 HEAD LOSS COEFFICIENT CURVES FOR GEOMETRIES I_a , & I_b , ROUGH BOUNDARIES



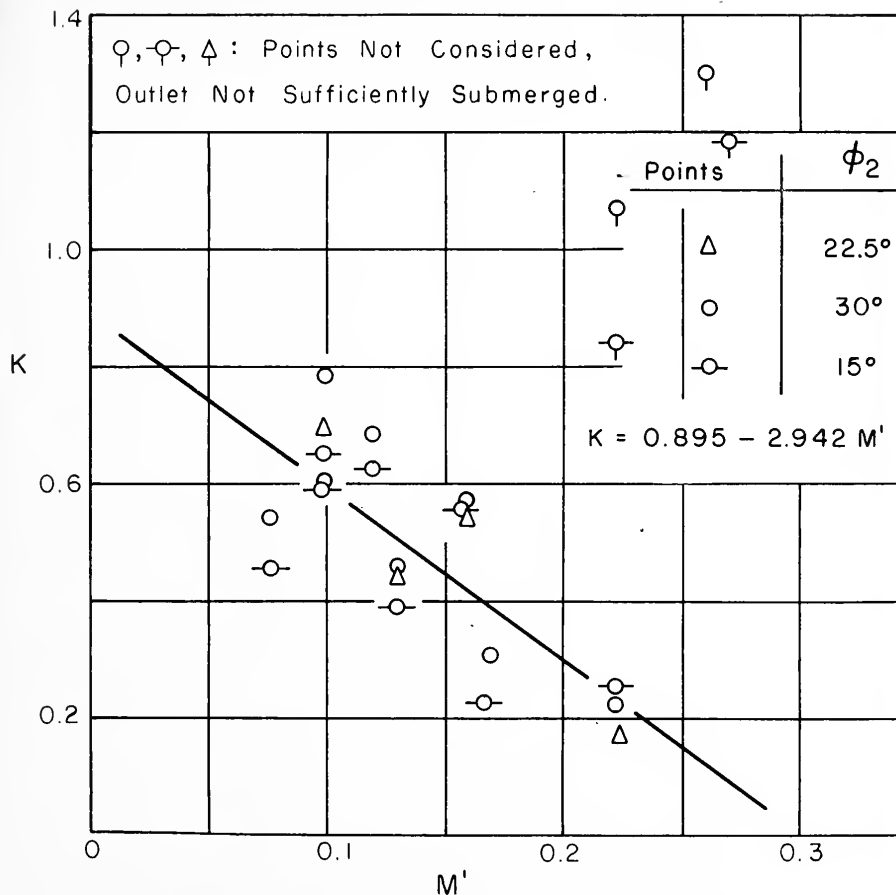


FIG. 53 HEAD LOSS COEFFICIENT CURVE FOR
GEOMETRY ∇_b , ROUGH BOUNDARIES

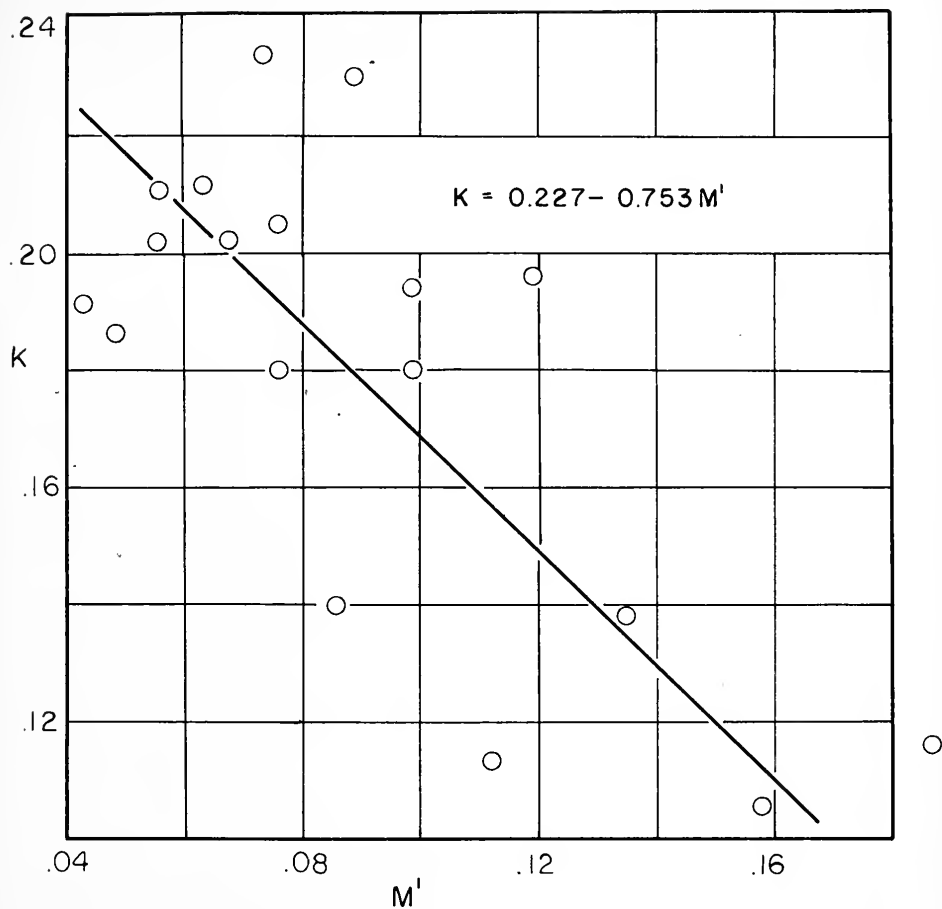


FIG. 54 HEAD LOSS COEFFICIENT CURVE FOR GEOMETRY VI, ROUGH BOUNDARIES

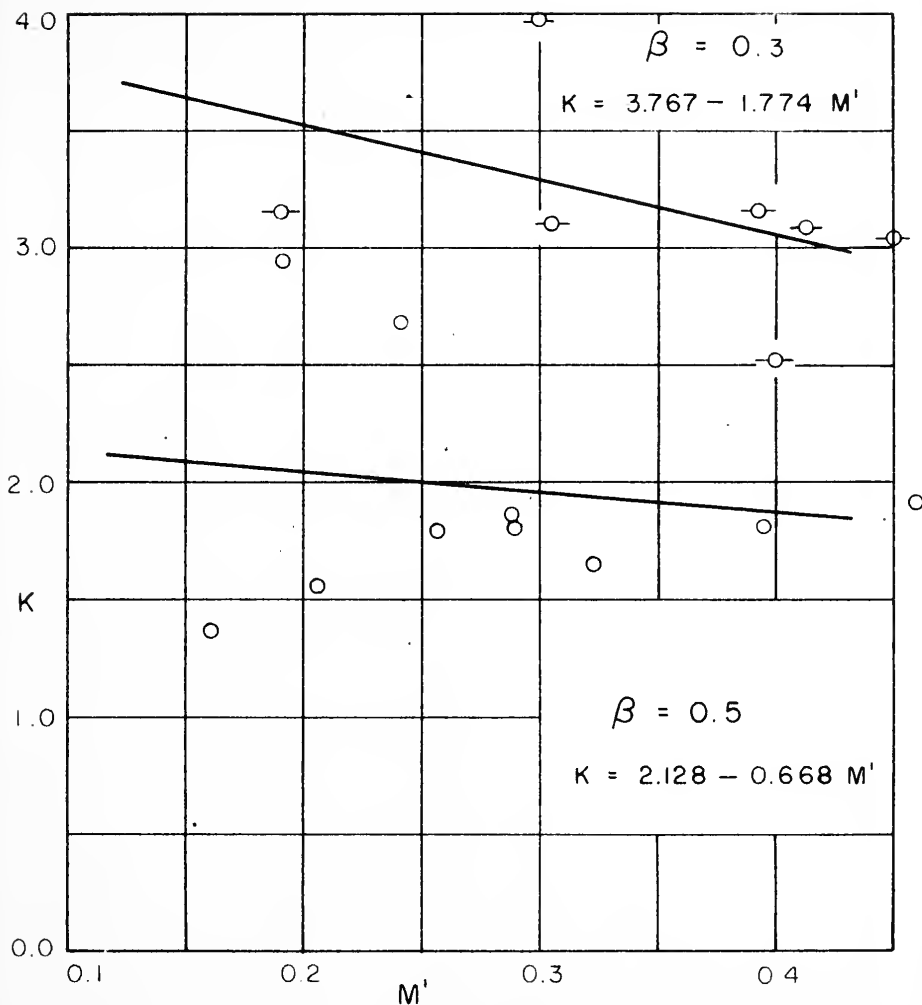


FIG. 55 HEAD LOSS COEFFICIENT CURVES FOR
GEOMETRY VII, ROUGH BOUNDARIES



General Backwater Equations for Geometries I-a,

I-b, V-b, VI and VII - Smooth and Rough Boundaries

The theoretical development of these equations was done in Chapter III, and earlier in this chapter the generalized backwater equation

$$\frac{Y_1}{Y_n} = C \left[\left(\frac{F_n}{M^*} \right)^2 \right]^\gamma \quad (36)$$

was plotted for the case of fully submerged discharge jet in the form (see Figure 33)

$$\frac{Y_1}{Y_n} - 1 = C \left[\left(\frac{F_n}{M^*} \right)^2 \right]^\gamma \quad (37)$$

If h_1^* is substituted for $Y_1 - Y_n$, equation (37) can be written in the following form:

$$\frac{h_1^*}{Y_n} = C \left[\left(\frac{F_n}{M^*} \right)^2 \right]^\gamma \quad (38)$$

This is the presentation used in the graphs at the end of this section. Figures 55 to 64 present the generalized backwater equations for the geometries considered. Significant values of the geometries are used as parameters.

Values for $\frac{h_1^*}{Y_n}$ and $\left(\frac{F_n}{M^*} \right)^2$ were calculated in the same computer program as used for the head loss considerations in the previous section. These points were to be plotted on a log log scale, so the computer program was also written to determine the slope of the best fitting line through these points. A least mean square routine for



log log plots was used (see Appendix C). For the smooth boundaries a sufficient number of data was available to use the least square method in finding the slope of the lines. In the case of rough boundaries, however, there was sometimes necessary to fit the lines by eye from the few data available.

The data used for the calculations are listed in runs 101 - 306, presented in Tables XVI - XXVII. The calculated values are listed in Tables XXX and XXXI.

There are some advantages in doing all these calculations in one computer program. Only one set of data has to be prepared and the computer stores the values in the memory once. The computer time used, therefore, becomes a minimum. For all the calculations pertaining to the figures (46 - 65) the time used by the IBM 7090 was less than 10 minutes.



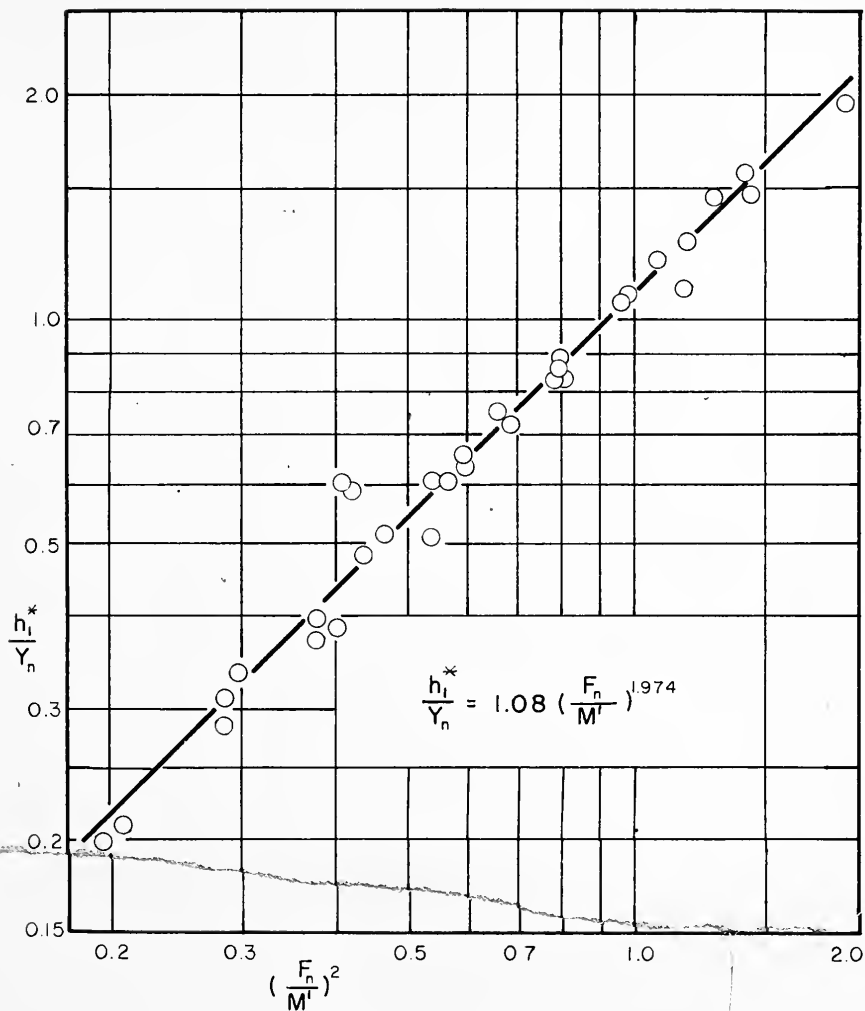


FIG. 56 GENERALIZED BACKWATER RATIO GEOMETRY

Ia, SMOOTH BOUNDARIES, $\frac{L}{b} = 0.0$



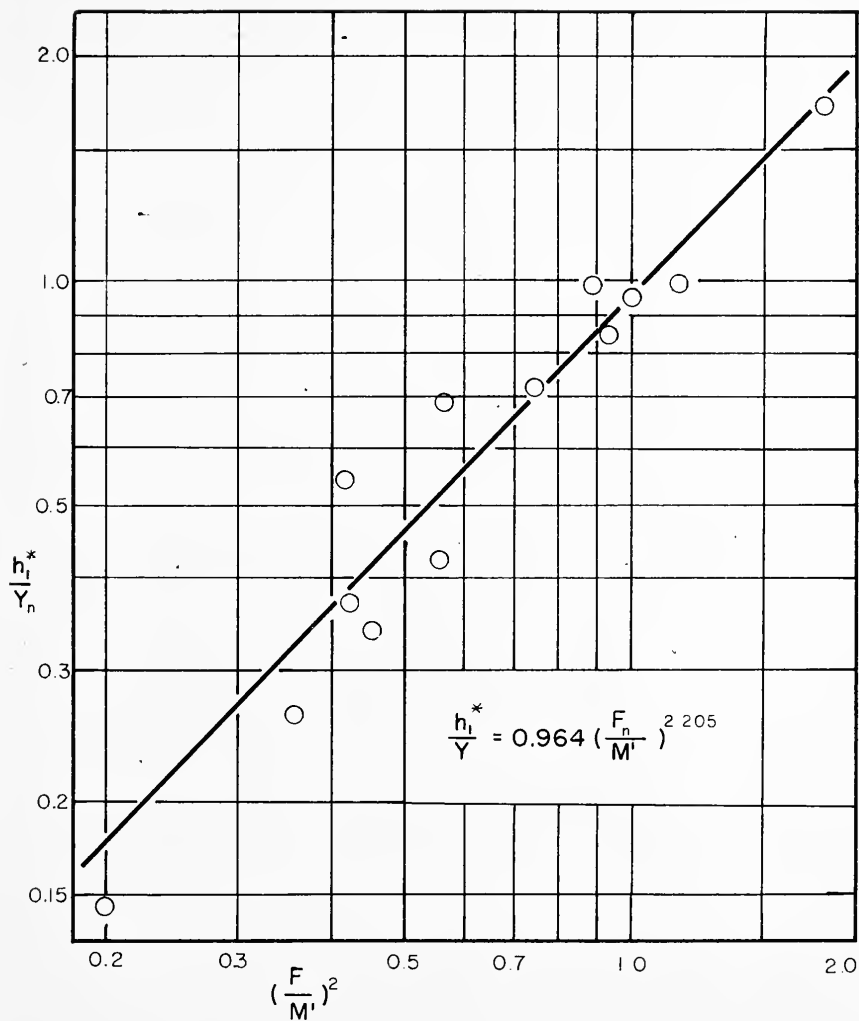


FIG. 57 GENERALIZED BACKWATER RATIO GEOMETRY
 Ib, SMOOTH BOUNDARIES, $\frac{L}{b} = 0.25$



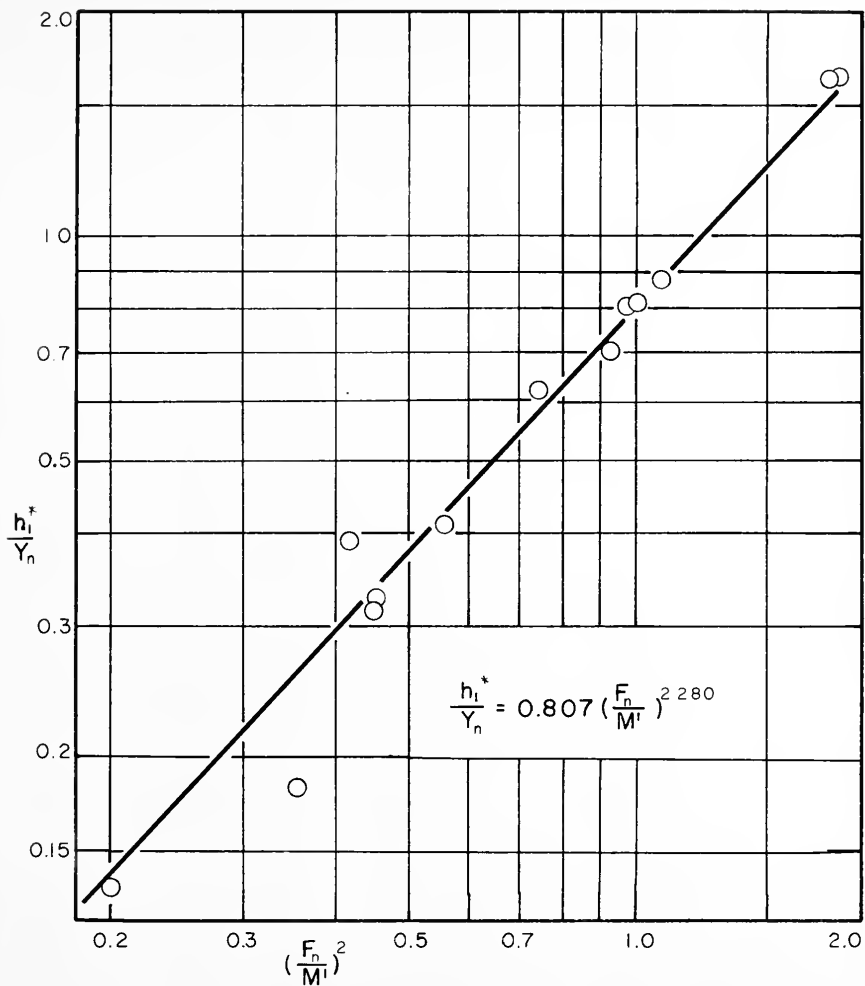


FIG. 58 GENERALIZED BACKWATER RATIO GEOMETRY
 1b, SMOOTH BOUNDARIES, $\frac{L}{b} = 0.50$



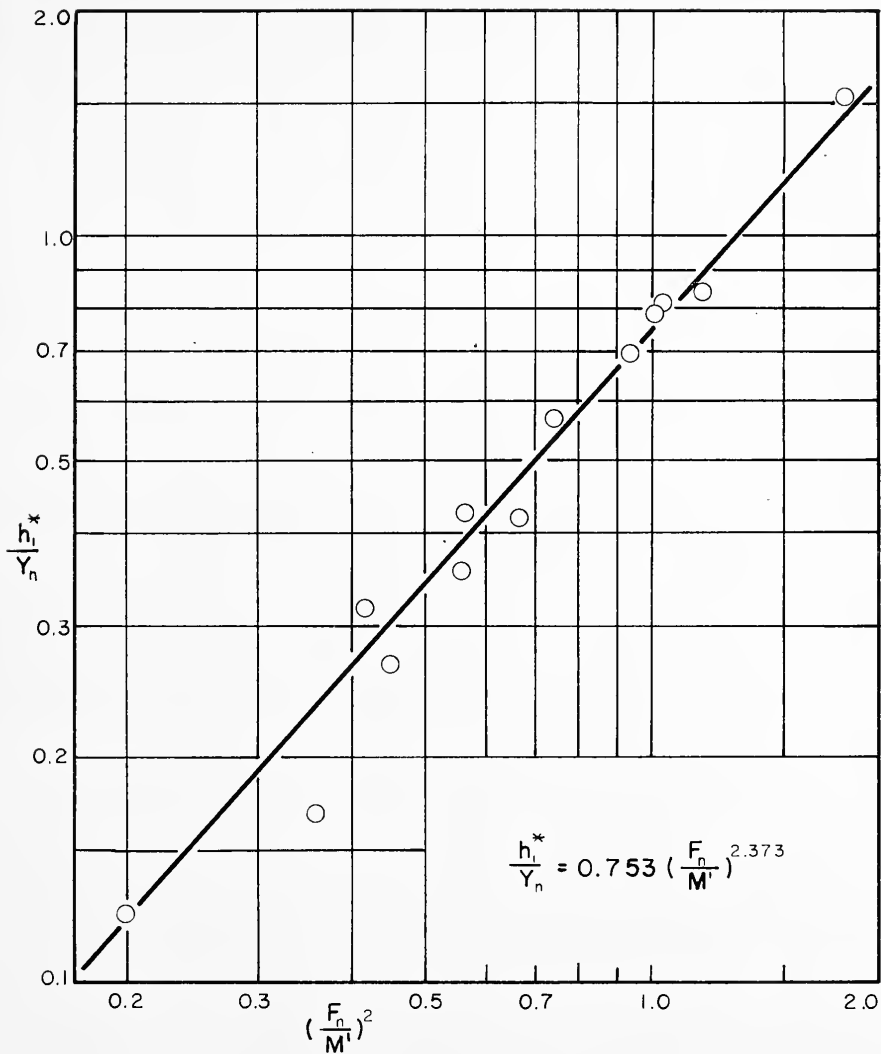


FIG. 59 GENERALIZED BACKWATER RATIO GEOMETRY
Ib, SMOOTH BOUNDARIES, $\frac{L}{b} = 0.75$

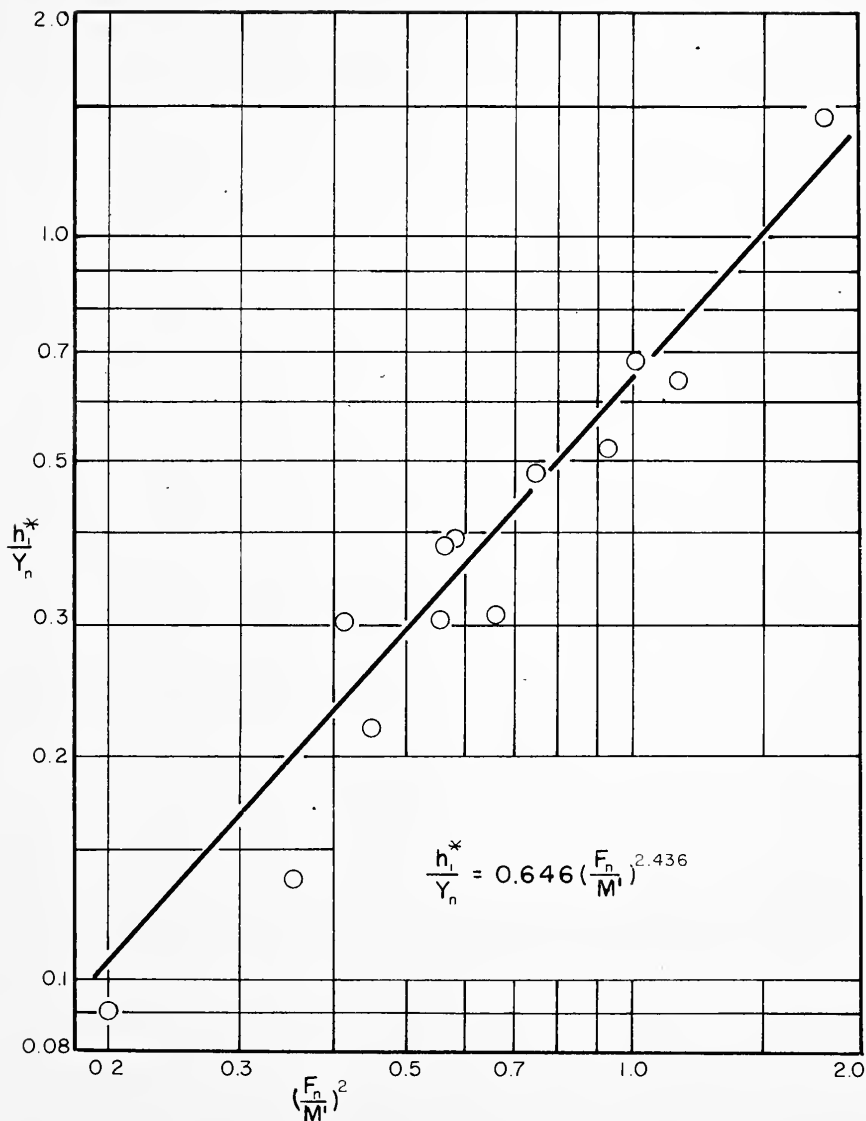


FIG. 60 GENERALIZED BACKWATER RATIO GEOMETRY
 1b, SMOOTH BOUNDARIES, $\frac{L}{b} = 1.0$



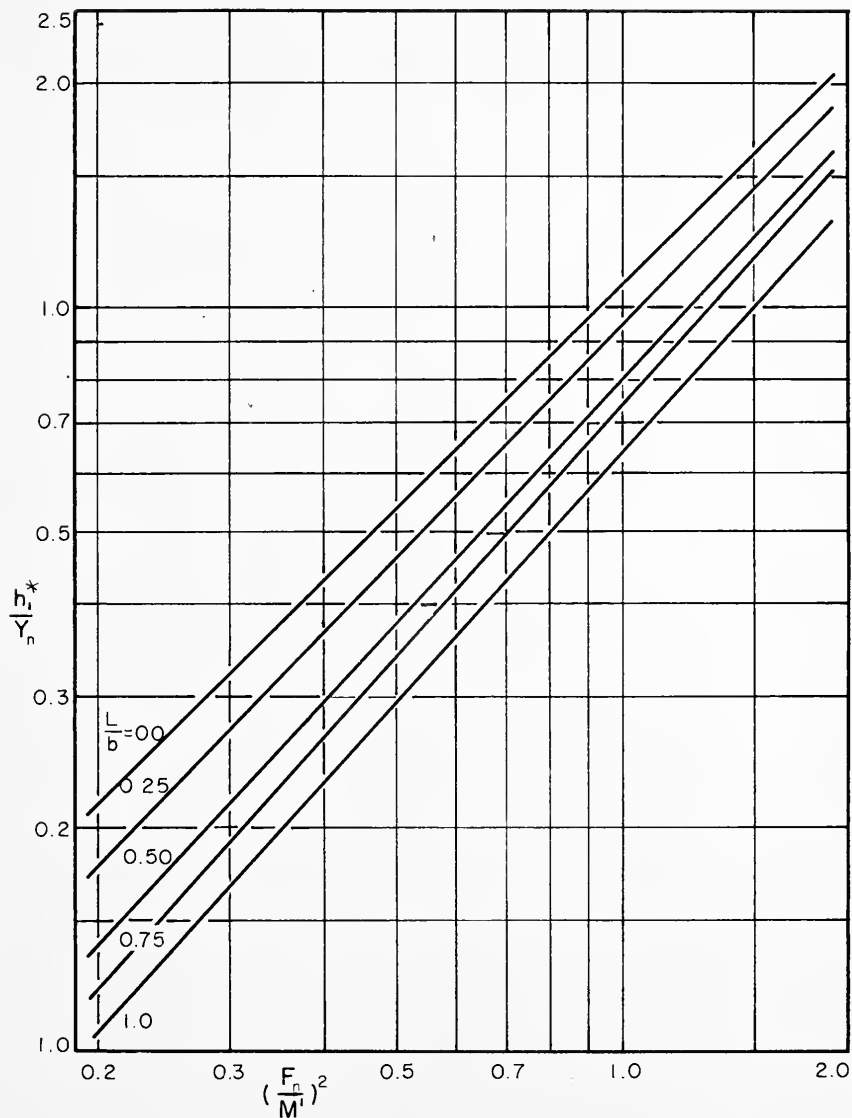


FIG. 61 SUMMARY OF BACKWATER RATIO CURVES FOR GEOMETRIES Ia AND Ib, SMOOTH BOUNDARIES



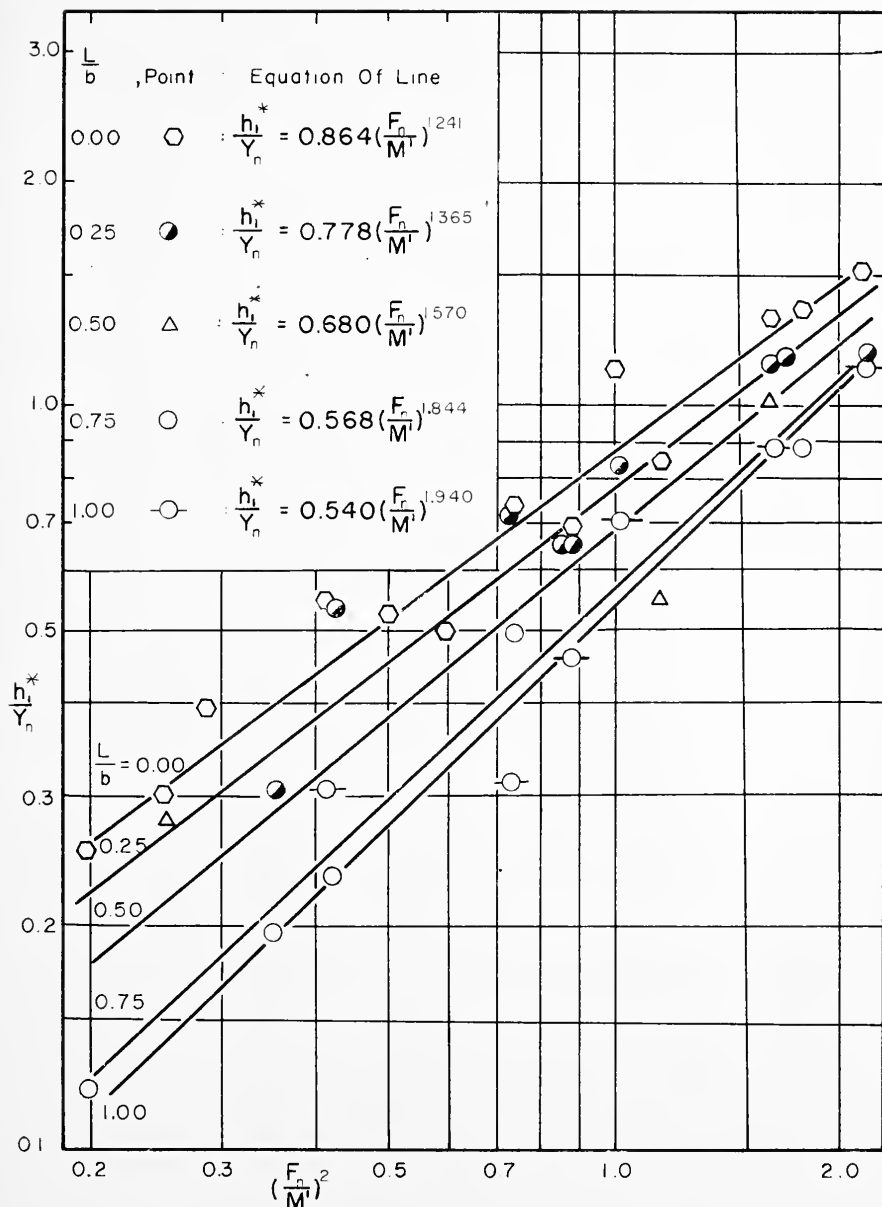


FIG. 62 GENERALIZED BACKWATER RATIO GEOMETRIES
Ia AND Ib, ROUGH BOUNDARIES

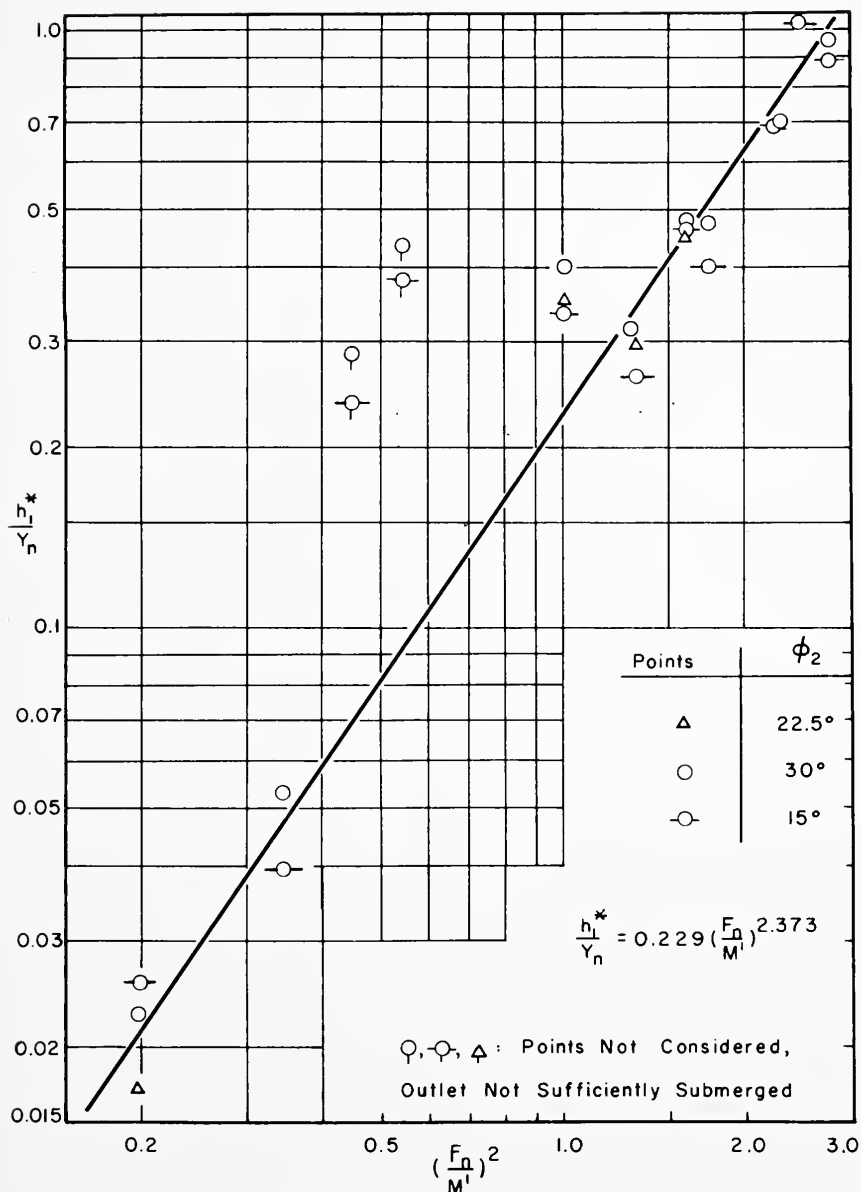


FIG. 63 GENERALIZED BACKWATER RATIO GEOMETRY ∇b ,
ROUGH BOUNDARIES



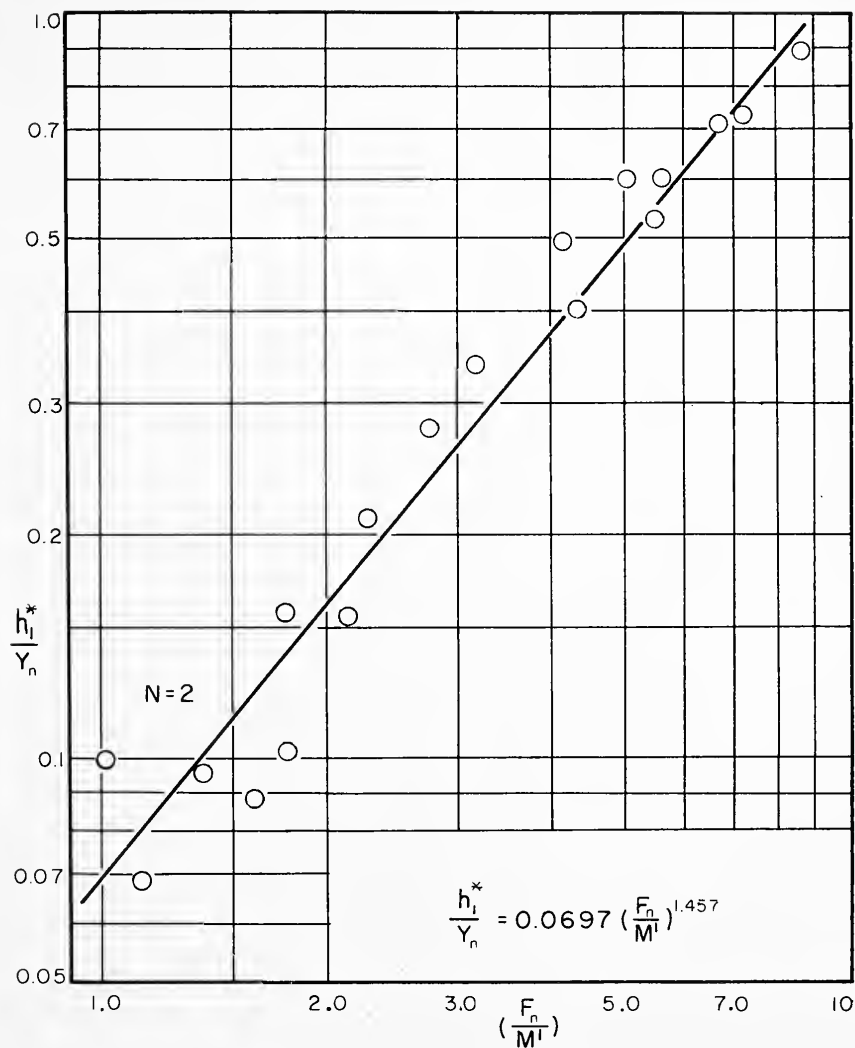


FIG. 64 GENERALIZED BACKWATER RATIO GEOMETRY
VI, ROUGH BOUNDARIES



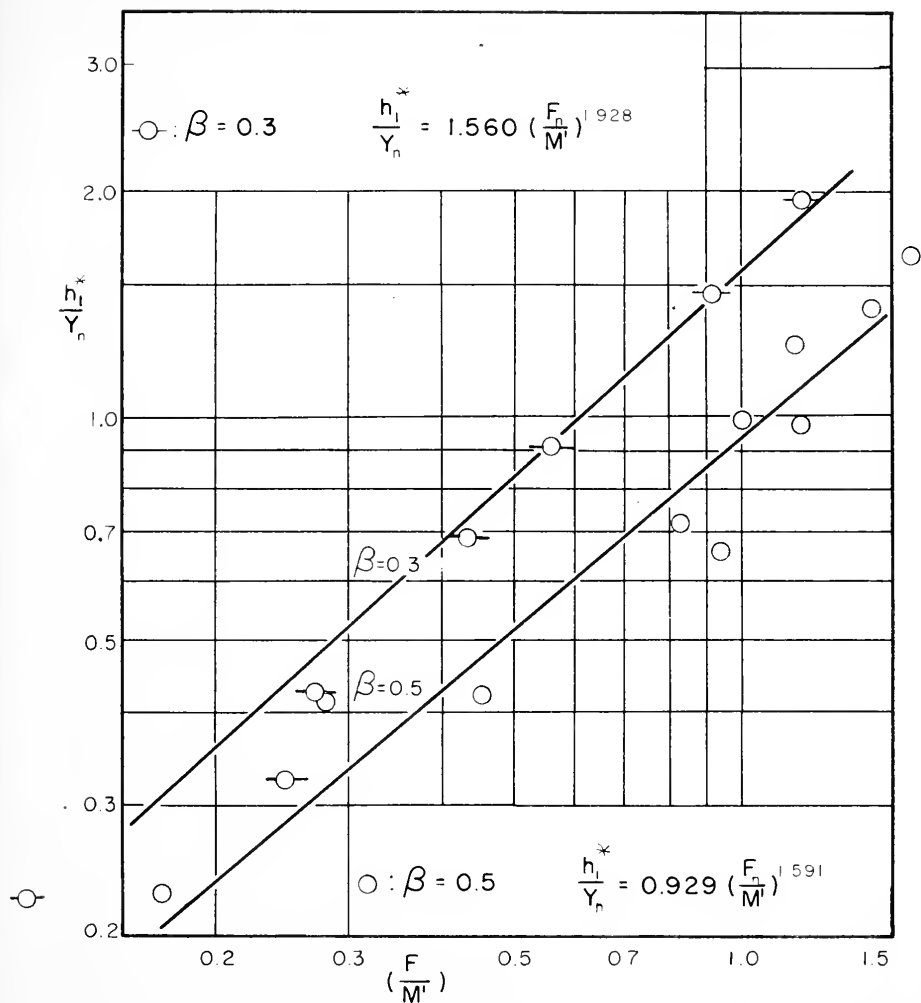


FIG. 65 GENERALIZED BACKWATER RATIO GEOMETRY
VII, ROUGH BOUNDARIES



CHAPTER VIII

FINDINGS, CONCLUSIONS AND RECOMMENDATIONS

The results of this report are applicable to bridges with submerged inlet and geometries I-a, I-b, V-b, VI and VII (see definition of geometries in Chapter V and figure 24). No eccentricity, entrance rounding or wing walls are counted for.

Findings

1. Equation of discharge for orifice type flow through a semi-circular submerged bridge constriction.
2. Semi-empirical expression for the occurrence of free surface flow and orifice type flow through the bridge opening.
3. Graphs presenting the discharge as a function of the ratio of the backwater depth to the arch span.
4. Graphs showing the ratio of the backwater to the normal depth as a function of the normal depth Froude number and the channel opening ratio.
5. Empirical generalized backwater equations derived for the several geometries from the graphs in point 4.
6. Graphs giving the value of the constriction head loss coefficient as a function of the channel opening ratio for the different test geometries.



Conclusions

7a. The backwater at submerged arch bridge constrictions perpendicular to the stream decreases as the length of the bridge in the direction of flow increases.

7b. For equal bridge length the backwater due to submerged arch bridges is further decreased when the constriction is skewed with respect to the direction of flow, at least for skew angles up to 30° .

8. The value of the head loss coefficient due to a submerged arch bridge constriction is independent of the normal depth Froude number as long as both inlet and outlet of the bridge are submerged.

9. For hydraulically short submerged arch bridges (that is where the barrel is not sufficiently long to allow the expanding depth of flow below the contraction to raise and fill the barrel), the backwater depth decreases for an increase in the normal depth Froude number.

10. To obtain a minimum backwater depth at a submerged arch bridge constriction the barrel should flow full (full conduit flow).

Recommendations

11. Further experiments as to the value of the head loss coefficient through different types of bridge constrictions including eccentricity, wing walls, entrance rounding and roughening of the inlet section.

12. Investigation of the separation and vortex phenomena at the bridge inlet.

BIBLIOGRAPHY



BIBLIOGRAPHY

1. Husain, S. T., "Preliminary Model Investigations of Hydraulic Characteristics of River Flow Under Arch Bridges," Masters Thesis, Purdue University, 1959.
2. Owen, H. J., "Design and Construction of Hydraulic Flume and Backwater Effects of Semi-Circular Constrictions in a Smooth Rectangular Channel," Masters Thesis, Purdue University, 1960.
3. Sooky, A. A., Husain, S. T., Owen, H. J. and Delleur, J. W., "Hydraulics of River Flow Under Arch Bridges - A Progress Report," Progress Report submitted to the Board of the Joint Highway Research Project, May 14, 1959, Purdue University.
4. Biery, P. F., "Hydraulics of Single Span Arch Bridge Constrictions," Masters Thesis, Purdue University, 1961.
5. Chang, T. P., Monthly Progress Report (49) Joint Highway Research Project, Purdue University.
6. Binnie, A. M., "The Flow of Water under a Sluice-Gate," Quart J. Mechn, appl. Math 5, Part 4, pp. 395-407, December 1952. AMR 6-2256.
7. Franke, P., "Jet Contraction in Flow under Sluice Gates in Rectangular Channels," Bautechnik 32, 8, pp. 257-259, August 1955, AMR 9-2240.
8. Albertson, M. L., Jensen, R. A., Dai, Y. B., and Rouse, H., "Diffusion of Submerged Jets," Trans. ASCE Vol. 115 (1950) pp. 639-697.
9. Henry, H. R., Discussion on Submerged Jets, Trans. ASCE Vol. 115 (1950) pp. 687-694.
10. Gibbings, J. C., and Dixon, J. R., "Two Dimensional Contracting Duct Flow," Quart Mech. Appl. Math. 10, 1, 24-41, Feb., 1957, AMR 10-2945, Sept. 1957.
11. Rouse, H., "Engineering Hydraulics," John Wiley and Sons, Inc., New York, 1949, Chapter I.
12. Rouse, H., Abul-Fetouh, A. H., "Characteristics of Irrotational Flow Through Axially Symmetric Orifices," Journ of appl Mich. Vol. 17, No. 4, Dec. 1950, Trans. ASME, Vol. 1743, pp. 421.



13. Von Mises, R., "Berechnung von Ausfluss und Überfallzahlen," Zeitschrift VDI, Vol. 61, 1947, pp. 447.
14. Chaturvedi, M. C., "Flow Characteristics of Axisymmetric Expansions," ASCE Proceedings, Vol. 89, No. HY3, May 1963, Part 1, pp. 61-92.
15. Highway Research Board, "Culvert Hydraulics," Research Report 15-B, National Academy of Sciences - National Research Council, publication no. 287, January 1953.
16. Highway Research Board, "Culvert-Flow Characteristics," Bulletin 126, National Academy of Science - National Research Council, publication no. 413, January 1956.
17. Rouse H., Metzler, D. E., "Hydraulics of Box Culverts," Bulletin 39, State University of Iowa, 1959.
18. Myers, G. E., Schaner, J. J. and Eustis, R. H., "Plane Turbulent Wall Jet Flow Development and Friction Factor," Trans. ASME, Series D., March 1963, pp. 47-54.
19. Chow, V. T., "Open Channel Hydraulics," McGraw-Hill Book Co., Inc., New York, 1959, Chapter 9.
20. Delleur, J. W., Biery, P. F., "Roughness Spacing in Rigid Open Channels," Report no. 5., Joint Highway Research Project, Purdue University, June 1961.
21. Streeter, V. L., "Fluid Dynamics," McGraw Hill Book Co., New York, 1948, pp. 174-177.
22. Kirchhoff, G. R., "Zur Theorie Freier Flüssigkeitsstrahlen," Crelle's Journal 1869.
23. French, J. L., "Hydraulics of Improved Inlet Structures for Pipe Culverts," Fourth Progress Report on Hydraulics of Culverts. National Bureau of Standards Report 7178, August 1961, p. 104, Also: First, Second and Third progress reports, National Bureau of Standards Report, 4444, 4911, 5306, respectively.
24. Izzard, C. F., Discussion of "Tranquil Flow Through Open-Channel Constrictions," by C. E. Kindswater and R. W. Carter, Trans. ASCE, Vol. 120, 1955, pp. 985-9.

APPENDIX A

NOTATIONS



APPENDIX A

NOTATIONS

SYMBOL	DIMENSIONS	DEFINITION
A	L^2	Area
A_1	L^2	Total depth water area at section 1, $A_1 = BY_1$
A_{n1}	L^2	Normal depth water area, $A_{n1} = BY_n$
A_{n2}	L^2	Total depth flow area at section 2
A_o	L^2	Area of bridge opening
B	L	Rectangular channel width
b^1	L	Diameter of circle of which the arch segment is a part
b	L	Span width at the springline of the arch
C		A coefficient
C	$L^{\frac{1}{2}}/T$	The Chezy roughness coefficient = $V_n / \sqrt{R_n S}$
C_c		Coefficient of contraction
C_d		Coefficient of discharge
C_v		Coefficient of velocity
d	L	Diameter of a circle
D	L	Hydraulic depth as defined by V. T. Chow
d'	L	Distance from the springline to the center of curvature of the arch

SYMBOL	DIMENSIONS	DEFINITION
E_{1-4}		Energy loss between section 1 and 4
e		eccentricity
F		Denotes a mathematical function
F_n		Normal depth Froude number = $V_n / \sqrt{gY_n}$
f		Denotes a mathematical function
G		Denotes a mathematical function
g		Denotes a mathematical function
g	L/T^2	Acceleration of gravity
H	L	Total energy head
h_1^*	L	$Y_1 - Y_n$
h		Static head
h_f	L	Headloss in constriction
K		Weir coefficient as defined in Francis weir formula
K		Head loss due to bridge constriction alone
L	L	Length of the bridge in the direction of flow
L_d	L	Distance between bridges
L_{1-4}	L	Distance between section 1 and 4



APPENDIX B

DEVELOPMENT OF THEORETICAL DISCHARGE EQUATION FOR ORIFICE
TYPE FLOW THROUGH SEMICIRCULAR OPENINGS

SYMBOL	DIMENSIONS	DEFINITION
M		Channel width ratio, b/B
M'		Channel opening ratio, A_o/A_n
M ₁		Mild slope backwater curve in an open channel
N		Number of spans
n	$L^{1/6}$	Manning's roughness coefficient
n		Subscript which refers to the normal depth for uniform flow
p	F/L^2	Pressure
Q _a	L^3/T	Actual discharge through opening
Q _t		Theoretical calculated discharge through opening
Q	L^3/T	Total flow
q	L^3/T	That portion of the total flow which could pass through the bridge without contraction
R	L	Hydraulic radius
R		Reynolds number $V_n R_n / \nu$
r	L	Radius of curvature of the arch

SYMBOL	DIMENSIONS	DEFINITION
S		Slope
S_o		Slope for normal depth flow in unconstricted channel
t	T	Time
V	L/T	Average velocity
V_o	L/T	Average velocity through constriction, Q/A_o
V_n	L/T	Average velocity when uniform, normal flow occurs, $Q/5Y_n$
V		Volt
Y	L	Depth of flow
Y_1	L	Depth of flow at section of maximum backwater
Y_n	L	Depth of the normal unstricted flow
Y_t	L	tailgate height
α		Kinetic energy coefficient
β		Segment factor d'/r
γ	F/L ³	Specific weight of water
ν	L ² /T	Kinematic viscosity of the fluid
ρ	FT ⁴ /L ⁴	Fluid mass density



APPENDIX B

DEVELOPMENT OF THEORETICAL DISCHARGE EQUATION FOR ORIFICE
TYPE FLOW THROUGH SEMICIRCULAR OPENINGS

Development of theoretical discharge equation for orifice type flow through Semicircular openings. With reference to Figure 5, and neglecting the velocity of approach the discharge is:

$$Q_t = \int V \, dA \quad (8)$$

where ,

$$V = \sqrt{2g (Y_1 - h)}$$

and

$$A = 2 \int_{h=0}^{h=r} \sqrt{r^2 - h^2} \, dh$$

Hence,

$$\begin{aligned} Q_t &= 2 \int_0^r \sqrt{2g (Y_1 - h)} \sqrt{r^2 - h^2} \, dh \\ &= 2 \sqrt{2g} \int_0^r (Y_1 - h)^{\frac{1}{2}} (r^2 - h^2)^{\frac{1}{2}} \, dh \end{aligned} \quad (9)$$

Take $Y_1^{\frac{1}{2}}$ and r outside the integral

$$Q_t = 2 \sqrt{2g} Y_1^{\frac{1}{2}} r \int_0^r \left(1 - \frac{h}{Y_1}\right)^{\frac{1}{2}} \left(1 - \frac{h^2}{r^2}\right)^{\frac{1}{2}} \, dh$$

Expanding each of the terms in the integrand into a binomial Series:

$$Q_t = 2 \sqrt{2g} Y_1^{\frac{1}{2}} r \int_0^r \left(1 - \frac{1}{2} X_1 - \frac{1}{8} X_1^2 - \frac{1}{16} X_1^3 - \frac{5}{128} X_1^4 \dots \right) \left(1 - \frac{1}{2} X_2 - \frac{1}{8} X_2^2 - \frac{1}{16} X_2^3 - \frac{5}{128} X_2^4 \dots \right) dh$$

where

$$X_1 = h/Y_1$$

$$X_2 = h^2/r^2$$

Multiply the two series together using the five leading terms, the integrand becomes:

$$\begin{aligned} \int_0^r & \left(1 - \frac{1}{2} X_1 - \frac{1}{8} X_1^2 - \frac{1}{16} X_1^3 - \frac{5}{128} X_1^4 - \frac{1}{2} X_2 + \frac{1}{4} X_1 X_2 \right. \\ & - \frac{1}{16} X_1^2 X_2 + \frac{1}{32} X_1^3 X_2 + \frac{5}{256} X_1^4 X_2 - \frac{1}{8} X_2^2 \\ & + \frac{1}{16} X_1 X_2^2 + \frac{1}{64} X_1^2 X_2^2 + \frac{1}{128} X_1^2 X_2^3 + \frac{1}{256} X_1^3 X_2^3 \\ & + \frac{5}{2048} X_1^4 X_2^2 - \frac{5}{128} X_2^4 + \frac{5}{256} X_1 X_2^4 + \frac{5}{1024} X_1^2 X_2^4 \\ & \left. + \frac{5}{2048} X_1^3 X_2^4 + \frac{5}{16384} X_1^4 X_2^4 \dots \right) dh \end{aligned}$$

Adding terms and substituting for X_1 and X_2 in the integrand

$$\begin{aligned} \int_0^r & \left[- \frac{5}{128} \left(\frac{h}{Y_1} \right)^4 + \frac{5}{256} \left(\frac{h}{Y_1} \right)^4 \left(\frac{h^2}{r^2} \right) + \frac{5}{1024} \left(\frac{h}{Y_1} \right)^4 \right. \\ & \left. \left(\frac{h^2}{r^2} \right)^2 + \frac{5}{2048} \left(\frac{h}{Y_1} \right)^4 \left(\frac{h^2}{r^2} \right)^3 - \frac{5}{128} \left(\frac{h^2}{r^2} \right)^4 + \frac{5}{256} \right] \end{aligned}$$



$$\left(\frac{h}{Y_1} \right) \left(\frac{h^2}{r^2} \right)^4 + 5/1024 \left(\frac{h}{Y_1} \right)^2 \left(\frac{h^2}{r^2} \right)^4 + 5/2048 \left(\frac{h}{Y_1} \right)^3 \left(\frac{h^2}{r^2} \right)^4 + 5/16,384 \left(\frac{h}{Y_1} \right)^4 \left(\frac{h^2}{r^2} \right)^4 \dots \Big] dh$$

Integrate and substitute for limits of integrand.

$$5r \left[\left(-1/128 \quad 1/5 + 1/256 \quad 1/7 + 1/1024 \quad 1/9 + 1/2048 \quad 1/11 + 1/16,384 \quad 1/13 \right) \left(\frac{r}{Y_1} \right)^4 + 1/2048 \quad 1/12 \left(\frac{r}{Y_1} \right)^3 + 1/1024 \quad 1/11 \left(\frac{r}{Y_1} \right)^2 + 1/256 \quad 1/10 \left(\frac{r}{Y_1} \right) - 1/128 \quad 1/9 \dots \right]$$

Simplifies to

$$r \left[-0.00435 + 0.00195 \left(\frac{r}{Y_1} \right) + 0.000455 \left(\frac{r}{Y_1} \right)^2 + 0.00020 \left(\frac{r}{Y_1} \right)^3 - 0.00430 \left(\frac{r}{Y_1} \right)^4 \dots \right]$$

Now, making the first term in the new series equal to unity and substituting the solved integrand back into the expression for the theoretical discharge, remembering that $2r = b$

$$Q_t = 0.4019 \sqrt{2g} Y_1^{\frac{5}{2}} b^2 \left[1 - 0.2136 \left(\frac{r}{Y_1} \right) - 0.03216 \left(\frac{r}{Y_1} \right)^2 - 0.0112 \left(\frac{r}{Y_1} \right)^3 - 0.005344 \left(\frac{r}{Y_1} \right)^4 \dots \right] \quad (10)$$

This result, using the five leading terms in the binomial series, can be written

$$Q_t = C_1 Y_1^{\frac{1}{2}} b^2 T \quad (11)$$

where

$$C_1 = 0.4019 \sqrt{2g} = 3.22$$

and

$$T = 1 - 0.2136 \left(\frac{r}{Y_1} \right) - 0.03216 \left(\frac{r}{Y_1} \right)^2 - 0.0112 \left(\frac{r}{Y_1} \right)^3 \\ - 0.005344 \left(\frac{r}{Y_1} \right)^4$$

The above theoretical discharge equation is valid for $Y_1 > r$ which means as long as the constriction is submerged.

APPENDIX C

DIGITAL COMPUTERS AND PROGRAM NOTES

APPENDIX C

DIGITAL COMPUTERS AND PROGRAM NOTES

LGP-30 Digital Computer

The LGP-30 is a stored program general - purpose computer marketed by the Royal McBee Corporation. It is designed for every day engineering problems and belongs to the more inexpensive class of computers. The three basic components of a computer memory unit, arithmetic unit, and control unit are assembled in one desk-size housing. The main memory of 4096 words is a magnetic drum which rotates at 4000 revolutions per minute, thus making possible a maximum access time of 15 milliseconds. The memory is arranged on the drum on 64 tracks, each track containing 64 sectors. Punched paper tape is the permanent file of information for the LGP-30. The primary input-output device is a tape typewriter. The input information to the LGP-30 is transmitted by means of punched tape that is fed into the computer's reader. Manually input is also possible by writing the instructions on a code typewriter, Flexowriter, on the machine.

The final answer is printed out on Flexowriter paper. The instructions needed to operate the LGP-30 consists of a series of 16 elementary instructions which are read and obeyed by the computer one after another. Instructions are the orders which tell the computer what we want it to do with the numbers which we have given it. Instructions are stored inside the machine before the operation of

the problem is started. Then these instructions are considered by the machine one by one and the data are processed accordingly. Instructions have two major portions. The first portion is a code, called the operation code, which tells the computer which operation is to be performed next, like "add". The second portion tells the computer where to find the number to be used in this operation. This portion is called the address portion.

Internal calculation is accomplished by directing to the computing section from memory, processing it, and directing it back to memory. The computing section consists of three working registers: the counter register, the instruction register and the accumulator register. The three registers are located on three separate recirculating tracks on the LGP-30 drum, in addition to the 64 tracks of memory.

The accumulator is the working register. It contains the results of addition, subtraction, multiplication etc., as these operations occur. It also contains one of the operands, prior to execution of an arithmetic instruction; the second operand is in memory at the work location specified by the address part of the instruction.

The instruction register contains the instruction being executed. Both the operator and the address of the instruction are located in this register. Words are transmitted from memory to this register. Generally, these words are instructions of a program stored in memory. The instruction register may be interrogated to determine the operation to be performed.

The counter register contains the location of the next instruction to be executed, i.e., if the counter register reads 4132, the



next instruction to be executed is stored at 4132 or track 41, sector 32. This register contains only the address part of a word. The address part of the instruction register may be transferred to the counter register. The address part of the counter register may be transferred through a plus 1 adder to memory by use of the instruction register command. During the execution of every operation 1 is added to the counter register automatically, so it will be ready to search for the next instruction, after it finishes the one being executed.

The program used in data calculations here was written as instructed in a manual published by the School of Electrical Engineering at Purdue University in April 1960. The manual is entitled, "LGP-30 Floating Point Interpretive System (H1-24.3) - Programming Notes."

The machine time required to execute and print out the answers for the data in the following program was about 4 hours. The same program could have been written much easier on the IBM 1620 or Fortran 7090 and the operation time would only have been a percentage of the time the LGP-30 used. The reason for using the LGP-30 was to compare the efficiency of the LGP-30 to the much more expensive IBM machines mentioned. Hence for all other programs the IBM machines were used.

Program for Calculation of Normal Depth when Discharge, Channel Width
and Slope, and Mannings Roughness Coefficient are Known

The mean velocity of a free stream in uniform steady state condition can be computed by the Manning formula:

$$V = \frac{1.486}{n} R^{2/3} S^{1/2} \quad (37a)$$

where: V = mean velocity in fps ($V = Q/A$)

n = roughness coefficient

R = hydraulic radius in ft ($R = A/P$)

S = slope of energy line

Q = discharge in cfs

A = cross sectional area in sq. ft.

P = wetted perimeter in ft.

when applying this formula to a rectangular channel:

$$A = By \quad \text{and} \quad P = B + 2y$$

where B = width of channel in ft.

y = depth of flow in ft.

when uniform steady state flow occurs $y = y_n$

Substituting into equation (37a) and rearranging gives

$$y_n = \frac{Q}{B^{5/3}} \frac{n}{1.486S^{1/2}} \left(\frac{B + 2y_n}{y_n} \right)^{2/3} \quad (37b)$$

The formula can not be solved for y_n explicitly so successive approximation was used. An approximate depth y_0 was chosen and


equation (37b) which is of from $Y = f(y)$ was calculated and $y_1 = f(y)$ was obtained. Then by doing the computations with the new y , a y_2 value was obtained etc. until the change of y in percentage is equal to or less than a given ϵ .

$$\frac{y_m - y_{m-1}}{y_{m-1}} \leq \epsilon$$

As a first approximation for the depth, $y = B$ was used.

Location	Address	Remarks
	;0004000'	
4000	r6300'	Special Instruction
4001	u0400'	" "
4002	i5000'	
4003	b5000'	S
4004	r0000'	\sqrt{S}
4005	h5018'	Store \sqrt{S}
4006	b5002'	B
4007	e5010'	$B^{5/3}$
4008	r5000'	$Q/B^{5/3}$
4009	m5004'	$Q/B^{5/3}$
4010	d5012'	$Q_n/1.486 B^{5/3}$
4011	d5013'	$Q_n/1.486 B^{5/3} S^{1/2}$
4012	h5020'	Store $Q_n/1.486 B^{5/3} S^{1/2}$
4013	b5002'	B
4014	h5022'	Store B as y_0
4015	b5022'	y_0
4016	h5024'	Store y_0
4017	m5016'	$2y_0$
4018	a5002'	$B + 2y_0$
4019	d5022'	$\frac{B + 2y_0}{y_0}$
4020	e5014'	$\frac{B + 2y_0}{y_0}^{2/3}$



Location	Address	Remarks
4021	m5020'	$y_1 = \frac{Q_n}{1.436 B^{5/3} S^{1/2}}$ $\left(\frac{B + 2y_0}{y_0} \right)^{2/3}$
4022	h5022'	Store y_1
4023	s5024'	$y_1 - y_0$
4024	d5024'	$\frac{y_1 - y_0}{y_0}$
4025	t0000'	$- \left \frac{y_1 - y_0}{y_0} \right $
4026	a5008'	$\epsilon - \left \frac{y_1 - y_0}{y_0} \right $
4027	t4015'	If $\left \frac{y_1 - y_0}{y_0} \right > \epsilon \rightarrow \alpha$ If $\left \frac{y_1 - y_0}{y_0} \right \leq \epsilon$
4028	p5000'	Print S 
4029	d0000'	Tab
4030	p5002'	Print B
4031	d0000'	Tab
4032	p5004'	Print n
4033	d0000'	Tab
4034	p5006'	Print Q
4035	d0000'	Tab
4036	p5022'	Print y
4037	m0000'	Car. Ret.
4038	u4002'	Start with new set of data
	.000 4002'	Constant data

;0004002' Instructions for data tape to move up and
i5006' give new Q value after each computed Y_n value
;0004028'
u4034' Go to
;0004034'
z5006' Print Q from memory
d0000' Tab
z5022' Print computed Y_n
;0004013'
b5028' B/10 (instead of 5002)
;0005040'
r6300' Special instruction
u0400'
i5028' Input to memory (B/10)
u4002' Go to
;0005040'



Data Location

Location		Content
Constant	5000	Slope $S = 0.001$
"	5002	Channel width $B = 4.955 \text{ ft.}$
"	5004	Mannings $n = 0.0110$
Variable	5006	Flow Rate Q
Constant	5008	Tolerance $\epsilon = 0.001$
"	5010	$5/3$
"	5012	1.486
"	5014	$2/3$
"	5016	2
"	5018	$\sqrt{S} = 0.25$
"	5028	$B/10$

The IBM 1620 Computer Using Fortran Programming

The word FORTRAN is derived from FORMula TRANslation. It is provided by IBM for the IBM 1620 Data Processing System and it allows engineers and scientists to write their problems and formulas in a language closely akin to their normal mathematical notation. The IBM 1620 then translates this language into a series of instructions which are used to solve the problem. Because the FORTRAN system assumes the responsibility of translating the problem for computer solution, the user of the IBM 1620 need not be excessively concerned with machine details.

Problems can be organized and specified for machine solution more quickly in FORTRAN language than in machine instructions such as the LBP-30 in using. The FORTRAN language is written as a compromise between the language of the computer and the language of the engineer and scientist. To satisfy the engineer and scientist, as many of the detailed computer control operations as possible are eliminated from the job of writing programs, and a problem statement format close to that of the mathematical equation is used. This condensed symbolic and mathematical form of the problem reduces the possibility of clerical errors, highlights and program logic, and makes it possible to quickly modify or change the problem.

A problem written in the FORTRAN language is made up of statements which can be identified by an arbitrary number if so desired. Three main types of statements are (1) arithmetic, (2) input-output, and (3) control. Arithmetic statements provide for computation of the problem. An example is $C = A + B$. This statement would cause

IBM 1620 to generate a series of machine instructions which would set the variable C equal to the sum of the variables A and B. Other types of arithmetic operations are multiply, represented by *, division, represented by /, and exponentiation represented by ** (e.g. $A**2$ is the same as A^2). The use of these operations would be illustrated by the FORTRAN statement:

$$X = A*B + C/Y - Y**3$$

which is equivalent to the mathematical expression:

$$X = AB + C/Y - Y^3$$

Input - output statements provide for transfers of data into and results out of the computer. A type of output statement is PRINT 1, X, Y which would cause the values of X and Y to be printed. Control statements regulate the sequence in which calculations are performed. Two of the control statements are STOP and IF. The STOP signifies the end of the problem. The IF statement provides for program decision depending upon whether or not the specified variable is less than, equal to, or greater than zero. The statement IF (X - Y) 10, 11, 12 will cause instructions to be compiled that will test the value of X - Y. If the value is less than zero ($X < Y$), statement 10 will be performed next. If X - Y equals zero ($X = Y$), then statement 11 will be performed and if X - Y is greater than zero ($X > Y$), then statement 12 will be performed.

Cost Comparisons - IBM 1620, LGP-30, IBM 7090

The IBM 1620 is a solid state digital computer, which means that the computer is built with primarily solid state devices such as transistors, distinguished from non-solid state devices such as

vacuum tubes which is the main structure of the LGP-30. Solid state devices are generally more reliable than non-solid state devices. The IBM also has an automatic built-in checking program that detects and permit corrections of the more common programming errors. LGP-30 has no automatic checking.

The cost of the LGP-30 is about \$50,000 while the IBM sells for from \$75,000 and up to \$200,000.

Another advantage of the IBM 1620 is that a problem specified in the FORTRAN language for this machine can be run with modifications on other IBM data processing systems using FORTRAN systems. Other programming systems such as GOTRAN, Symbolic Programming System and package subroutines can also be used by the IBM computers. Other IBM computers such as the IBM 7090, also used for data computation in this study, costs about \$3,000,000. IBM 7090 is also a solid state digital computer, but its price, speed of computation and capacity of memory makes it more suitable for a larger concern or Research Institute.

The following programs are written in the FORTRAN language and processed on the IBM 1620 or 7090 computers.

Program for Prandtl Tube Calibration

$$\text{Velocity} = f(\text{Voltage})$$

Assuming the relation:

$$\Delta h = BV$$

Δh is in cm.

$$\text{Let: } \Delta h = Y$$

$$V = X$$

Then $Y = B X$

Now compute B by least square method:

$$\sum (Y_i - BX_i)^2 = \min \rightarrow \frac{d \sum (Y_i - BX_i)^2}{dB} = 0$$

$$\sum 2 (Y_i - BX_i) (-X_i) = 0$$

$$\sum X_i Y_i - B \sum X_i^2 = 0$$

$$B = \frac{\sum_{i=1}^n X_i Y_i}{\sum_{i=1}^n X_i^2}$$

The correlation coefficient

$$R_{xy} = \frac{\sum_{i=1}^n X_i Y_i - \frac{1}{n} \sum_{i=1}^n X_i \sum_{i=1}^n Y_i}{\left[\sum_{i=1}^n Y_i^2 - \frac{1}{n} \left(\sum_{i=1}^n Y_i \right)^2 \right] \left[\sum_{i=1}^n X_i^2 - \frac{1}{n} \left(\sum_{i=1}^n X_i \right)^2 \right]}$$

Since:

$$V_v = C \sqrt{2g \Delta h}$$

where:

V_v is in fps.

Δh is in feet

i.e. for Prandtl tube:

$$V_v = \sqrt{2g \Delta h^{ft}}$$

converge Δh from ft to cm:

$$V_v^{\text{fps}} = \sqrt{2g (0.032808) \Delta h^{\text{cm}}}$$

$$V_v = \sqrt{2 \times 32.174 \times 0.032808 \text{ BV}}$$

$$V_v = C\sqrt{V}$$

where

$$C = \sqrt{2 \times 32.174 \times 0.032808 \text{ B}}$$

The program is written to compute B, R, C for the measured data.

Program IBM 1620

```

2 DATA FITTING FOR    VELOCITY = F(VOLTAGE)    BY IBM 1620.

DIMENSION X(300),Y(300)

17 READ 1,N,J

1 FORMAT (15,15)

TYPE 2

2 FORMAT(////////24H H(CM) = B TIMES VOLTAGE)

TYPE 3

3 FORMAT (48H VELOCITY (FPS) = C TIMES SQUARE ROOT OF VOLTAGE//)

TYPE 4

4 FORMAT (3X,1HJ,10X,1HP,11X,3HRXY,11X,1HC/)

CONST = 2.0*32.174*0.03280833

K = 1

L = J

M = 1

P = J

14 SXY = 0.0

SXSQ = 0.0

SX = 0.0

```



```

SY = 0.0
SYSQ = 0.0
10 DO 7 I = K,J
    SXY = SXY + X(I)*Y(I)
    SXSQ = SXSQ + X(I)**2
    SX = SX + X(I)
    SY = SY + Y(I)
7 SYSQ = SYSQ + Y(I)**2
B = SXY / SXSQ
RXY = ( SXY-SX*SY/P)/SQRT((SYSQ-SY**2/P)*(SXSQ-SX**2/P))
C = SQRT(CONST * B)
TYPE 8,J,B,RXY,C
8 FORMAT (15,F13.5,F13.5,F13.5)
IF (J - N) 9,11,15
9 K = J + 1
J = J + 1
P = J
GO TO 10
11 GO TO (12,17),M
12 TYPE 13
13 FORMAT (/)
K = L + 1
P = J - L
M = 2
GO TO 14
15 TYPE 16

```


16 FORMAT (6H ERROR)

GO TO 17

END

Program for calculation of curves in test selection charts. (see fig. 26 & 27)

Development of tailgate height eqn. from Francis weir formula:

$$Q = KB \left[\left(H + \frac{V^2 \alpha}{2g} \right)^{3/2} - \left(\frac{V^2 \alpha}{2g} \right)^{3/2} \right] \quad (37)$$

where Q = discharge cfs.

B = effective length of crest, ft.

H = measured head on crest, ft, upstream from weir
beyond beginning of surface curve.

V = velocity of approach

K = weir coefficient

Set

Y_t = tailgate height

Y_n = normal depth of flow

Then eqn (37) can be written in the following way:

$$\frac{Q}{KB} = \left(Y_n - Y_t + \frac{V^2 \alpha}{2g} \right)^{3/2} - \left(\frac{V^2 \alpha}{2g} \right)^{3/2} \quad (38)$$

rewrite (38)

$$\left[\frac{Q}{KB} + \left(\frac{V^2 \alpha}{2g} \right)^{3/2} \right]^{2/3} = Y_n - Y_t + \frac{V^2 \alpha}{2g}$$

Now solve for Y_t :

$$Y_t = Y_n + \alpha \frac{V^2}{2g} - \left[\frac{Q}{KB} + \left(\alpha \frac{V^2}{2g} \right)^{3/2} \right]^{2/3}$$

but

$$V = \frac{Q}{A} = \frac{Q}{5Y_n}$$

and

$$Y_t = \alpha \frac{Q^2}{2g B^2 Y_n^2} + Y_n - \left[\frac{Q}{KB} + \left(\frac{\alpha Q^2}{2g B^2 Y_n^2} \right)^{3/2} \right]^{2/3} \quad (39)$$

when substitution the constant values

α = assumed to be unity

$K = 4.205$

$B = 4.955 \text{ ft.}$

The tailgate equation is found to be

$$Y_t = \left[\frac{Q^2}{1581 Y_n^2} + Y_n \right] - \left[\frac{Q}{20.056} + \left(\frac{Q^2}{1581 Y_n^2} \right)^{3/2} \right]^{2/3} \quad (40)$$

The Y_t values are calculated in the program and plotted versus Y_n with Q as parameter in the nomographic charts in fig. 26 and 27.

Program IBM 1620

```
20 DO 10 I=10,45,5
```

```
PN=0.0
```

```
PI=I
```

```
Q=.1*PI
```

```
PRINT 4
```

```
4 FORMAT (30H      Q      YN      YT      )
```

```
8 READ 6,Y
```

```
6 FORMAT (F4.0)
```

```
PN=PN+1.0
```



```

N=PN
D=1.
A=(D*(Q**2/((1581.0)*(Y**2)))+Y)
B=((D*(Q**2/(1581.0*(Y**2))))**1.5)
C=((C/20.836)+B)**(2./3.)
YT=A-C
PUNCH 2,Q,Y,YT
2 FORMAT (F10.5,2X,F10.5,2X,F11.6)
IF (N-42) 8,10,10
10 CONTINUE
PAUSE
GO TO 8
END

```

Program to find Theoretical Discharge Q_t , and Coefficient of Discharge C_d .

From equation (11), Chapter III

$$Q_t = C_1 Y_1^{\frac{3}{2}} b^2 T \quad (11)$$

where

$$C_1 = 3.22 C_d$$

and

$$\begin{aligned}
 T = 1 - 0.1068 \left(\frac{b}{Y_1} \right) - 0.00804 \left(\frac{b}{Y_1} \right)^2 - 0.0014 \left(\frac{b}{Y_1} \right)^3 \\
 - 0.000335 \left(\frac{b}{Y_1} \right)^4
 \end{aligned}$$

Note: $b = 2r$

Equation (11) is programmed and with b , Y_1 , Y_n , Q_a and F_n as given data, the print-out will be:

$$Q_t, C_d, (A_o/A_n)(Y_1/Y_n)^{\frac{1}{2}}, F_n, Y_1/Y_n, \left(\frac{F_n}{A_n}\right)^2$$

Program IBM 1620

```

PRINT 80
80 FORMAT(49H QT CD AO/AN*YI/YN FN YI/YN (FN*AN/AO)**2
20 READ 10,QA,F,YN,Z,P
10 FORMAT (F2.1,2X,F2.2,2X,F4.2,2X,F3.1,2X,F4.2)
B=4.955
YN=YN*(.0328)
H=((.0328)*X(P))
H=((.0328)*(P))
Y=((.0833)*(Z))
C=((.000335)*((Y/H)**4))
A=(1.-(.1068*(Y/H))- (.00304*((Y/H)**2))- (.0014*(Y/H)**3))-C
D=((3.22)*((H)**(.5))*(Y**2))
QT=A*D
CD=QA/QT
AN=YN*B
AC=(3.14/8.)*(Y**2)
AI=H*B
AA=(AO/AN)*((H/YN)**.5)
AB=H/YN
AC=((F*AN)/AO)**2

```



```

PRINT 90,QT,CD,AA,F,AB,AC
90 FORMAT (F4.1,F7.3,F8.4,F14.2,F7.3,F9.3)
IF (Z-18.) 20,100,100
100 PRINT 110
110 FORMAT(49H-----)
GO TO 20
END

```

Program for calculation of the plotting values for the log log graph with axis $(\frac{Y}{Y_n} - 1)$ versus $(\frac{F_n}{F})^2$, and C_d

Program IBM 1620

```

PRINT 80
80 FORMAT(49H QA CD AC/AN*(YI/YN)1/2 FN YI/YN (FN*AN/AC)2
20 READ 10,QA,F,YN,Z,P
10 FORMAT (F2.1,2X,F2.2,2X,F4.2,2X,F3.1,2X,F4.2)
B=4.955
YN=YN*(.0328)
H=((.0328)*(P))
Y=((.0833)*(Z))
C=((.000335)*((Y/H)**4))
A=(1.-(.1068*(Y/H))- (.00804*((Y/H)**2))- (.0014*(Y/H)**3))-C
D=((3.22)*((H)**(.5))*(Y**2))
QT=A*D

CD=QA/QT
AN=YN*B
AC (3.14/8.)*(Y**2)

```



```

AI=H*B
AA=(AC/AI)*(H/YN)**.5)
AB=H/YN
AC=((F*AN)/AO)**2
PRINT 90,QA,CD,AA,F,AB,AC
90 FORMAT (F4.1,F7.3,F8.4,F14.2,F7.3,F9.3)'
IF (Z-18.) 20,100,100
100 PRINT 110
110 FORMAT (49H ----- )
GO TO 20
END

```

Program for finding normal depth Froude number, F_n , when given discharge, Q , and normal depth Y_n .

Program equation:
$$F_n = \frac{Q}{B Y_n} / (g Y_n)^{\frac{1}{2}} = \frac{0.0355Q}{Y_n^{3/2}}$$

Program IBM 1620

```

PRINT 20
20 FORMAT (49H      QA      YN      FN      )
40 READ 10,QA,YN
10 FORMAT (F8.7,2X,F8.8)
FN=((0.0355*QA)/(YN**1.5))
PRINT 30,QA,YN,FN
30 FORMAT (F6.3,F9.5,F8.4)
GO TO 40
END

```


Program for calculation of plotting values K versus M' , $\frac{h_1^*}{Y_n}$ versus $(\frac{F_n}{M'})^2$ and the slope of the best fitting line through the points on arithmetic and log log scale respectively.

The programmed equations are

$$K = \frac{h_1^*}{V_0^2/2g} - \alpha \left[\left(\frac{A_0}{A_y} \right)^2 - \left(\frac{A_0}{A_1} \right)^2 \right] \quad (35)$$

and

$$K = C_1 + C_2 M'$$

where C_1 and C_2 are the constants computed to determine the slope of the line (see figures 46 - 55).

$$\frac{h_1^*}{Y_n} = f \left(\frac{F_n}{M'} \right)^2$$

and

$$\frac{h_1^*}{Y_n} = C \left(\frac{F_n}{M'} \right)^2 \gamma \quad (38)$$

where C and γ are the constants computed to determine the slope of the line (see figures 56 - 65)

Program IBM 7090

1 AKS=0.00

1 AKS=0.00

AMIS=0.00

AMSS=0.00

AKMS=0.00

ZELSUM=0.00

ZILS=0.00

ZELSS=0.00

ZELZS=0.00

M=1

READINPUTTAPES,90,ALPHA,PHI,G,B

90 FORMAT(4F10.5)

100 READINPUTTAPES,91,I,Q,YNI,YI,AO,PAR

91 FORMAT(15,F5.2,4F10.4)

YN=YNI/PHI

AMI=AO/(YN1*B)

ETA=SQRIF(G*YNI)

FN=Q/(B*YN1*ETA)

RHO=B*YN1

V=Q/AO

Z=2.0*G*PHI*(YI-YN)/V**2

PI=B*PHI*YI

OMEGA=AO/PI

AK=Z-ALPHA*(AMI**2-OMEGA**2)

AMS=AMI**2

AKAM=AK*AMI

ZI=(YI-YN)/YN

ZE=(FN/AMI)**2

ZIL=LOGF(ZI)

ZEL=LOGF(ZE)

ZELS=ZEL**2

ZELZ=ZEL*ZIL


```

WRITEOUTPUTTAPE6,92,I,AK,AMI,AMS,AKAM,FM,PHY
WRITEOUTPUTTAPE6,92,I,ZI,ZE,ZIL,ZEL,ZELS,ZELZ
92 FORMAT(15,6F15.5//)
AKS=AKS+AK
AMIS=AMIS+AMI
AMSS=AMSS+AMS
AKAMS=AKAMS+AKAM
ZILS=ZILS+ZIL
ZELSS=ZELSS+ZELS
ZELSUM=ZELSUM+ZEL
ZELZS=ZELZS+ZELZ
M=M+1
IF(M-17)20,20,21
20 GOTO100
21 WRITEOUTPUTTAPE6,93,M,AKS,AMIS,AMSS,AKAMS
WRITEOUTPUTTAPE6,93,M,ZILS,ZELSUM,ZELSS,ZELZS
93 FORMAT(15,4F15.5//)
CONSB=((AMIS*AKS)-(17.0*AKAMS))/((AMIS**2-17.0*AMSS)
CONSA=(AKS-AMIS*CONSB)/17.0
CONB=((ZELSUM*ZILS)-(17.0*ZELZS))/((ZELSUM**2-17.0*ZELSS)
CONA=(ZILS-ZELSUM*CONB)/17.0
WRITEOUTPUTTAPE6,94,CONSA,CONSB,CONA,CONB
94 FORMAT(4F15.5)
GOTO1
END(1,0,0,0,0,0,1,0,0,1,0,0,0,0,0)

```


APPENDIX D

TABLES

[illegible]

TABLE XXXI - CALCULATED VALUES - RUN N. 141 - 306

Run No.	K	M	$\frac{h_1}{Y_1}$	$\frac{F_1}{(Y_1)^2}$	$\frac{1}{g^2 b^5/c}$	$\frac{Y_1}{b}$	Run No.	K	M	$\frac{h_1}{Y_1}$	$\frac{F_1}{(Y_1)^2}$	$\frac{1}{g^2 b^5/c}$	$\frac{Y_1}{b}$
141	1.527	.154	.390	.415	.262	.843	222	1.580	.252	.1285	.353	.453	.665
142	1.466	.154	.366	.415	.262	.835	223	1.585	.252	.1296	.353	.460	.662
143	1.431	.223	.144	.200	.128	.610	224	1.398	.158	1.1157	1.617	1.075	.353
144	1.333	.223	.134	.200	.128	.606	225	1.246	.158	1.021	1.617	.953	1.010
145	1.227	.223	.123	.200	.128	.606	226	1.079	.158	.890	1.617	.853	.943
146	.897	.223	.090	.200	.128	.588	227	1.073	.135	1.1177	2.159	.441	1.270
147	2.430	.134	.688	.503	.253	1.100	228	1.036	.135	1.1337	2.159	.441	1.250
148	1.577	.134	.447	.503	.253	1.065	229	1.419	.211	.643	.866	.253	.770
149	1.503	.134	.427	.503	.253	1.050	230	1.411	.211	.646	.866	.253	.764
150	1.403	.134	.398	.503	.253	1.030	231	1.459	.304	.434	.467	.160	.870
151	1.891	.113	.719	1.874	.441	1.890	232	.654	.160	.333	1.011	.553	1.667
152	1.788	.113	1.025	1.874	.441	1.839	233	.251	.263	.455	.266	1.8	.564
153	1.684	.113	1.531	1.874	.441	1.771	234	.694	.160	.353	1.011	.553	1.82
154	1.602	.113	1.457	1.874	.441	1.718	235	.134	.223	.417	.260	.128	.512
155	1.941	.176	.728	.740	.253	.968	236	.780	.160	.400	1.011	.553	1.120
156	1.872	.176	.627	.740	.253	.910	237	.442	.223	.462	.260	.128	.524
157	1.523	.176	.572	.740	.253	.880	238	.452	.276	.444	1.749	.529	1.200
158	1.283	.176	.483	.740	.253	.823	239	.226	.171	.060	.345	.192	.721
159	1.440	.254	.262	.350	.160	.589	240	.537	.076	.173	1.749	.529	1.537
160	1.000	.254	.182	.350	.160	.553	241	.357	.171	.054	.345	.192	.721
161	.922	.254	.168	.350	.160	.545	242	.371	.171	.054	.345	.192	.721
162	.760	.254	.136	.350	.160	.521	243	.442	.136	.245	.145	.353	.796
163	1.807	.151	.852	.493	.303	1.187	244	.403	.136	.314	1.355	.553	.860
164	1.428	.154	.703	.493	.303	1.091	245	.552	.200	.682	2.274	.529	1.344
165	1.474	.154	.690	.493	.303	1.086	246	1.024	.223	.234	.429	.192	.635
166	1.109	.154	.525	.493	.303	.780	247	.447	.160	.099	2.274	.529	1.334
167	1.487	.223	.449	.555	.254	.918	248	1.382	.223	.228	.429	.192	.609
168	1.375	.223	.334	.555	.254	.762	249	.557	.152	.463	1.617	.553	.731
169	1.154	.223	.250	.555	.254	.680	250	.541	.152	.456	1.617	.553	.723
170	.959	.223	.200	.555	.254	.650	251	.573	.158	.476	1.617	.553	.738
171	1.880	.146	1.100	1.154	.354	1.486	252	.627	.120	.282	2.756	.529	1.222
172	1.706	.146	.995	1.154	.354	1.400	253	1.362	.276	.368	2.544	.192	.587
173	1.500	.146	.875	1.154	.354	1.265	254	.445	.160	.064	2.756	.529	1.295
174	1.442	.146	.862	1.154	.354	1.200	255	1.543	.270	.432	.544	.192	.609
175	1.104	.146	.649	1.154	.354	1.160	256	.211	.056	.337	3.179	.710	1.430
176	1.499	.202	.624	.556	.224	.835	257	.174	.056	.099	1.011	.553	.794
177	1.255	.202	.411	.556	.224	.828	258	.082	.154	.017	.415	.262	.593
178	1.455	.202	.355	.556	.224	.795	259	.186	.056	.448	.435	.192	.575
179	1.077	.202	.250	.556	.224	.765	260	.139	.086	.077	1.373	.441	.993
180	1.211	.356	1.494	1.277	.256	.830	261	.171	.134	.220	.563	.253	.724
181	1.247	.184	.420	.662	.256	.912	262	.091	.043	.529	5.562	1.062	2.102
182	.919	.184	.210	.662	.256	.846	263	.179	.076	.159	1.749	.529	1.204
183	1.993	.155	2.173	2.160	.441	1.856	264	.661	.118	.652	.718	.303	.850
184	2.197	.211	.991	.886	.253	.970	265	.235	.073	.247	4.196	.710	1.220
185	2.069	.211	.967	.886	.253	.922	266	.056	.130	.034	1.345	.553	.627
186	1.681	.304	.370	.427	.160	.578	267	.211	.063	.603	5.620	.885	1.510
187	1.375	.243	.214	.450	.160	.557	268	.113	.112	.104	1.789	.441	.778
188	1.555	.100	.790	1.111	.166	.550	269	.245	.168	.016	.754	.453	.505
189	1.728	.344	.840	.427	.160	.538	270	.453	.056	.734	7.155	1.342	1.896
190	1.899	.187	1.692	1.131	.363	1.104	271	.181	.079	2.142	2.274	.529	.996
191	2.204	.170	1.565	1.401	.354	1.496	272	.065	.154	.331	.933	.303	.660
192	1.865	.170	1.284	1.401	.354	1.324	273	.231	.089	.601	5.697	.710	1.070
193	2.202	.100	1.117	1.011	.354	1.690	274	.106	.152	.089	1.217	.553	.944
194	2.618	.154	.546	.445	.204	.990	275	.206	.076	.714	6.793	.885	1.340
195	2.749	.197	.392	.483	.159	.867	276	.139	.135	.195	2.159	.441	.975
196	2.500	.223	.252	.200	.128	.609	277	.262	.168	.894	8.071	1.062	1.668
197	1.500	.112	1.352	1.789	.441	1.660	278	.196	.120	.280	2.756	.529	.813
198	1.949	.175	.724	.735	.153	.974	279	.110	.187	.069	1.131	.303	.565
199	2.082	.212	.569	.501	.199	.784							
200	1.680	.252	.497	.553	.160	.610							
201	1.599	.158	1.312	1.207	.353	1.155							
202	1.370	.135	1.499	2.159	.441	1.463							
203	1.515	.211	.686	.886	.253	.85							
204	1.603	.256	.497	.604	.199	.635	285	1.855	.288	1.647	1.697	.045	.560
205	1.448	.100	.846	1.154	.354	1.320	286	1.786	.257	1.401	1.513	.045	.508
206	1.466	.150	.826	1.011	.353	1.370	287	1.368	.277	1.368	1.217	.045	.520
207	1.338	.100	.710	1.011	.353	1.370	288	1.366	.161	.658	.949	.045	.559
208	2.589	.154	.540	.445	.202	.980	289	2.941	.190	.445	.280	.018	.404
209	1.421	.154	.307	.445	.202	.837	290	3.045	.450	1.960	1.202	.120	.575
210	1.199	.223	.121	.200	.128	.597	291	3.082	.413	1.486	.913	.109	.526
211	1.398	.158	1.350	1.217	.353	1.465	292	3.148	.392	.910	.554	.087	.425
212	1.199	.223	.121	.200	.128	.597	293	3.093	.306	.884	.432	.087	.482
213	.960	.112	.868	1.789	.441	1.320	294	3.151	.191	.429	.270	.087	.654
214	1.939	.175	.720	.734	.253	.970	300	1.919	.461	1.263	1.189	.069	.380
215	1.336	.175	.498	.734	.253	.845	301	1.814	.395	.996	1.019	.069	.392
216	1.119	.175	.417	.734	.253	.801	302	1.650	.323	.721	.832	.069	.413
217	1.419	.211	.643	.886	.253	1.250	303	1.816	.389	.621	.653	.054	.381
218	.941	.140	.551	1.154	.354	1.095	304	2.886	.222	.228	.168	.036	.392
219	.723	.140	.424	1.154	.354	1.003	305	2.523	.400	.322	.247	.168	.413
220	1.674	.252	.302	.353	.160	.613	306	3.972	.306	.225	.113	.131	.510

